LEABHARLANN CHOLÁISTE NA TRÍONÓIDE, BAILE ÁTHA CLIATH | TRINITY COLLEGE LIBRARY DUBLIN
Ollscoil Átha Cliath | The University of Dublin

Terms and Conditions of Use of Digitised Theses from Trinity College Library Dublin

Copyright statement

All material supplied by Trinity College Library is protected by copyright (under the Copyright and Related Rights Act, 2000 as amended) and other relevant Intellectual Property Rights. By accessing and using a Digitised Thesis from Trinity College Library you acknowledge that all Intellectual Property Rights in any Works supplied are the sole and exclusive property of the copyright and/or other IPR holder. Specific copyright holders may not be explicitly identified. Use of materials from other sources within a thesis should not be construed as a claim over them.

A non-exclusive, non-transferable licence is hereby granted to those using or reproducing, in whole or in part, the material for valid purposes, providing the copyright owners are acknowledged using the normal conventions. Where specific permission to use material is required, this is identified and such permission must be sought from the copyright holder or agency cited.

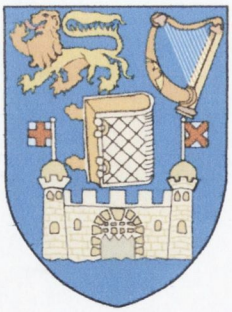
Liability statement

By using a Digitised Thesis, I accept that Trinity College Dublin bears no legal responsibility for the accuracy, legality or comprehensiveness of materials contained within the thesis, and that Trinity College Dublin accepts no liability for indirect, consequential, or incidental, damages or losses arising from use of the thesis for whatever reason. Information located in a thesis may be subject to specific use constraints, details of which may not be explicitly described. It is the responsibility of potential and actual users to be aware of such constraints and to abide by them. By making use of material from a digitised thesis, you accept these copyright and disclaimer provisions. Where it is brought to the attention of Trinity College Library that there may be a breach of copyright or other restraint, it is the policy to withdraw or take down access to a thesis while the issue is being resolved.

Access Agreement

By using a Digitised Thesis from Trinity College Library you are bound by the following Terms & Conditions. Please read them carefully.

I have read and I understand the following statement: All material supplied via a Digitised Thesis from Trinity College Library is protected by copyright and other intellectual property rights, and duplication or sale of all or part of any of a thesis is not permitted, except that material may be duplicated by you for your research use or for educational purposes in electronic or print form providing the copyright owners are acknowledged using the normal conventions. You must obtain permission for any other use. Electronic or print copies may not be offered, whether for sale or otherwise to anyone. This copy has been supplied on the understanding that it is copyright material and that no quotation from the thesis may be published without proper acknowledgement.



Local Investigations of Switchable Rotaxane Molecules at Interfaces Using Atomic Force Microscopy

By

Alan Anthony Farrell

A thesis submitted for the degree of

Doctor of Philosophy

at the

University of Dublin

2008

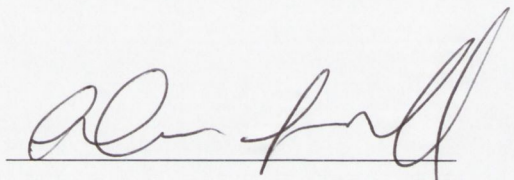
TRINITY COLLEGE
0 5 AUG 2008
LIBRARY DUBLIN
THESIS
8498

Declaration

I declare that the work in this dissertation has not been previously submitted as an exercise for a degree to this or any other university.

The work described herein is entirely my own work, except where stated in the text.

I agree that Trinity College Library may lend or copy this thesis on request.



Alan Farrell

Summary

Rotaxane molecules (interlocked molecules consisting of two parts bonded mechanically) have an inherent multi-stability. The relative positions of the sub-molecular components can be altered through external stimuli, a functionality that has been proven in solution-phase experiments. There has however, been no local, molecular-scale demonstration that the functionality of these molecules can be retained if the molecules are fixed to a surface.

In this work, Hydrogen bond assembled, switchable rotaxane molecules, assembled at a surface in thin films through a solvent deposition technique, have been studied locally by atomic force microscopy (AFM). Through this information, the effect of film preparation conditions, solvent character, and molecular structure upon potential rotaxane mobility at surfaces has been analysed. A set of experimental protocols has been established to produce well-ordered, molecularly-thin films, in which the rotaxanes are least likely to Hydrogen bond to neighbouring molecules.

Using Frequency Modulation AFM in ambient conditions, the local, molecular-scale, structure of these films has been observed for the first time. By recording an AFM signal called dissipation at the molecular-scale, which reflects the local dynamic properties of the molecules, a method for the detection of rotaxane switching is proposed. The local investigations are extended to longer, more complicated, rotaxane molecular 'shuttles' (so-called because of the character of the motion of the sub-molecular components). The switching technique is also developed further to include the rotaxane shuttle architectures, and using mixed monolayer films of rotaxanes, the molecular-scale AFM signals of the shuttling molecules during the switching process can be compared to a non-functional, yet similar, 'reference' rotaxane molecule.

Acknowledgements

I would like to thank Science Foundation Ireland for funding this project for the 4 years I was in Trinity College. I also wish to acknowledge the Leigh group in Edinburgh for willingly giving over so much rotaxane material for me to study. Also in Edinburgh Euan Kay has been especially helpful, with excellent feedback on my early efforts to describe rotaxanes on paper.

Thank you to Suzi, for all your patience and time throughout my time in your group, and for having faith in me. I learned so much from all my co-workers, especially Takayuki Uchihashi, who says he doesn't like students but can't help being a wonderful teacher. Thank you to Michael Higgins for helping me to find my feet in the world of AFM. Thank you to Takeshi Fukuma for your countless hours of patience and for trusting me to operate your AFM alone so soon after you spent months building it. I would like to thank Camilla Kelly for helping me get things done, and for your common sense and sense of humour. Jason Kilpatrick, your 'mod' skills will never be matched, thanks for all your help.

What a bunch of guys, couldn't ask for better; Andy, Barry, Simo, Rowan, Siobhán, I enjoyed all of your company so much – there was never a morning without a laugh. I'll be in touch with you all soon.

To my friends, I hope you all still remember me – I'll make up for the evenings missed as soon as I have slept some more.

I would like to give a huge thank you to my family, especially my parents; for allowing me to vent, and always having a smile to greet me, even after my extended absences without contact. To Andrea, for helping me to get to work on the savings of a PhD. Most importantly I want to thank Anne-Marie, for your love and support, and for keeping me sane, I can hardly believe I'm typing these words at last.

Table of Contents

DECLARATION ..... **II**

SUMMARY ..... **III**

ACKNOWLEDGEMENTS ..... **IV**

LIST OF FIGURES ..... **VIII**

LIST OF ABBREVIATIONS ..... **XII**

LIST OF PUBLICATIONS ..... **XIII**

CHAPTER 1: INTRODUCTION **1**

1.1 Nano Function 1
1.2 Nanotechnology – advancing technology 1
1.3 Self Assembly I – mimicking Nature 2
1.4 Interlocked Molecular Architectures 2
1.5 Self-assembly II - molecules and atoms at surfaces 4
1.6 Probe Microscopies 5
1.7 Thesis Overview: 7
1.8 References 9

CHAPTER 2: MATERIALS **11**

2.1 Introduction 11
2.2 The Mechanical Bond - Interlocked molecules 11
2.3 Multistable Rotaxanes 12
2.3.1 Mechanism of switching *13*
2.3.2 Switching Stimuli *14*
2.3.4 Property Changes *14*
2.4 H-Bond Assembled Rotaxanes 15
2.4.1 H-Bond Assembled Rotaxanes: Activation with light *17*
2.4.2 H-Bond Assembled Rotaxanes: Light Activation extended to Shuttles *19*
2.4.3 Mechanism of H-Bond Assembled Rotaxane Molecular Shuttle Switching *19*
2.4.4 H-Bond Assembled Rotaxane Switching: Other Stimuli *20*
2.5 Rotaxanes at Surfaces 21
2.5.1 Current Evidence for Rotaxane sub-molecular motion at surfaces *22*
2.5.2 Observations with probe microscopy *25*
2.6 H-Bond Assembled Rotaxanes at surfaces 28
2.6.1 H-Bond-Assembled Rotaxanes on the Au(111) Surface *29*
2.6.2 H-Bond-Assembled Rotaxanes on the HOPG surface *31*
2.7 Conclusions 32
2.8 References 33

CHAPTER 3: EXPERIMENTAL TECHNIQUES **37**

3.1 Introduction 37
3.2 Sample Preparation 38
3.2.1 Choice of deposition technique: drop casting *38*
3.2.2 Choice of substrate: HOPG *38*
3.1.3 Other Substrates *39*
3.2 Atomic Force Microscopy 42
3.2.1 Introduction *42*
3.2.2 Principle of Operation *42*
3.3 Dynamic AFM 43
3.3.1 Amplitude Modulation AFM *45*
3.3.2 Frequency Modulation AFM *47*
3.3.3 Energy Dissipation in FM-AFM *49*
3.4 AFM probes. 52
3.4.1 Measurement of lever displacement *52*
3.4.2 Calibration of levers *52*
3.4.3 Calibration of spring constant *53*

3.4.4 Sader Method for Lever Calibration 54
3.4.5 Cantilever Hydrodynamic Considerations 55
3.5 Experimental Setup/AFM Modifications 57
3.5.1 Imaging modes for rotaxanes on HOPG 57
3.5.2 FM-AFM Imaging: Avoiding Instrumental Artefacts 59
3.5.3 AFM Modifications - Introduction 59
3.5.4 AFM Scanner Modification 61
3.5.5 Magnetic Activation 62
3.5.6 Design of the coil assembly 63
3.5.7 Ultra-sensitive AFM experiments 64
3.6 Conclusions 65
3.6 References 65

CHAPTER 4: THE EFFECT OF SOLVENT UPON MOLECULARLY THIN ROTAXANE FILM FORMATION 68

4.1 Introduction 68
4.2 Sample preparation 69
4.2.1 Materials 69
4.2.2 Solvent evaporation times 70
4.3 Film Characterisation 70
4.3.1 Surface coverage calculation 71
4.4 Rotaxane Film morphology 71
4.4.1 Morphology of other rotaxane functionalities 72
4.5 Effect of solvent basicity on rotaxane film structure 73
4.6 Effect of surface coverage on rotaxane film structure 75
4.7 Conclusions 77
4.8 References 78

CHAPTER 5: QUANTITATIVE CONSERVATIVE AND DISSIPATIVE FORCE IMAGING OF ROTAXANES AT THE MESO AND MOLECULAR SCALE 79

5.1 Introduction 79
5.2 Imaging in ambient vs UHV conditions – challenges overcome during this work 80
5.3 Experiment 82
5.4 Meso-scale imaging in UHV and ambient conditions 83
5.5 Molecular-scale imaging in UHV conditions 84
5.5.1 Rotaxane surface reconstruction 84
5.6 Molecular-scale imaging in air 85
5.7 Quantitative force measurements in ambient conditions 86
5.8 Energy dissipation in FM-AFM 87
5.9 Imaging molecular mobility at surfaces 88
5.10 Energy dissipation maps 88
5.10.1 Meso-scale 88
5.10.2 Molecular-scale 89
5.11 Conclusions 90
5.12 References 91

CHAPTER 6: USING MIXED ROTAXANE THIN FILMS TO INVESTIGATE THE EFFECTS OF ROTAXANE STRUCTURE ON MECHANICAL AND MORPHOLOGICAL PROPERTIES OF ROTAXANE THIN FILMS 93

6.1 Introduction 93
6.2 Mixed monolayers 94
6.3 Energy Dissipation in FM-AFM 95
6.4 Experimental 97
6.4.1 Materials 97
6.4.2 Rotaxane Film Preparation 97
6.4.3 FM-AFM Imaging 98
6.5 Controlling the surface concentration of rotaxane thin films / The effect of packing on the observed molecular-scale structure 99
6.6 High-resolution structure in a closely-packed film of unsymmetric rotaxanes 100
6.7 Multi-component rotaxane thin films 103

6.8 OBSEVATION OF FILM CHARACTERISTICS USEFUL FOR THE DETECTION OF MOLECULAR SWITCHING EVENTS 107
6.8.1 Observing molecular-scale structures in mixed monolayers *107*
6.8.2 Dissipation contrast *108*
6.8.3 Effect of chemical structure on observed contrast *109*
6.8.4 Optimum scan conditions for molecular resolution and dissipation contrast observation *112*
6.9 ATTEMPTS AT DIRECT OBSERVATION OF EXTERNALLY STIMULATED ROTAXANE MOTION AT A SURFACE 114
6.10 CONCLUSIONS 116
6.11 REFERENCES 116

CHAPTER 7: CONCLUSIONS AND OUTLOOK 118

7.1 INTRODUCTION 118
7.2 CONCLUSIONS 118
7.3 OUTLOOK 119
7.4 REFERENCES 123

LIST OF FIGURES

Figure 1.1: Some Interlocked structures; the Olympic flag, and a simple model of rotaxane structure. 'A' and 'B' can be any molecular species, and are not bonded chemically. 3
Figure 2.1: Reaction mechanism for the production of the first ever rotaxane molecule. This is adapted from the 1995 review by Amabilino and Stoddart.[1] 12
Figure 2.2: Illustration of the Free Energy of the rotaxane molecule as a function of position of the macrocycle along a thread. The sites of minimum energy are the "stations", and when switching of one of these stations occurs, the free energy difference between the stations is changed. This figure is adapted from the 2003 publication by Altieri et al.[6] 14
Figure 2.3: Illustration of the synthesis of a simple H-Bond assembled Fumaramide rotaxane with a single station and minimal thread length. The rigid fumaramide structure holds the H-Bond donor groups in a position that templates the formation of macrocycles. This figure is adapted from the 2001 publication by Gatti et al.[22] 16
Figure 2.4: Rotaxane crystal structures and the yields for rotaxane formation associated with the H-Bonding template of the station. Structure (b) can only be produced by photoisomerisation of (a). This figure is adapted from the publication by Altieri et al.[6] 18
Figure 2.5: Light activated H-Bond assembled molecular shuttle. The rotaxane thread has two stations, (a Fumaramide and a Succinamide group), and a 12 Carbon Spacer. This figure is adapted from the publication by Altieri et al.[6] 20
Figure 2.6: Electrochemically activated H-Bond assembled molecular shuttle. The rotaxane thread has two stations, (a Succinamide and a Naphthalimide group), and a 12 Carbon Spacer. This figure is adapted from the publication by Altieri et al.[29] 21
Figure 3.1: Illustration of the HOPG lattice structure. This structure is stacked sheets of graphene, and is easily cleavable because of the relatively weak bonding between the stacked sheets. Image Source: Wikipedia (http://en.wikipedia.org/wiki/Graphite - fetched July 2007) 39
Figure 3.2: AFM image of thin film of rotaxane molecular shuttle (of the kind discussed in section 2.4.4) physisorbed on a SAM of 11-mercaptoundecanoic acid on Au(111). This film was prepared according to the method of Cecchet et al.[3, 4] 40
Figure 3.3: AFM image of thin film of Fumaramide rotaxane (section 2.4) physisorbed on a methylated silicon surface. This film was prepared by exposing a clean silicon 001 surface to Methylsilane vapour. The surface has an RMS roughness of 450 pm. 41
Figure 3.4: AFM image of Exo-pyridyl Fumaramide Rotaxane deposited on a freshly cleaved Mica(0001) surface. The rotaxane molecule has formed crystallites but not spread on the surface. 41
Figure 3.5: Principle of AFM operation. 43
Figure 3.6: Graph of the Lennard-Jones force law (eq. 3.5). 45
Figure 3.7: Typical AM-AFM interaction curves (Phase and Amplitude). The curve was measured on a HOPG surface using a Silicon tip (with a native oxide layer) with radius approx. 10 nm (as specified by supplier). 46
Figure 3.8: Typical FM-AFM interaction curves (Frequency and Excitation Voltage). The curve was measured on a HOPG surface using a Silicon tip (with a native oxide layer) with radius approx. 10 nm (box value). Point 'a' is a point where the tip-sample separation is large and no perturbation is experienced. Point 'b' is the point of minimum force (i.e. maximum net attractive force). At point 'c' the tip and sample are close together and repel each other. 48
Figure 3.9: Proposed model for the inverted Topography and Dissipation signals seen during FM-AFM scanning. 51
Figure 3.10: Cantilever frequency shift in liquid as the cantilever/tip ensemble approaches the surface. The long range shift (a) shows significant deviation due to hydrodynamic damping. This effect however is unimportant over the region of interest (b) (last 200 nm). This interaction was measured using a silicon tip under water as an approach to a HOPG surface was made. 56
Figure 3.11: Measurement of hydrodynamic damping. This was observed in Ambient conditions. 57
Figure 3.12: AM-AFM image of a rotaxane thin film on HOPG. The square in the centre of the image is where a Contact Mode scan (500 nm x 500 nm) was performed previously. In the Contact Mode scan no topographic details were observed. The AFM mode was changed to AM mode and the scan size was zoomed out to observe the damage done by tip ploughing. 58
Figure 3.13: Photograph of AFM scanner modifications. The new piezo tube sits in a hole in a heavy stainless steel fitting. This fitting is carried along by the original flexure scanner. A software modification allows disable the original scanner and move the sample with the piezo tube. This allowed significant reduction of the positional noise caused by having such a large scan range on the original scanner. 61

Figure 3.14: Illustrations of the main methods used for AFM cantilever activation. 62
Figure 3.15: Comparison of the activation spectra for a cantilever with attached magnet for the three different coil setups. This figure also shows photographs of the Magnetic Activation modification used with the Asylum MFP-3D, and the modified scanner. 63
Figure 3.16: Signal flow and feedback diagram of home-built low noise AFM operation in FM-AFM mode. 64
Figure 4.1: Rotaxane molecular structures of IF (Isophthalyl Fumaramide rotaxane), EF (Exo-pyridyl Fumaramide), ISN (Isophthalyl Succinamide-Naphthalimide Shuttle) and ESN (Exo-pyridyl Succinamide-Naphthalimide Shuttle). 69
Figure 4.2: AFM topography images of (a) IF and (b) EF sub-monolayer films on HOPG. Scan sizes 2 μm. 71
Figure 4.3: AFM topography images of (a) ISN and (b) ESN sub-monolayer films on HOPG. Scan sizes 1 μm. 72
Figure 4.4: AFM topography images of EF sub-monolayer films on HOPG as deposited from a range of solvents. Scan sizes 1 μm. 73
Figure 4.5: Film height of rotaxane IF monolayer films for five different solvents, plotted against solvent hydrogen-bond basicity (β). Numbers in brackets are the percentage coverage of the films for those measurements. 74
Figure 4.6: Rotaxane crystal structures; (a) IF as recrystallised from DMSO, (b) EF as recrystallised from DMSO , (c) IF as recrystallised from CHCl3/MeCN (non hydrogen-bonding solvent). 75
Figure 4.7: AFM topography images of EF sub-monolayer films on HOPG as deposited from chloroform for a range of surface coverages; (a) 20%, (b) 50%, (c) 78% and (d) 95%. Scan sizes: (a), (c), (d) 2 μm, (b) 1 μm. 76
Figure 4.8: AFM topography images of EF sub-monolayer films on HOPG as deposited from DMSO for a range of surface coverages; (a) 14%, (b) 29%, (c) 55% and (d) 88%. Scan sizes 2 μm. 76
Figure 4.9: Film height of rotaxane IF monolayer films for chloroform and DMSO, plotted as a function of surface coverage. 77
Figure 5.1: Molecular structure of exopyridyl fumaramide rotaxane (EF). 82
Figure 5.2 Meso-scale FM-AFM images of an EF thin film on HOPG (a) in UHV before annealing (464 nm x 558 nm, cantilever: Nanosensors NCH, Δf = - 15 Hz, a = 8 nm), (b) in UHV after annealing (500 nm x 500 nm, cantilever: NCH, Δf = - 20 Hz, a = 8 nm), (c) in ambient conditions no annealing (500 nm x 500 nm, cantilever: Nanosensors EFM, Δf = - 25 Hz, a = 9.6 nm, Q = 154). 83
Figure 5.3: Molecular-scale UHV FM-AFM images of an EF thin film on HOPG. (a), (b), (c) Before annealing and (d) annealed sample, [(a): 9 nm x 9 nm, Δf = - 150 Hz, a = 6.5 nm, (b): 9 nm x 9 nm, Δf = - 150 Hz, a = 6.5 nm, (c): 9 nm x 9 nm, Δf = - 170 Hz, a = 6.5 nm, (d): 9 nm x 9 nm, Δf = - 180 Hz, a = 5.9 nm; measured lattice parameters: asurf = 1.65 nm ±0.1 nm, bsurf = 1.35 ±0.1 nm, $\theta = 70° \pm 2°$]. 84
Figure 5.4: Apparent equilibrium reconstruction of the EF film on HOPG after annealing with parameters: a_{surf} = 1.65 nm, b_{surf} = 1.37, $\theta = 68°$. 85
Figure 5.5: Molecular-scale ambient FM-AFM topography image of EF thin film on HOPG (70 nm x 70 nm, cantilever: Nanosensors NCHR + magnet, a = 10.8 nm, Δf = - 35 Hz). 85
Figure 5.6: Typical frequency, force and dissipation vs. tip-sample distance curves in ambient conditions, dots: raw data, line: smoothed data (Cantilever: NCHR + magnet, Q = 510, a = 8.9 nm). 87
Figure 5.7: Molecular-scale UHV FM-AFM images of an EF thin film on HOPG. Simultaneous topography (a) and dissipation (b) images (23.2 nm x 27.9 nm, cantilever: NCH, Δf = - 100 Hz, a = 8.9 nm). 88
Figure 5.8: Meso-scale ambient FM-AFM simultaneous topography (a) and dissipation (b) images of an EF thin film on HOPG (500 nm x 500 nm, Δf = - 26 Hz, a = 11.8 nm). 89
Figure 5.9: Molecular-scale ambient FM-AFM simultaneous topography (a) and dissipation (b) images of an EF thin film on HOPG (30 nm x 30 nm, Δf = - 52 Hz, a = 8.9 nm). 89
Figure 6.1: Molecular structures and nomenclature for the rotaxane molecules used in the experiments presented in this chapter. The macrocycles are distinguished by being Isophthalyl (X, Y = CH) and Exopyridyl (X, Y = N). The various "stations" (areas of the rotaxane thread where the thread-macrocycle interaction energy is locally minimized) are Fumaramide, Succinamide and Naphthalimide. A CX prefix corresponds to the number of carbon atoms in the thread backbone (e.g. C12 for a 12 Carbon chain). Hence the name in (a) is EF, a rotaxane with an exopyridyl-functionalised macrocycle and a single fumaramide station; (b) is a C12-ESN, which would correspond to an exopyridyl succinamide naphthalimide benzylic amide hydrogen-bond-assembled rotaxane molecular shuttle; (c)

corresponds to an isophthalyl/exopyridyl macrocycle with fumaramide-succinamide stations and a 12 carbon thread 98
Figure 6.2: FM-AFM (ambient conditions) topography images showing molecular-scale details of C12-IFS on HOPG as deposited from acetone. The surface concentration in (a) and (b) is arbitrarily γ, and the surface concentration of (c) is 3γ and that of (d) is 4γ. The films in (c) and (d) were made by adding molecules to (a) and (c) respectively by repeating the film deposition process. Thus the sequence of images shows the gradual completion of a rotaxane monolayer. 100
Figure 6.3: FM-AFM (ambient conditions) topography images showing high-resolution molecular-scale details of C12-IFS on HOPG deposited from acetone. The molecules are part of a compressed film as in Figure 6.2 (c). In image (a) it can be seen that the main rows actually have a fine double-row structure (indicated by the arrow); image (b) is the retrace topography image, which also shows the double-row structure, indicating that this is a true structure and not noise. The FFT of image (a) (inset) reveals a periodic distance of 5.3 nm between the double-rows. 102
Figure 6.4: FM-AFM topography image of a two-component rotaxane film on HOPG, formed using EF and IFS partial components deposited in the order EF then IFS. The meso-scale image shows that the mixed films retain the morphological characteristics of the individual components' films. The brighter, more ordered regions are the EF molecule (region A) (which can be compared to the image in Figure 4.2(b) and the molecules in region B are IFS molecules (which can be compared to the image in Figure 6.2(a)). Region C is the HOPG surface. 104
Figure 6.5: FM-AFM (ambient conditions) topography images of multi-component rotaxane films on HOPG formed using EF and EFS molecules. The images show clearly the distinct morphologies of the individual component molecular films. The film in image (a) was formed by depositing sub-monolayer coverage of the shorter EF molecule to form a partial film, followed by sub-monolayer coverage of the EFS molecule. There appears to be a build-up of the EFS molecule on the already-formed EF portion of the film. The film in image (b) was formed in the reverse order to (a), i.e. a partial monolayer coverage of EFS followed by a partial coverage of EF. The film characteristics in (b) are different to (a); the film in (b) has smaller EF domains relative to (a) and the EF portion does not have any apparent coverage of EFS molecules. 105
Figure 6.6: FM-AFM (ambient conditions) topography images of a multi-component rotaxane film on HOPG, formed using EF and IFS partial components deposited in the order EF then IFS. The images clearly show the molecular-scale details of both film components. These molecular-scale characteristics correspond to those of the individual components seen in Figure 4.2(b) (EF) and Figure 6.2(a) (IFS). 106
Figure 6.7: FM-AFM (ambient conditions) topography (a) and excitation voltage (proportional to dissipation) images of a multi-component rotaxane film on HOPG, formed using EF and EFS partial components deposited in the order EF then EFS. The dissipation image shows three clear regions of contrast corresponding to the EFS molecules (brightest), EF molecules and HOPG (smooth dark regions). 109
Figure 6.8: FM-AFM (ambient conditions) topography (a) and excitation voltage (proportional to dissipation) images of a multi-component rotaxane film on HOPG, formed using EF and IFS partial components deposited in the order EF then IFS. The dissipation image shows three clear regions of contrast corresponding to the EF molecules (brightest), IFS molecules and HOPG (smooth dark regions). The contrast between EF and IFS regions is inverted with respect to the contrast seen in Figure 7. 111
Figure 6.9: FM-AFM (ambient conditions) topography (a), (b) and (c) and excitation voltage (d) (proportional to dissipation) images of a two-component rotaxane film on HOPG, formed using EF and ESN partial components deposited in the order EF then ESN. Image (a) shows clearly the distinct molecular reconstructions of the EF film (bottom part of the image) and ESN molecules (upper part of the image). Image (b) is a zoomed image of the same region where the molecular types can be identified by the morphologies of the partial components of the film (the EF being the more ordered component of the film in the lower part of the image); section 4.4, comparing Figure 4.2(b) to 4.3(b) the morphologies films of the individual components can be compared. Images (c) and (d) are corresponding topography and dissipation images respectively which illustrate that we can simultaneously observe and compare the molecular reconstruction and dissipation contrast of the individual film components. 113
Figure 6.10: FM-AFM (ambient conditions) topography (a), (b) and (c) and excitation voltage (d) (proportional to dissipation) images of a C12-IFS monolayer on HOPG. (a) is a half-monolayer; this half-monolayer was then irradiated to switch some of the Fumaramide groups to Succinamide, hence altering the thread-macrocycle interaction strength. (b) Shows that same half-monolayer after irradiation plus another half-monolayer of unswitched C12-IFS. Higher-resolution topography and

dissipation images of the mixed switched/unswitched monolayer are shown in (c) and (d) respectively. *115*
*Figure 7.1: A series of FM-AFM topography and dissipation images of a contaminated HOPG surface in ambient conditions during exposure of the surface to UV radiation at (***254 nm, 5mW/cm2***) for 1 hour*..... *121*
Figure 7.2: Illustration of AM-AFM study of Electrochemically switchable H-bond assembled rotaxane monolayer thin film. (a) is the molecular schematic. (b), (c) and (d) are the Topography, Phase and Current signals recorded while the tip-sample bias was varied Bias was varied (RHS of (d)). Image (e) is the resulting film structure showing the removal of rotaxane material. (f) shows the phase vs. Bias curve while the tip is engaged close to the surface in typical imaging conditions..... *122*

LIST OF ABBREVIATIONS

AFM	Atomic Force Microscope
AGC	Automatic Gain Controller
AM-AFM	Amplitude Modulation Atomic Force Microscopy
ATP	Adenosine triphosphate
CuPc	Copper Phthalocyanine
CV	Cyclic Voltammagram
DC	Direct Current (used to signify 'static' as opposed to 'dynamic')
DMSO	Dimethyl Sulfoxide
DNA	Deoxyribonucleic acid
FFT	Fast Fourier Transform
FM-AFM	Frequency Modulation Atomic Force Microscopy
FPGA	Field-Programmable Gate Array
H-Bond	Hydrogen Bond
HOPG	Highly-Oriented Pyrolytic Graphite
HPLC	High Performance Liquid Chromatography
HREELS	High-Resolution Electron Energy-Loss Spectroscopy
LB	Langmuir-Blodgett
MAD Mode	Magnetically-Activated Dynamic Mode
MFP-3D	Molecular Force Probe-Three Dimensional
MHz	MegaHertz
ML	Monolayer
MSTJ	Molecular Switch Tunnel Junction
NMR	Nuclear Magnetic Resonance
OBD	Optical Beam Deflection
PLL	Phase-Locked Loop
RNA	Ribonucleic acid
SAM	Self-Assembled monolayer
SEM	Scanning Electron Microscope
STM	Scanning Tunneling Microscope
THF	Tetrahydrofuran
UHV	Ultra-High Vacuum
UV	Ultra Violet
XPS	X-ray Photoelectron Spectroscopy
XR	X-ray Reflectometry

Rotaxane Nomenclature:

IF	Isophthalyl Fumaramide
EF	Exo-pyridyl Fumaramide
ISN	Isophthalyl Succinamide-Naphthalimide
ESN	Exo-pyridyl Succinamide-Naphthalimide
IFS	Isophthalyl Fumaramide-Succinamide
EFS	Exo-pyridyl Fumaramide-Succinamide

LIST OF PUBLICATIONS

Some of the work contained in this thesis has also been published in scientific literature and presented to peers at international conferences.

Papers – Peer Reviewed

1. A.A. Farrell, T. Fukuma, T. Uchihashi, E.R. Kay, G. Bottari, D.A. Leigh, H. Yamada, and S.P. Jarvis, "Conservative and Dissipative Force Imaging of Switchable Rotaxanes with Frequency Modulation Atomic Force Microscopy", *Phys. Rev. B* **2005** (72) 125430.

2. A.A. Farrell, E.R. Kay, G. Bottari, D.A. Leigh, and S.P. Jarvis, "The Effect Of Solvent Upon Molecularly Thin Rotaxane Film Formation", *Appl. Surf. Sci.* **2007** (253) 6090.

3. J.E. Sader, T. Uchihashi, M.J. Higgins, A. Farrell, Y. Nakayama, S.P. Jarvis, "Quantitative Force Measurements Using Frequency Modulation Atomic Force Microscopy - Theoretical Foundations", *Nanotechnology* **2005** (16) S94.

Oral Presentations

- 7th International Symposium on Atomically Controlled Surfaces, Interfaces and Nanostructures (ACSIN7) Nara, Japan, 2003.
- Workshop on Capabilities of Scanning Probe Microscopy Research in SFI Nanoscience Laboratories, Dublin, 2005.
- Microscopical Society of Ireland 29th Annual Symposium, Dublin, 2005.

Poster Presentations

- Trends in Nanotechnology (TNT2004), Segovia, Spain, 2004.
- International Symposium on Surface Science and Nanotechnology (ISSS-4), Saitama, Japan, 2005.
- International Conference on Nanotechnology (ICN+T 2006), Basel, Switzerland, 2006.

Chapter 1: Introduction

"There's Plenty of Room at the Bottom"

Feynman, R. P. *The Pleasure of Finding Things Out* (Perseus Books: Cambridge, Massachusetts,1999). www.its.caltech.edu/~feynman

1.1 Nano Function

The understanding, manipulation and utilization of the nanoscale interactions and functionality of molecules have many benefits, including: (i) the potential for miniaturization of current technologies which could, in theory, allow for significant response time and storage capacity increases, whilst simultaneously reducing cost; (ii) devices that would otherwise not exist, like artificial superhydrophobic surfaces[1] and chemical-specific sensors can be created.[2]

In general, properties of nanoscale materials do not scale to macroscale systems and so must be investigated at the nanoscale. One of the core foundations of nanoscience is that when dimensions approach a few atomic diameters matter no longer behaves according to the laws of classical physics. For example, in electronic device manufacture quantum tunnelling effects must be considered, while nanoparticles of these dimensions have very large surface area to volume ratios, meaning that often the properties of the surface dominate in lieu of the bulk material properties. Fluid flow at length-scales similar to that of the constituent fluid elements cannot be modelled by classical fluid flow models.

1.2 Nanotechnology – advancing technology

There are two ways that the ongoing miniaturization of technology can continue. One way is through refinement and scaling down of current "top-down" processes (where the device is sculpted from the greater whole). Already the limits of this approach are being encountered – the newest semi-conductor production technologies must use immersion lithography for accurate pattern definition. This effectively reduces the wavelength of the light used by a factor equal to the refractive index of the liquid. The alternative approach is the use of bottom-up processes, where the patterned structures are built through self-assembly of the constituents. An example of current research in

this area is the investigation of the growth of semiconducting nanowires directly on Silicon substrates with specific orientations.[3]

In the interim between current state-of-the-art and the adoption of purely 'bottom-up' strategies, there will of course be techniques that share traits of both approaches. For example the self-assembly of a block copolymer material on a surface already lithographically patterned can serve to reduce existing feature sizes.[4]

1.3 Self Assembly I – mimicking Nature

The concept of self-assembly is core to all of nanoscience, both from the perspective of chemical synthesis and from the perspective of surface patterning. Ever since the elucidation of the double-helix structure of DNA, which is stabilized by selective Hydrogen-bonding, there has been a revolution in the field of chemical synthesis. The principles of biomolecular organization are being understood, adapted and applied to synthetic systems. Functional nano-devices are present in every living being. Large Ribonucleic Acid (RNA) complexes have been observed to function as molecular factories,[5] unzipping DNA, reading the encoded information and assembling a protein. Adenosine Triphosphate (ATP) Snthase has the form of a molecular motor,[6] and is involved in the production of ATP, the compound that transports chemical energy within cells. It is the highly specialized functionality, and programmed self-assembly that has evolved over millions of years, that Man seeks to understand and mimic.

1.4 Interlocked Molecular Architectures

With all the recent excitement in the scientific community about the possibilities of nanotechnology, many scientists have been re-examining complex interlocked molecular architectures – previously considered mainly as beautiful curiosities. Some interlocked architectures are illustrated in Figure *1.1*. A "Catenane" is composed of interlocked macrocycles in similar fashion to the Olympic rings, while a typical "Rotaxane" architecture is one (or more) macrocycle(s) threaded by a dumbbell-shaped sub-molecule.

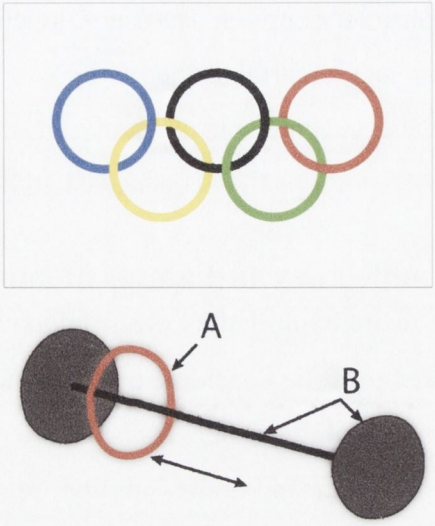


Figure 1.1: Some Interlocked structures; the Olympic flag, and a simple model of rotaxane structure. 'A' and 'B' can be any molecular species, and are not bonded chemically.

It is perhaps the resemblance of the motions of interlocked molecules to everyday mechanical machines, and the intuitive stimulus-response characteristics so easily described in these terms, that has led to their common association with the very heart of nanoscience. However, just because the behaviour of these molecules is so easily explained by analogy with the macroscopic world, does not mean that their potential functionality in nanoscale devices is diminished. This year, researchers at the University of California, Los Angeles, in collaboration with Hewlett-Packard, announced a working molecular memory based on the reversible translational motion of macrocycles inside an interlocked molecular architecture.[7] Although many would argue that these devices are slow, or that for true molecular electronics applications we need molecules that can function as transistors and systems that exhibit gain, this level of control at the molecular level is remarkable.

Nevertheless, the exact underlying mechanism for the functionality of these devices remains a mystery, despite much evidence by secondary and/or averaging techniques, it has proven impossible to elucidate definitively, and without opposition, the exact mechanism of, for example, the Stoddart-Heath molecular switches,[8] or indeed to say for sure if the motion of the molecular components in the solid state is the explanation for the functionality of the device. Furthermore, direct observation of these effects would be invaluable in refining these potential device components, which could lead to the possibility of building devices that can actually rival the functionality and versatility of silicon technology. This is where a fundamental study of model systems

such as simple rotaxanes, at surfaces, is necessary to elucidate basic facts about molecule-molecule and molecule-surface interactions and their effect on sub-molecular mobility in rotaxane and catenane molecular machines.

1.5 Self-assembly II - molecules and atoms at surfaces

If molecular machines are to be exploited as electronic switches or sensing devices there are four key factors that must be considered: functionality, order, addressability, and durability. The functionality of the molecules is the most important factor, and the other three factors, especially order and addressability are somewhat integrated. The rotaxanes' surface properties are explored in this thesis with these ideas in mind.

Many elegant molecular systems have been designed with specific functionalities that involve molecular rearrangements or some kind of reaction taking place.[9] For the most part the functionality of these systems is tested in solution environments. In most cases it remains to be proven that the molecular system in question functions as intended when confined at a surface. Ordering of atoms and molecules can be achieved through self-assembly via physorption or chemisorption if the molecular or atomic size is tailored to the atomic pattern of the surface. As an example a sulfide functional group will easily bind to Gold, and molecules with this functionality form monolayers on the Au(111) surface (Self-Assembled Monolayers (SAMs)).[10] The molecules in a SAM are typically long alkyl chains with a sulfide functionality to bind to the surface. The long alkyl chains can be modified to incorporate H-bonding groups, so that neighbouring molecules pack more closely together with a subsequent increase in film order.

The current means of accessing a device is through tiny metal connects, where the solid state device has been sculpted from a greater whole. Addressing individual molecular devices would seem to be beyond the scope of lithographic patterning. Not only will the device need to function, and assemble into a pattern, but scaling to the outside world will require that the connections to these devices are also self-assembled. One might imagine incorporation of patterned nanowires for the connection of neighbouring devices, with scaling upwards involving successively larger patterned nanowires.

This thesis explores the self-assembly at surfaces of interlocked rotaxane molecules, themselves made through a templated self-assembly process (discussed in *section 2.4*). Self-assembly at a surface is complementary to molecular self-assembly. The understanding of this field has been primarily driven by investigations using probe microscopy investigations, which is the primary tool of the experimental data presented in Chapters *4*, *5* and *6*.

1.6 Probe Microscopies

The invention of the Atomic Force Microscope (AFM) came as an offshoot of the Scanning Tunneling Microscope (STM). The existence of a tunneling current, through an insulating barrier, between two conducting surfaces in close proximity is predicted by quantum mechanics. Tunneling through a vacuum barrier was first demonstrated experimentally by Binnig *et al.* by controllably bringing a sharp conducting tip in close proximity to a conducting surface.[11] By scanning the tip over the surface at a constant value of tunnel current a topographic picture of the surface with unprecedented resolution was produced.[12] The tunnelling current is extremely sensitive to distance (the tunnelling current varies exponentially with distance), so atomic resolution was demonstrated relatively quickly by this method.[13] Although the STM does not measure force, researchers noticed that the STM could measure large atomic-scale corrugations that could not be explained by a conducting model alone – the scanning tip was experiencing a force.

Binnig *et al.* constructed the first AFM by using an STM to sense the motion of a cantilever made of gold foil with a sharp diamond attached as the tip which was brought into proximity to an insulating sample.[14] This technique was capable of imaging non-conducting samples because the motion (or deflection) of the cantilever was dependent upon the force experienced by the tip. Now a sample could be imaged by scanning the tip over the surface at a constant value of deflection, which produced a topographic picture of the surface corresponding to a region of constant force between the tip and sample. The STM was soon replaced as the means of measuring the lever displacement by optical methods like specular laser reflection,[15] and interferometry.[16] This simple "contact mode" AFM technique was able to successfully

obtain lattice images of various surfaces, including Graphite,[17] amino acid crystals,[18] and NaCl.[19] The lack of observation of atomic- and molecular-scale defects, and the fact that the load applied during imaging was typically much greater than the loading limit for a single atom, meant that the images obtained were not yet truly atomic images. By carefully balancing the applied load in aqueous conditions however, Ohnesorge *et al.* were able to resolve atomic-scale kinks, which corresponded to point-like defects, along mono-atomic step lines of calcite.[20]

Eventually in 1995 by adopting a technique that measured the frequency response of a deliberately oscillated cantilever, as the attached tip approached the surface, Giessibl *et al.* could obtain the first images of the Si(111) 7x7 structure in Ultra-High Vacuum (UHV).[21] The technique was capable of much reduced loading forces on the sample during imaging. Later that year single defects and their motion was observed.[22] As ideal experimental parameters were gradually (empirically) determined, obtaining true atomic resolution in UHV became more and more routine.

Some groups turned the attention of their ultra-sensitive dynamic AFMs towards the study of molecular films for their potential applications as functional devices. By investigating molecular films such as SAMs on Au(111),[23] and Fullerenes on Si,[24] this technique has added a new dimension to the knowledge already garnered by STM of these molecules. Since the AFM does not require a conducting or semiconducting surface, the AFM can investigate systems that the STM cannot, so larger molecules or even living biological systems can be investigated.

The adoption of dynamic modes of operation (discussed thoroughly in Chapter 3) and the resulting increase in sensitivity has allowed high-resolution molecular studies to be carried out. In addition, extra channels of information are accessible, which give insight into local material properties because of the measurable energy loss from tip to sample. This energy loss (dissipation – Chapter 3) has a material dependence and molecular scale contrast, and is exploited in this work.

1.7 Thesis Overview:

This thesis has been undertaken during a period of rapid development/excitement in the fields of AFM, Rotaxanes and Interlocked Architectures.

With regard to the importance of self-assembly emphasised above, in this thesis I investigated rotaxane molecular machines with a view to clarifying two of the fundamental questions about these molecules when incorporated at a surface. That is, will they assemble (can we make films with order), and will they function under the confining influence of the surface. The kind of understanding I have been looking for is one that can be applied to a range of molecules as opposed to specific molecules, with a view to establishing rules for rotaxane assembly to maximize retention of functional properties that have been established in the solution phase.

Initially I studied the formation of rotaxane films from various solvent types. I first observed that certain macrocycle functionalities resulted in films that were substrate-aligned, and also that the packing seemed to depend upon the nature of the solvent used during deposition. The substrate-alignment inferred that at the molecular scale molecules should be aligned. This was the first known evidence of local molecular-scale packing information for rotaxane molecules.

One of the initial intentions of this work was to investigate rotaxanes at a molecular level. The Jarvis research group had members who had historically been involved in molecular-scale investigations of DNA, SAMS etc. under UHV conditions. At the time the UHV environment was the only place such investigations were possible (because of the enhanced sensitivity associated with the lack of damping of AFM lever oscillations). I developed a fruitful collaboration with a UHV AFM laboratory in Kyoto University, Japan. I studied the ordered rotaxane films and established a surface reconstruction model. This model is discussed in Chapter 5.

I brought my knowledge and experience gained during this time back to the Laboratory in Ireland. Because the rotaxane films were created in ambient conditions and then transferred to the UHV environment, I had high confidence that the reconstructions would still be present in ambient conditions, with the only obstacle being instrument sensitivity. I modified an Asylum MFP-3D^{TM} AFM (*section 3.5*) and

using the Frequency Modulation AFM technique (*section 3.3.2*) managed to achieve molecular resolution in air. These measurements also verified that the local molecular-scale tip-sample energy transfer could be measured. At this time there really was only one other study of molecules done outside of UHV, which was done on a chemically adsorbed, close-packed, highly uniform SAM on Au sample – much different to the physically adsorbed and easily displaced rotaxane films I was studying. This other study was in fact carried out by the group I collaborated with in Japan, using a modification of a completely different AFM system.

A lot of the work was done at the beginning of my time as a PhD student into the study of the formation of ordered rotaxane films, and while it was exciting to be developing cutting-edge molecular-resolution-capable equipment I felt that there was important information to be gleaned from this early data. I therefore revisited the film preparation work with a view to expanding the data-set to gain some real statistics about the film formation process. Another reason was that the switching experiments of rotaxanes at surfaces that I was trying were producing unclear results, and it became apparent that I needed to be sure that the film deposition conditions were optimal for maximizing the potential for rotaxane functionality. Some of the experiments I carried out included systematically varying the important solvent parameters during rotaxane deposition. This work is described in Chapter *4*.

During this time Dr. Takeshi Fukuma, a collaborator of mine from Kyoto, came to Ireland to work with our group. He brought considerable expertise to the group and built an advanced low-noise AFM. In parallel with expanding the solvent data set and analysing this data I began working with Dr. Fukumas instrument to establish experimental protocols for examining the even more challenging long-chain rotaxane shuttles.

The final analysis of the solvent data was therefore done subsequent to the work described in Chapter *5* and most of that in Chapter *6*. However the chapters are presented in the order of initiation of the work for ease of understanding. The data presented in Chapter *4* and the resulting publication[25] suggest that acetone is not an ideal solvent for rotaxane film formation to favour the occurrence of sub-molecular motion. By no means does this invalidate the data in Chapters *5* and *6*, in which I

continued working with acetone in order to maintain experimental consistency. This is important especially when using previous results to aid in the calculation of a molecular-scale model for the rotaxane shuttle surface reconstruction (the values calculated in *section 5.5.1*, were used to aid in the calculation of the model illustrated in Chapter *6*, Figure *6.3*).

I thereafter achieved simultaneous molecular-scale resolution of 2 rotaxanes - a reference (non-shuttle) and a switchable shuttle, with simultaneous imaging of material dependant – rotaxane molecular type dependant energy dissipation contrast. (this work is described in *section 6.8*). This gives us multiple channels through which to detect rotaxane switching. At the time of submitting this thesis, to the best of my knowledge, there have been no other published molecular resolution studies of rotaxanes in a film. Furthermore due to the challenges of high-resolution imaging very few other ambient molecular-scale studies have been done (for a review of other work in this area see *section 5.2*).

1.8 References

1. Erbil, H. Y.; Demirel, A. L.; Avci, Y.; Mert, O., *Science* **2003** (299) 1377.
2. Snow, E. S.; Perkins, F. K.; Houser, E. J.; Badescu, S. C.; Reinecke, T. L., *Science* **2005** (307) 1942.
3. Hsin, C. L.; He, J. H.; Lee, C. Y.; Wu, W. W.; Yeh, P. H.; Chen, L. J.; Wang, Z. L., *Nano Lett.* **2007** (7) 1799.
4. Kim, S. O.; Solak, H. H.; Stoykovich, M. P.; Ferrier, N. J.; de Pablo, J. J.; Nealey, P. F., *Nature* **2003** (424) 411.
5. Cate, J. H.; Yusupov, M. M.; Yusupova, G. Z.; Earnest, T. N.; Noller, H. F., *Science* **1999** (285) 2095.
6. Boyer, P. D., *Nature* **1999** (402) 247.
7. Green, J. E.; Wook Choi, J.; Boukai, A.; Bunimovich, Y.; Johnston-Halperin, E.; DeIonno, E.; Luo, Y.; Sheriff, B. A.; Xu, K.; Shik Shin, Y.; Tseng, H.-R.; Stoddart, J. F.; Heath, J. R., *Nature* **2007** (445) 414.
8. Service, R. F., *Science* **2003** (302) 556.
9. Credi, A., *Journal of Physics-Condensed Matter* **2006** (18) S1779.
10. Prime, K. L.; Whitesides, G. M., *Science* **1991** (252) 1164.
11. Binnig, G.; Rohrer, H.; Gerber, C.; Weibel, E., *Appl. Phys. Lett.* **1982** (40) 178.
12. Binning, G.; Rohrer, H.; Gerber, C.; Weibel, E., *Phys. Rev. Lett.* **1982** (49) 57.
13. Binnig, G.; Rohrer, H.; Gerber, C.; Weibel, E., *Phys. Rev. Lett.* **1983** (50) 120.
14. Binnig, G.; Quate, C. F.; Gerber, C., *Phys. Rev. Lett.* **1986** (56) 930.
15. Meyer, G.; Amer, N. M., *Appl. Phys. Lett.* **1988** (53) 1045.
16. McClelland, G. M.; Erlandson, R.; Chiang, S., In *Review of Progress in Quantitative Non-Destructive Evaluation*, Thompson, D. O.; Chimenti, D. E., Eds. Plenum: New York, 1987; Vol. 6, p 1307.

17. Binnig, G.; Gerber, C.; Stoll, E.; Albrecht, T. R.; Quate, C. F., *Europhys. Lett.* **1987** (3) 1281.
18. Marti, O.; Elings, V.; Haugan, M.; Bracker, C. E.; Schneir, J.; Drakes, B.; Gould, S. A.; Gurley, J.; Hellemans, L.; Shaw, K.; Weisenhorn, A. L.; Zasadzinski, J.; Hansma, P. K., *Journal of Microscopy-Oxford* **1988** (152) 803.
19. Meyer, G.; Amer, N. M., *Appl. Phys. Lett.* **1990** (56) 2100.
20. Ohnesorge, F.; Binnig, G., *Science* **1993** (260) 1451.
21. Giessibl, F. J., *Science (Washington, D. C., 1883-)* **1995** (267) 68.
22. Sugawara, Y.; Ohta, M.; Ueyama, H.; Morita, S., *Science* **1995** (270) 1646.
23. Uchihashi, T.; Ishida, T.; Komiyama, M.; Ashino, M.; Sugawara, Y.; Mizutani, W.; Yokoyama, K.; Morita, S.; Tokumoto, H.; Ishikawa, M., *Appl. Surf. Sci.* **2000** (157) 244–250.
24. Kobayashi, K.; Yamada, H.; Horiuchi, T.; Matsushige, K., *Appl. Surf. Sci.* **1999** (140) 281.
25. Farrell, A. A.; Kay, E. R.; Bottari, G.; Leigh, D. A.; Jarvis, S. P., *Appl. Surf. Sci.* **2007** (253) 6090.

Chapter 2: Materials

2.1 Introduction

In this chapter I present a detailed background of interlocked molecules, especially rotaxanes, as well as the current status of research in this field. Particular attention is paid to the functionality of these molecules, including the various stimuli that can activate their inherent multistability. I introduce the family of Hydrogen bond assembled rotaxanes that are the focus of the work presented in this thesis, detailing their synthesis, structure and functionality. Previous investigations of interlocked molecules and rotaxanes, and their functionality, at surfaces, are detailed, noting in particular the application of probe microscopy in these studies. This background helps better plan experiments for detection of rotaxane functionality at surfaces and to understand the results presented in chapters 4, 5 and 6.

2.2 The Mechanical Bond - Interlocked molecules

Some of the interesting interlocked architectures, introduced in Chapter 1, include catenanes (consisting of two interlocked macrocycles), rotaxanes (consisting of a macrocycle trapped onto a linear thread part by two large steric blocking groups, and pseudorotaxanes similar to a rotaxane, yet without the need for a steric blocker. A key point is that they are still single molecules, but connected by a physical rather than a chemical bond. Their interlocked nature implies an inherent multistability – that is co-conformational energy minima of perhaps similar, perhaps very distinct values – and this multisability suggests that with a little imagination we can control this bistability by some external means.

Catenanes, from the Latin *catena* meaning chain, are molecules which contain two or more interlocked rings, which are inseperable without the breaking of a covalent bond. Rotaxanes, from the Latin *rota* meaning wheel, and *axis* meaning axle, are comprised of a dumbbell-shaped component, in the form of a rod and two bulky stopper groups, around which there are encircling macrocyclic component(s). The stoppers of the dumbbell prevent the macrocycle(s) 'de-threading' from the rod. When these stopper groups are absent from the ends of the rod, or if the bulky groups are of insufficient size to stop potential 'slipping' or 'de-threading' of the macrocycle, we refer to the

corresponding complexes as *pseudorotaxanes*. The nomenclature employed with these systems involves placing (in square brackets) the number of the components before the name of the compounds or complexes.Thus, a [2]catenane is comprised of two interlocked macrocycles, a [2]rotaxane is comprised of one dumbbell component and one macrocycle, and a pseudo[2]rotaxane is comprised of one macrocycle with a rodlike molecule inserted through its center.

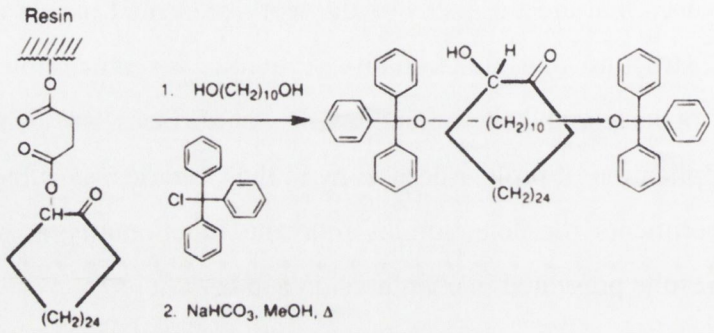


Figure 2.1: Reaction mechanism for the production of the first ever rotaxane molecule. This is adapted from the 1995 review by Amabilino and Stoddart.[1]

The first synthesis of a [2]rotaxane as shown in Figure *2.1* was reported by Harrison and Harrison in 1967.[2] They called it a "hooplane", and it was created by the "statistical" approach, which is the chance formation of the macrocycle while it is being threaded by the dumbbell molecule part. This method has since been superceded by the "directed" or "templated" synthesis of rotaxanes, first demonstrated in the case of a rotaxane by Schill *et al.*[3, 4] The template that brings the rotaxane components together at the time of rotaxane formation can be a covalent bond, a coordinative bind, or a noncovalent bond.

2.3 Multistable Rotaxanes

A rotaxane can be designed in such a way that the thread can have a single or multiple "recognition sites" for the macrocycle. In fact it is often one of these recognition sites that template the rotaxane formation in the first place. A cleverly designed rotaxane can have multiple recognition sites, one of which usually has stronger non-covalent interactions than the other. Such rotaxanes can often be switched between different co-conformational states upon application of an external stimulus. The first such "molecular shuttle" was demonstrated by Bissel, Stoddart *et al.*[5] in 1994. The

rotaxane could be reversibly switched between two states by changing the proton concentration in solution or by electrochemical means, which caused the ring to move controllably between the two stations on the ring. To characterize the macrocycle's movement between stations, ^{1}H NMR and ultra violet/visible spectroscopy were employed. The authors noted that:

"Nature abounds with molecular switching devices which perform a variety of functions, such as the transport of metabolites across cell membranes or the signalling of nerve impulses. These processes are commonly controlled by stimuli such as changes in ion concentrations and electrical potentials."

This illustrates how the skills of molecular engineers are approaching levels where we can imitate Nature's approach of building complex nanostructures through bottom-up self-assembly processes, while also designing the functionality of the structures to suit our own needs.

2.3.1 Mechanism of switching

In the case of all stimuli-rensponsive molecular shuttles, the stimulus does not intrinsically induce motion of the macrocycle, rather it alters the equilibrium between different translational co-conformers, by altering the affinities, of the binding stations to the macrocycle, relative to each other. Either the binding strength of the less populated station is increased, that of the populated station is decreased, or both. The mechanism for the rotaxane shuttling is hence a biased Brownian motion mechanism as illustrated in Figure *2.2*. Once the relative binding affinities of the stations are reversed, the macrocycle will statistically spend more time on the station to which it has greater affinity.

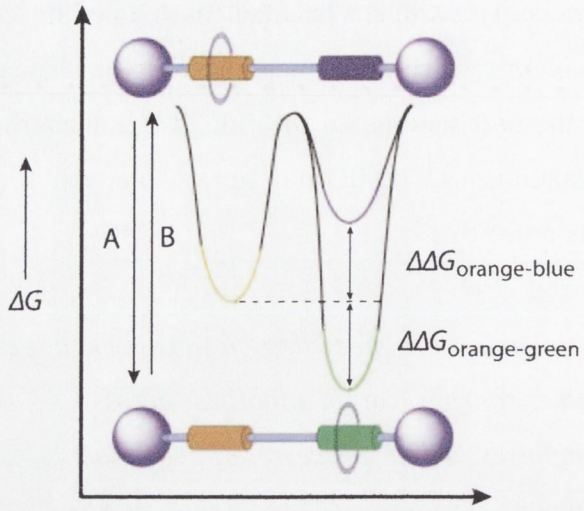


Figure 2.2: Illustration of the Free Energy of the rotaxane molecule as a function of position of the macrocycle along a thread. The sites of minimum energy are the "stations", and when switching of one of these stations occurs, the free energy difference between the stations is changed. This figure is adapted from the 2003 publication by Altieri *et al.*[6]

2.3.2 Switching Stimuli

There are many other switching stimuli that can be used to switch molecular shuttles besides the chemical and electrochemical means mentioned above. Changing the solvent environment can cause the rotaxane to switch between stations.[7] As a good example of how such a rotaxane stimulus-response can be employed, recently a rotaxane-containing-polymer showed switching properties in the presence of different solvent vapours.[8] These rotaxanes can also be switched by heat energy.[9] Perhaps the most fascinating and beautiful method of molecular shuttle switching control is the use of light as a switching stimulus. This is because light as a stimulus allows one to easily imagine applications such as integrated light-activated transistors, recordable films and photo-sensitive coatings. Light-switching of rotaxanes was first reported by Murakami *et al.*[10] A common switching method in rotaxanes is the *E*|*Z* isomerisation of a carbon-carbon or nitrogen-nitrogen double bond in one of the stations,[9, 11] thereby altering the macrocycle-thread binding energy, and hence changing the equilibrium between the stations.

2.3.4 Property Changes

Although the switching of the macrocycle positions in rotaxane molecular-shuttles can now be accomplished in a number of ways,[12, 13] an important consideration is

creating shuttles that undergo a property change based on this motion.[5, 14-17] To date a few systems have been created where a positional change of the nanoscale sub-units has been used to vary physical properties such as fluorescence,[8, 18-20] induced circular dichroism[17] and conductivity.[21] Typically organic molecules show characteristic electrical or optical or chemical properties that are greatly sensitive to the molecular structure and conformation, and this is the fundamental reason why rotaxane molecules have attracted a lot of attention as possible future molecular devices.[27-29] The flow behind the operation of a rotaxane molecular shuttle device is therefore: the station-macrocycle interactions are altered, which results molecular structure change (i.e. shuttling occurs), and as a result of the new structure the electrical/optical/chemical properties can be different.

One of the interesting studies at the heart of this thesis involves a method for the detection of rotaxane switching locally. Now clearly if a rotaxane has two or more distinct co-conformations into which we can transform it, and if the molecules were to be recrystallised, the material properties of the crystals would depend upon the co-conformation of the molecules when the crystal is formed. Therefore it would seem that confirming a property change of the molecules is something that could be done for all switchable rotaxanes, but which is heavily dependent upon whether that property is relevant to the state of the molecules or is a property change that can be detected in a given state. This thesis proposes a method to detect locally (i.e. at the molecular scale) if a molecule has switched based on high-resolution AFM signals from both conservative and dissipative force interactions. The theory behind the method will be discussed in chapter 3, and the development of the technique is detailed in chapters 5 and 6.

2.4 H-Bond Assembled Rotaxanes

In this study we investigated the behaviour at surfaces of a specific family of hydrogen-bond assembled rotaxanes. This is a particular family of rotaxanes where a benzylic amide macrocycle (a strong hydrogen-bond donor through the amide NH groups) is assembled by a templated synthesis around a "recognition site" (a hydrogen-bond accepting group) on the thread as the last step in the rotaxane synthesis.[22] One of the simplest and certainly the most elegant of these rotaxanes is

illustrated in Figure *2.3*. This rotaxane's thread contains a single fumaramide recognition site that templates the assembly benzylic amide macrocycles to form rotaxanes in exceptionally high yields. The fumaramide unit is a very rigid structure; the two hydrogen-bond accepting groups of the recognition site are in a fixed arrangement complementary to the hydrogen-bond donating sites of the macrocycle.

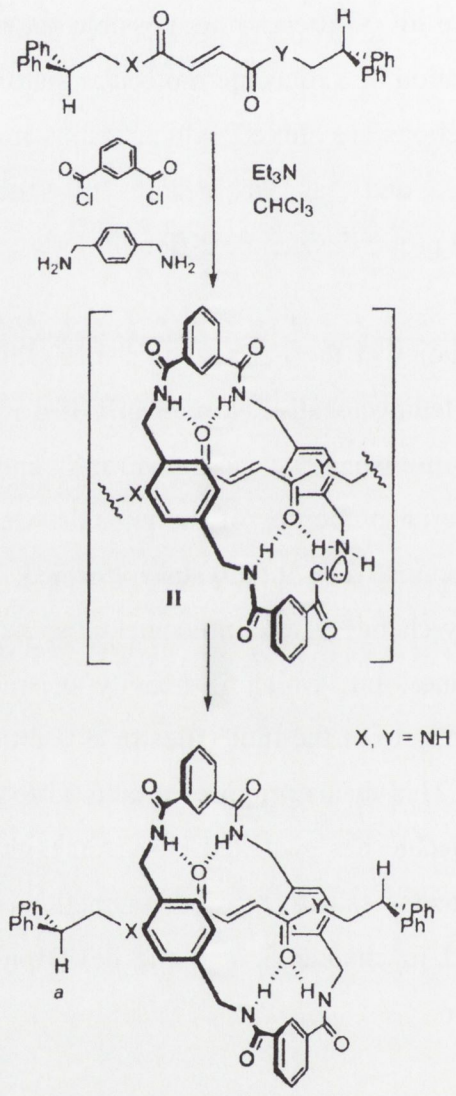


Figure 2.3: Illustration of the synthesis of a simple H-Bond assembled Fumaramide rotaxane with a single station and minimal thread length. The rigid fumaramide structure holds the H-Bond donor groups in a position that templates the formation of macrocycles. This figure is adapted from the 2001 publication by Gatti *et al.*[22]

The preparation of the fumaramide rotaxane is a two-step process, as illustrated in Figure *2.3*.[23, 24] The rigid fumaramide thread is first synthesised from a commercially available amine and bis-acid chloride. In the next step, to form the macrocycle around the thread, four equivalents of xylylene diamine and isophthaloyl dichloride are used.

The resulting rotaxane can easily be isolated without chromatography, by filtration followed by spontaneous crystallization upon addition of water to a dimethylformamide solution of the crude product. This method results in a yield for rotaxane synthesis of 97%, which has not been matched for any other rotaxane synthesis to the best of my knowledge. The fumaramide template is very effective as a rotaxane former because it so perfectly templates the formation of a benzylic amide macrocycle, in a relaxed (i.e. low energy) chair-type conformation. The fact that the fumaramide unit is structurally rigid means that no internal degrees of freedom are lost upon rotaxane formation, and also means that the thread does not fold and hydrogen-bond to itself.

2.4.1 H-Bond Assembled Rotaxanes: Activation with light

Cleverly, the double-bond in the fumaramide group, the feature that gives it structural rigidity and makes it such an effective template for rotaxane synthesis is the very same feature that allows us to geometrically change the thread after rotaxane formation, thus altering the nature of the thread-macrocycle interaction, and therefore altering the strength of this interaction.[25] While the *E*-isomer (fumaramide) (Figure *2.4 (a)*), is a perfect hydrogen-bonding motif, its *Z*-isomer (maleamide) is quite the opposite (Figure *2.4 (b)*), only allowing hydrogen-bonding to one of the two isophthalimide groups of the macrocycle.[26]

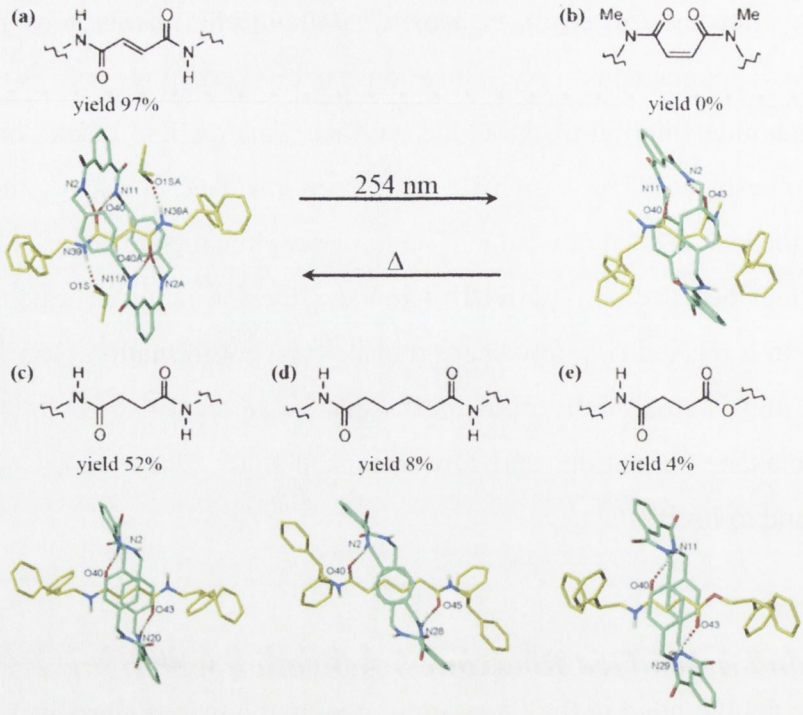


Figure 2.4: Rotaxane crystal structures and the yields for rotaxane formation associated with the H-Bonding template of the station. Structure (b) can only be produced by photoisomerisation of (a). This figure is adapted from the publication by Altieri *et al.*[6]

Irradiation at 254 nm for 30 mins results in a 50% conversion of fumaramide to maleamide rotaxane after the converted solution is passed through a silica pad. The unconverted rotaxanes can be recycled and the process repeated, resulting eventually in >90% conversion. For the macrocycle to pirouette around the thread, a rotation of 180° about the axis plus a formal chair-flip of the macrocycle must occur. The rate for half-circumrotation of the macrocycle around a fumaramide station was measured by ^{1}H NMR experiments to be 1 Hz at 223 K. For the maleamide station (converted station), the macrocycle spinning rate was >1.1 x 10^6 Hz at 223 K. This means that we can achieve a post-assembly photoconversion of a precise hydrogen-bonding, rotaxane-forming template to a motif that does not template the formation of a mechanical bond. The resulting mismatch in recognition sites drastically reduces the energy barrier to macrocycle pirouetting, resulting in a 10^6 x increase in the spinning rate. This is an example of controlled large-amplitude internal molecular motion. The fumaramide template can be recovered by heating at 125° C for 48 hours.

2.4.2 H-Bond Assembled Rotaxanes: Light Activation extended to Shuttles

The photochemical and thermal interconversion of fumaramide units was used as the basis for a series of molecular shuttles, ([2]rotaxanes where there are two or more binding stations on the thread).[6, 20] These stimuli-responsive shuttles allow for the controlled movement of the macrocycle between the stations.

It has been found that the macrocycle binding affinity of a station is related to its ability to template the formation of a rotaxane.[6, 25, 26] When considering the single-binding-site [2]rotaxanes formed using the templates shown in Figure *2.4* (fumaramide, maleamide and succinamide) the rotaxane yields for the typical macrocycle-templating reaction are found to be 97%, 0% and 52% for these three threads. The succinamide (succ-) is an intermediate hydrogen-bonding station, so use of a succ- station as the secondary station on a thread with another fumaramide/maleamide unit allows production of a kind of molecular shuttle, a rotaxane that acts as a 2-pole, stimulus-rensponsive switch.

2.4.3 Mechanism of H-Bond Assembled Rotaxane Molecular Shuttle Switching

The mechanism for the rotaxane shuttling is a biased Brownian motion mechanism as illustrated earlier in Figure *2.2*. When the light-switchable molecular shuttle (Figure *2.5*) is irradiated with UV light at 254 nm the fumaramide station is converted to a maleamide station; switching from maleamide back to fumaramide is achieved by heating or reversible Michael addition. For rotaxane molecular shuttles, the stimulus does not inherently induce motion of the macrocycle, rather it alters the equilibrium between different translational co-conformers, by altering the affinity of the binding stations relative to each other. Either the binding station of the less populated station is increased or that of the populated station is decreased, or both. Once the relative binding affinities of the stations are reversed, the macrocycle will statistically spend more time on the station to which it has greater affinity.

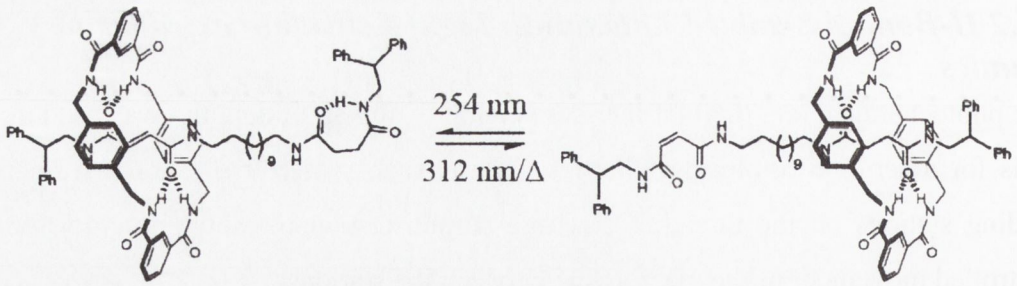


Figure 2.5: Light activated H-Bond assembled molecular shuttle. The rotaxane thread has two stations, (a Fumaramide and a Succinamide group), and a 12 Carbon Spacer. This figure is adapted from the publication by Altieri *et al.*[6]

In a Fumaramide-Succinamide (Fum-Succ) molecular shuttle, the occupancy of the stations as calculated through ^{1}H NMR was >95% on the fumaramide station, while in the Maleamide-Succinamide (Mal-Succ) (UV switched) configuration the occupancy was 15:85 in favour of the non-photoactive succinamide station. This clearly illustrated that the macrocycle's discrimination for different stations is excellent. In the Fum-Succ configuration, the stations offer very similar hydrogen-bonding surfaces, however the ratio is very high in favour of Fumaramide. This, as illustrated in Figure *2.5* is due to the ability of the succ-station to self-bind, when not occupied, as compensation.[6] In the case of the 2-pole fumaramide/maleamide station, the 2-way control over the isomerisation of the station means that the position of the macrocycle on either station of the molecular shuttle can be controlled.

2.4.4 H-Bond Assembled Rotaxane Switching: Other Stimuli

Light is not the only kind of stimulus that can be used to control sub-molecular movement in hydrogen-bonded rotaxanes. Other stimuli include solvent type,[23, 27] and electrochemical stimulus.[28, 29] As an example the molecular shuttle in Figure *2.6* consists of a benzylic amide macrocycle mechanically linked onto a thread molecule containing two potential hydrogen-bond acceptor moieties - a succinamide (*succ*) station and a redox-active 3,6-di-*tert*-butyl-1,8-naphthalimide16 (*ni*) station - separated by a 12-Carbon (C12) aliphatic spacer.

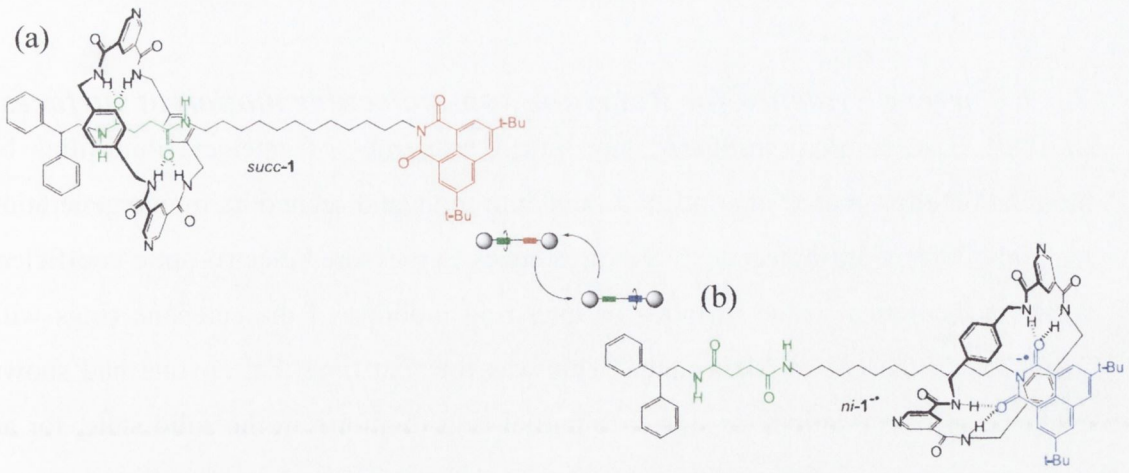


Figure 2.6: Electrochemically activated H-Bond assembled molecular shuttle. The rotaxane thread has two stations, (a Succinamide and a Naphthalimide group), and a 12 Carbon Spacer. This figure is adapted from the publication by Altieri *et al.*[29]

To minimize its free energy, the macrocycle in Figure *2.6(a)* sits over the succinamide station in non-hydrogen-bonding solvents, so that this co-conformation predominates. When a naphthalimide group is reduced to the corresponding radical anion there is a large increase in electron density on the group, and hence a large increase in hydrogen-bond accepting ability.[30-32] In the rotaxane (Figure *2.6(b)*) this change in oxidation state reverses the relative hydrogen-bonding abilities of the two thread stations so that the rotaxane adopts this co-conformation.

2.5 Rotaxanes at Surfaces

Rotaxane molecules also have been studied at surfaces, and the findings have provided valuable insights for their incorporation in "smart" materials, sensors or nanoscale devices. Extending the controllable switching of rotaxanes to solid-state devices however is not a straightforward process, for the simple reason that when confined to a surface, or in a crystal, the number of degrees of freedom (necessary for the activated switching mechanisms found in rotaxanes) is drastically reduced. Through further studies of how these switchable molecules self-assemble, pack, align, and function, we can hope to find conditions where the molecular bistability and not the effect of the surface determine their behaviour, a point well illustrated in the review of the surface-specific work of the Stoddart group on rotaxanes.[33] It will be seen that the work performed in this thesis directly addresses many of the issues important for the functionality of surface-attached rotaxanes.

2.5.1 Current Evidence for Rotaxane sub-molecular motion at surfaces

In 1999 Gase *et al.* investigated the optical properties of catenane thin films by modulation elipsometry and optical second harmonic and second harmonic generation methods.[34] They attributed the large differences in measured electro-optic coefficient with the theoretical value to intra- or inter-ring motions of the catenane rings with frequency in the DC to MHz range. This was the first time that anyone had shown evidence of ring rotation, (in this case partial ring rotation), in the solid state, for an interlocked molecular species.

In 2001, the "Breakthrough of the Year" in Science magazine was an array of devices arranged in crossbar architecture, with each junction consisting of a single layer of catenane molecules sandwiched between SiO_2 and a sputtered Titanium overlayer.[35] The devices showed bistable current/voltage characteristics when a voltage was changed from +2 to -2 Volts. This was attributed to the concerted circumrotation of catenane macrocycles between two co-conformations upon oxidation and reduction of the molecule. Indeed the fact that the response of the devices showed hysteresis lent weight to the explanation that the switching was an activated process, as is the switching of a rotaxane molecular shuttle. Some controversy arose as to the exact mechanism of these devices,[36] commonly known as "Stoddart-Heath" bistable molecular switches,[37, 38] and also known as a two terminal, molecular switch tunnel junctions (MSTJs).[39] This controversy was a result of a question about the sputtered layer of Ti on top of the rotaxane thin film. Many researchers argued that the effect of this layer on the film was unknown and it seemed likely that the deposition process would be damaging to the organic film. Also this layer meant that researchers were "blind" to the switching part of the device. As a result the groups involved in this research have shown a lot of interesting evidence for co-conformational switching in interlocked molecules, and have refined their device recently to a 160-kilobit molecular electronic memory, patterned at the same scale as electronic devices expected to be available by 2020.[40] If it is truly to be proven that these devices act as supposed then the molecules need to be addressed locally, something this thesis explores in Chapters 5 and 6.

In 2004 the Stoddart group showed that a disulfide-tethered bistable rotaxane on a Gold surface at a solution interface functioned properly when this interface was electrochemically activated. The cyclic voltammagrams (CVs) showed details that corresponded to the proposed switching mechanism of the devices.[41] In a subsequent publication it was shown that the macrocycles can actually move relative to the surface.[42] Langmuir-Blodgett (LB) double layers of these switchable rotaxanes were deposited onto a SiO_2 surface at a high surface pressure and investigated with X-ray photoelectron spectroscopy (XPS). XPS was used to track nitrogen (N) which is present in the macrocycle of the rotaxane only, proposed to be the mobile part of the rotaxane. The N 1s photoemission of the thin film was measured and then the film was immersed in an aqueous solution of oxidant to induce switching. The sample was again probed with XPS and the observed differences in the two N 1s spectra were attributed to mechanical switching. In a further experiment involving a condensed rotaxane LB film at the air-water interface the group investigated structural aspects of the mechanical shuttling using X-ray reflectometry (XR) to probe the out-of-plane structure of the oxidized and unoxidized rotaxanes.[43] The XR profiles showed peaks of high electron density which the authors ascribed to the locations of the stations along the molecular thread. The relative densities of the peaks changed significantly upon oxidation of the films, which corresponded to a shift of the electron distribution towards the water surface, in agreement with a translation of the macrocycle towards the water surface.

Most of the above experiments were designed to elucidate the specific behaviour of the rotaxanes inside the MSTJs, however one of the difficulties is obviously that inside the devices the molecular layer is directly covered with a sputtered layer of TiO_2, which is not something that can easily be replicated in surface experiments. Furthermore although motion is often observed in these experiments the motion is never locally measured at the molecular level, and often the molecules are exposed to a solution, the Brownian motion of which could be said to provide the activation necessary to allow the rotaxane switching. While the experiments are very ingenious and do seem to show that the molecules can be switched under certain specific conditions, the extent to which the surface experiments (and in particular the air-water interface experiments) can be applied to the MSTJ devices is somewhat limited because of the experimental differences to the MSTJ architecture.

Katz *et al.* demonstrated the electrochemical switching of a thiol-functionalised rotaxane on a Gold electrode.[44] In this rotaxane it is the macrocycle part of the rotaxane that is oxidized/reduced, which upon reduction loses a local π-donor-acceptor stabilizing interaction with the thread station, the motion of the macrocycle down the molecular thread towards the electrode is stimulated by an electrostatic attraction to the electrode. They characterised the positions of the oxidized and reduced macrocycle by chronoamperic and impedence measurements. They made interesting contact angle measurements of the electrodes, in situ, which showed that this switching of the macrocycle position was a way to reversibly control the hydrophilic and hydrophobic properties of the surface. They subsequently investigated the dynamics of the motion of the macrocycle and found that the rate-constants were related to the viscosity of the solution by adding glycerol to the solution.[45] The rotaxanes in the more viscous environments shuttled more slowly, which was similar to the effects found by Flood *et al.*[46] and Choi *et al.*[47] when they varied the switching environments from solvent to Sol-Gel (although in these studies the molecules were not anchored at one end). The self-assembly of rotaxanes on titanium dioxide nanoparticles has also been studied using NMR and cyclic voltammetry,[48-50] and it was found that the molecules are electronically addressable and switchable in this state.

While Katz *et al.* showed that by switching a surface of rotaxanes electrochemically the contact angle hydrophobicity/hydrophilicity can be controlled, [44] this was taken a step further when Bernà *et al.* used a similar phenomenon to move a solvent droplet up an incline upon rotaxane switching.[51] The rotaxane molecular shuttle from this study has two stations, a fluorinated fumaramide station and a succinamide station and is physically adsorbed on a carboxy-terminated self-assembled monolayer (SAM) on Au(111). Upon irradiation at 254 nm the relative non-covalent macrocycle-station binding strengths were reversed, and through biased Brownian motion the rotaxane components moved relative to each other to expose the fluorinated station. The regions irradiated hence had a higher hydrophobicity. By irradiating locally at one side of the droplet the researchers could cause it to visibly move (mm-scale) because of an induced hydrophobicity gradient and for certain solvents could cause the drop to move uphill after rotaxane switching. In order to expose the fluorinated groups the

molecule would need to undergo co-conformational rearrangement, therefore this is compelling evidence that sub-molecular motion occurs in this case for a surface-attached rotaxane.

One of the most intruiging pieces of evidence of mechanical switching in rotaxanes is from the case of linear artificial molecular muscles.[52-54] These devices consist of a [3]rotaxane (i.e. a rotaxane with two macrocycles), with both of the rings tethered with disulfide to a microcantilever coated with gold on one side, and observations are made in a liquid environment.[55] The rotaxane is constructed in such a way that it is symmetrical (which in fact facilitates the synthesis of this complex molecule) with four binding stations on the thread in total, two towards the ends of the molecular thread, where the macrocycles sit when in the initial configuration, and two more stations towards the centre of the molecule. When oxidant is flowed into the system the rotaxane is switched and both macrocycles move towards the centre of the molecule. This results in a surface stress on the lever and an upwards bending of 35 nm on a 500 *x* 100 *x* 1 (length *x* width *x* thickness) micron silicon microcantilever coated with gold on one side.[55]

One more example of how these nanometre scale movements are translated into macroscopic effects is the case of a rotaxane that is known to switch between stations depending on the environment it is in (i.e. depending on the solvent). The macrocycle contains a fluorescent anthracene station, and in polar solvents the macrocycle is positioned over this station, quenching its fluorescence.[20] These rotaxanes were incorporated into a polymer film, and by lithographically exposing parts of the surface to DMSO vapour the rotaxanes were switched and the surface could be patterned.[8] The fluorescence patterns were visible to the naked eye (at least a photograph was taken) when the sample was irradiated with UV light after patterning.

2.5.2 Observations with probe microscopy

Probe microscopy has been employed for various experiments involving rotaxanes to elucidate their properties at surfaces. There are a number of reasons however, why there has not been much published high-resolution structural data of close-packed rotaxane films at surfaces. The Scanning Tunneling Microscope (STM) can only

operate if the substrate under investigation is conducting or semi-conducting, and can also be applied to extremely thin insulating films on a conductive surface. If the insulating film (in general this will be a film of organic molecules) is not thin enough, ploughing of the STM probe will occur. This happens when the tip must be closer than the thickness of the molecular film to the underlying substrate for a detectable tunnelling current to flow. To date only Samori *et al.* have published high resolution STM images of interlocked molecule (catenane) domains, which were self-assembled on Highly-Oriented Pyrolytic Graphite (HOPG), which because of the flexible nature of the molecules and the very large size of the macrocycles, were able to form very flat-lying structures (i.e. films with a small thickness).[56] To obtain structural information of soft non-conducting molecules would therefore seem to be more the domain of Atomic Force Microscopy (AFM). The expense and difficulty of ultra-high vacuum (UHV) AFM experiments, is usually reserved for a more fundamental type of experiment, and also it is usually undesirable to introduce organic species into a UHV environment. Most rotaxane probe microscopy experiments as a result have been performed in ambient conditions.

Some groups have achieved more success with the imaging and manipulation of isolated rotaxanes at surfaces. Shigekawa *et al.* were able to show that the end of an STM tip can be used to manipulate cyclodextrin beads along the length of a "molecular necklace",[57, 58] Although technically it would be better if the molecules were switched and the beads/macrocycles moved by biased Brownian motion as is the case in solutions, this nevertheless is an important result. This result demonstrated that conditions could be met where the fine balance between molecule-substrate and intra-molecule interactions (i.e. between the sub-molecular components) could be found and interrupted. Cacialli *et al.* imaged thin films of these same molecules with Amplitude Modulation AFM (AM-AFM),[59] as did Kumaki *et al.*,[60] although these molecules did not show any of the random movements observed in their other studies of polymer chains.[61] This is the opposite to the case experienced by Biscarini *et al.* who proposed that the Catenane molecules were too mobile for STM imaging.[62] This illustrates the importance of balancing the surface forces experienced by the rotaxanes.

AFM has also been used as a tool to establish the general morphology of films, e.g. establishing if a film is smooth or whether or not the molecules arrange into

domains[33, 63] and the examination of the spatial correlation of rotaxane thin films.[64, 65] In the literature of the field there is a distinct lack of high resolution structural information however, or information about the conformation of the rotaxanes, whether chemisorbed or physisorbed on the surface. This only serves to highlight the difficulty of such experiments in ambient conditions, where water layers and molecular contaminants are usually present. It would appear that some groups have almost achieved molecular resolution in e.g. SAMS with thiol-functionalised rotaxanes embedded,[66] unfortunately the features of the molecules tend to be indistinct. Nevertheless the general morphology of rotaxane and catenane thin films can be used to demonstrate that switching behaviour at surfaces can occur. A good example is the demonstration of conformational self-recognition of catenane molecules.[67] In this case it was found that molecules are desorbed from a mica surface, and resorb to form a film with different morphology through interaction with other molecules in a solution phase, if the molecules in solution have a different conformation to the surface-bound molecules. The stable energy conformations of the molecules in solution were switched by changing the solvent.

Another way of applying the AFM to rotaxane thin films is in their manipulation by the AFM probe for information storage. Some groups have used electrochemical methods to apparently switch rotaxanes beneath the tip, and to produce patterns.[68] These images do not show distinct order in the sample or molecular-scale characteristics. Moulin *et al.* have proposed a method for extremely dense information storage through the reconfiguration of large amounts of rotaxanes into patterns with a characteristic length-scale when manipulated through contact mode AFM scanning.[65] This self-organization at the meso-scale occurs via the low energy barrier to intra-molecular rearrangement that exists because of the mechanical bond.[69] It would seem to me that a possible explanation for this reconfiguration is the recrystallisation of the molecules in a tip-sample water meniscus bridge until a critical mass of rotaxanes is achieved and the molecules are no longer pulled along with the meniscus. In ambient conditions with no humidity control thin layers of water will be present on both the tip and sample, and when the tip is brought in close enough proximity to the sample a bridging effect can occur.

AFM was also used to provide a comparison of the packing interaction in a crystal of H-Bond assembled rotaxanes with the packing interaction in a crystal of the thread molecule alone.[70] The scratching force required to make a comparable indent in the crystal was measured. This indentation happens when the shearing force exerted by the tip exceeds the adhesion forces within the crystal. The minimum load force required for scratching a comparable amount of material from a crystal is qualitatively related to the adhesion force, which depends on the packing interactions. This experiment illustrated that the rotaxanes are more mobile in the solid state (in bulk crystal), than the thread molecules alone in crystalline state.

The thesis of Alberto Credi showed an example of attempting to switch a rotaxane monolayer with an electric field by examining the effect on the rotaxane monolayer AFM image.[71] Unfortunately they were unsuccessful, which once again illustrates the difficulty of such experiments and our lack of knowledge about the possibility of sub-molecular motion at surfaces. Interestingly there have been many examples in the literature of the switching of the properties of organic monolayers by stimuli such as light, and the detection of the switching by probe microscopy, however none of these molecules were rotaxanes that switched macrocycle positions.[72-78]

2.6 H-Bond Assembled Rotaxanes at surfaces

To exploit fumaramide rotaxanes as molecular-scale devices it is first necessary to build a foundation of knowledge about their integration with solid surfaces as thin films. To date most of the work with fumaramide rotaxanes has focussed mainly on their interaction with two types of surface, the Au(111) surface and the HOPG (1111) surface.

The adsorption of H-Bond assembled rotaxanes directly on the Au(111) surface has been studied, as well as the adsorption of the component parts (the rotaxane thread and macrocycle). To a lesser extent rotaxane adsorption on a Silver surface has been explored. A clean, highly crystalline Au(111) surface is relatively easy to produce by Gold evaporation onto Mica. The assembly of thiol-functionalised rotaxanes on Au(111) has also been investigated, as well as rotaxanes physisorbed on carboxy-terminated self-assembled monolayers (SAMs) on Gold. The other main set of

experiments has involved the ideal HOPG(0001) surface, commonly used by probe microscopists because of its large and extremely flat terraces and small unit cell. To date the rotaxane-related studies involving HOPG have investigated the morphologies of thick multilayer films using probe microscopy. Special attention has been focussed on the self-assembly of clusters of molecules at multiple length-scales, along with the influence of perturbation by the scanning tip on the films.

In this thesis, the focus is to investigate molecularly-thin films *locally* (i.e. at the molecular-scale) with advanced Atomic Force Microscopy techniques to gain insight into how we can control, by our surface preparation techniques, the interactions that are important in retaining molecular functionality in thin films at a solid surface. Since we will be concentrating on a specific family of rotaxanes and their behaviour at surfaces, it is useful to review the previous studies on these molecules, because they can help us to understand our present work and corroborate our results. An important example of this is the work of Biscarini *et al.*[70] By a statistical treatment of rotaxane crystal structures they were able to predict which of a series of rotaxanes including many fumaramide rotaxanes would most likely show motion in the solid state. The criteria important to this motion are low crystal packing density and weak macrocycle interactions between neighbouring molecules. They demonstrated that these properties can coexist in certain rotaxanes, especially the fumaramide rotaxanes when recrystallised from hydrogen-bonding solvents. This is something that is examined in this thesis (Chapter *4*) and it will be shown that the volume of the film is also greater for rotaxanes deposited at surfaces from hydrogen-bonding solvents than non-hydrogen-bonding solvents.

2.6.1 H-Bond-Assembled Rotaxanes on the Au(111) Surface

Studies carried out, using high-resolution electron energy-loss spectroscopy (HREELS) and X-ray photoelectron Spectroscopy (XPS), on thiol-functionalised catenane and rotaxane thin films adsorbed from solution on to Au(111), revealed no long-range order in the resulting films.[79] When the films were annealed larger domains were observed and it was found that there was an unwanted extra chemisorption of carbonyl/amide groups on the gold surface in the case of both the rotaxane and catenane. The films of the catenane were of better quality in terms of

uniformity. It seems that research of this method of surface attachment was abandoned in favour of investigating the individual components' interactions with the gold surface. This is an example of the importance of having the surface attachment group as part of the macrocycle as opposed to the thread, as mentioned later in this thesis (see section *4.1.1* for further discussion). For this rotaxane the thiol-functionality was part of the thread,[79] and since the molecules did not behave in a way that would allow a large number of internal degrees of freedom (there was extra amide chemisorption) the results were probably not considered promising in terms of device fabrication. This meant going back and redesigning the molecules, which first meant the difficult and complicated redesign of a thread with a sulfide functional group. If the surface attachment were through the macrocycle rather than through the thread, redesign of the thread would be much less complicated; it was decided to be impractical to produce more molecules in such a series. Studies in this area turned to simple rotaxanes and their components adsorbed on Gold directly and adsorbed to SAMs.[79-81]

The benzylic amide macrocycle was studied on Au(111) as a function of coverage as deposited by vacuum sublimitation, using HREELS,[80] and XPS.[81] These studies revealed that the component has a flat-lying molecular orientation, accompanied by chemisorption by the amide functional groups and also via the carbonyl functionality in the initial stages of film formation. The structures observed involved considerable distortion of the adsorbed macrocycle from its crystal structure. As further layers were deposited the films showed a less selective geometry, where non-parallel orientations began to prevail with a decrease in film order. These studies also stressed that there are strong macrocycle-macrocycle interactions in these films.

The vapour deposition on Ag(111) and Au(111) of thin films of the simple fumaramide rotaxane (Section *2.4*) were studied by XPS, HREELS and molecular dynamics simulations as a next step in these series of experiments.[82] It was found that the molecule adsorbs intact and that chemisorption at low coverage is driven by interactions between the three amide functions of fumaramide rotaxane and the surfaces. The rotaxane prefers to orient the macrocycle part of the molecule as close to the surface as possible, leading to a "collapsed x-like" structure with two phenyl

rings parallel to the substrate and three amide groups within bonding distance of the substrate.

This was followed by a coverage-dependant study of the fumaramide rotaxane and its component parts' adsorption on Au(111) by HREELS.[83] Once more chemisorption of the macrocycle and rotaxane was evident from the presence of Au-O stretching vibrations. The phenyl rings orient predominantly parallel to the Au(111) surface at up to 0.5-ML coverage for the rotaxane and 1-ML coverage for the macrocycle. The thread showed no evidence of chemisorption, and the absence of a preferential orientation, which according to simulations was due to the substantially higher mobility of the thread. This is indeed a promising result in terms of the mobility of the thread at a Gold surface, with no evidence of its adsorption when in a film as part of the rotaxane.

2.6.2 H-Bond-Assembled Rotaxanes on the HOPG surface

One of the earliest probe microscopy experiments on interlocked molecules was carried out in 1999 on H-bond assembled catenanes on HOPG.[62] Attempts were made to image the molecules with STM in ambient conditions as deposited at low surface concentration from methanol solution. Only occasionally could the molecules be observed, perhaps because they were mobile on HOPG as the authors suggest, or perhaps because of high forces between the tip and sample that displaced the molecules instead of allowing the tip to pass over the molecules. Apparently some sub-molecular features were observed on rare occasions though, that suggested that the adsorption of the catenane is driven by electrostatic attraction of carbonyl groups and HOPG.

Recently work has been done to examine the evolution of thin films (many multilayers thick however) of simple fumaramide rotaxanes on HOPG during the annealing process,[65] using AFM, bright field transmission electron microscopy, selected area electron diffraction and molecular mechanics simulations. These layers are a lot thicker than the molecularly thin films that are dealt with in this thesis. At first the rotaxane film is spin coated to form a uniform film a few multilyers thick. As this film is annealed it dewets, forming nanosized droplets. These droplets coalesce by

ripening to form patterns with distance correlation. These larger droplets coalesce and form crystallites and eventually larger crystals as they incorporate surrounding droplets. The nanostructures are metastable because the inherent degrees of freedom permitted in the rotaxane architecture can favour the re-organization and nucleation of the film. The large-scale reorganisation can occur because concerted, small-amplitude, internal motions can occur without disruption of packing, and intermolecular contacts allow low energy trajectories for reorganization. This drastic reorganisation of the thin films certainly suggests that the molecules retain some of their flexibility at this surface although the molecules are imparted a lot of extra energy during the annealing process. However, the occurrence of "concerted movements" suggests inter-molecular hydrogen bonding, something which one would ideally hope to avoid in a molecular-scale device. This inter-molecular hydrogen bonding that can occur is something that I am able to address through my studies (see sections *4.5* & *4.6*). The researchers were unable to perform high-resolution STM measurements which meant that they could not provide conclusive evidence of the arrangement of the rotaxane molecules relative to the graphite lattice. This is another important area that my studies were able to address by adopting a highly-sensitive dynamic AFM technique to locally investigate molecularly thin films (see Chapters *5* & *6*).

2.7 Conclusions

By examining the field of mechanical molecular switches at surfaces in depth, it is clear that there are immense possibilities for exploitation of rotaxanes as devices. Already fascinating applications are emerging, such as the recent work of Green, Stoddart, Heath *et al.*, who demonstrated super-high-density electronic memory based on interlocked molecular functionality.[40] There is however much that needs to be understood about the basic principles of these systems, especially the burning question: Can these molecules actually do what we think they are doing at surfaces – are they operating as switching devices? In this thesis I will show that probe microscopy has the potential to shed some light on this area, in particular through local, molecular-scale investigations of the structural and dynamic properties of rotaxane thin films. In chapters 4, 5 & 6 of this thesis I have addressed a number of the issues raised in this chapter. Amongst other things, I have helped determine the best film growth conditions to minimize the intermolecular H-bonding in H-bond

assembled rotaxanes and created film structures where the rotaxane is surface-attached via the macrocycle. I have also established the surface reconstruction of the molecules locally by AFM, and by local energy transfer mapping, come closer to a way of locally detecting the co-conformational changes in rotaxanes at surfaces. I have established the effects of long thread lengths on molecular packing and measured the nanostructures of thin films of various molecular shuttles. I have also self-assembled mixed monolayers of rotaxanes with distinct and identifiable domains having different functionalities; so that in this way I can locally compare structural differences and measure tip-sample energy-transfer differences (dissipation – an AFM measurement discussed thoroughly in the next chapter) as a function of rotaxane type, conformation, and functionality.

2.8 References

1. Amabilino, D. B.; Stoddart, J. F., *Chem. Rev.* **1995** (95) 2725.
2. Harrison, I. T.; Harrison, S., *J. Am. Chem. Soc.* **1967** (89) 5723.
3. Schill, G.; Henschel, R., *Annalen Der Chemie-Justus Liebig* **1970** (731) 113.
4. Schill, G.; Zollenko.H, *Annalen Der Chemie-Justus Liebig* **1969** (721) 53.
5. Bissell, R. A.; Cordova, E.; Kaifer, A. E.; Stoddart, J. F., *Nature* **1994** (369) 133.
6. Altieri, A.; Bottari, G.; Dehez, F.; Leigh, D. A.; Wong, J. K. Y.; Zerbetto, F., *Angewandte Chemie-International Edition* **2003** (42) 2296.
7. Da Ros, T.; Guldi, D. M.; Morales, A. F.; Leigh, D. A.; Prato, M.; Turco, R., *Org. Lett.* **2003** (5) 689.
8. Leigh, D. A.; Morales, M. A. F.; Perez, E. M.; Wong, J. K. Y.; Saiz, C. G.; Slawin, A. M. Z.; Carmichael, A. J.; Haddleton, D. M.; Brouwer, A. M.; Buma, W. J.; Wurpel, G. W. H.; Leon, S.; Zerbetto, F., *Angewandte Chemie-International Edition* **2005** (44) 3062.
9. Bottari, G.; Dehez, F.; Leigh, D. A.; Nash, P. J.; Perez, E. M.; Wong, J. K. Y.; Zerbetto, F., *Angewandte Chemie-International Edition* **2003** (42) 5886.
10. Murakami, H.; Kawabuchi, A.; Kotoo, K.; Kunitake, M.; Nakashima, N., *J. Am. Chem. Soc.* **1997** (119) 7605.
11. Stanier, C. A.; Alderman, S. J.; Claridge, T. D. W.; Anderson, H. L., *Angewandte Chemie International Edition* **2002** (41) 1769.
12. Sauvage, J. P.; DietrichBuchecker, C.; Eds., *Molecular Catenanes, Rotaxanes and Knots*. Wiley-VCH: Weinheim, 1999.
13. Balzani, V.; Credi, A.; Raymo, F. M.; Stoddart, J. F., *Angewandte Chemie-International Edition* **2000** (39) 3349.
14. Muraoka, T.; Kinbara, K.; Kobayashi, Y.; Aida, T., *J. Am. Chem. Soc.* **2003** (125) 5612.
15. Jimenez-Molero, M. C.; Dietrich-Buchecker, C.; Sauvage, J. P., *Chemistry-a European Journal* **2002** (8) 1456.
16. Collier, C. P.; Wong, E. W.; Belohradsky, M.; Raymo, F. M.; Stoddart, J. F.; Kuekes, P. J.; Williams, R. S.; Heath, J. R., *Science* **1999** (285) 391.

17. Bottari, G.; Leigh, D. A.; Perez, E. M., *J. Am. Chem. Soc.* **2003** (125) 13360.
18. Qu, D. H.; Wang, G. C.; Ren, J.; Tian, H., *Org. Lett.* **2004** (6) 2085.
19. Wang, Q. C.; Qu, D. H.; Ren, J.; Chen, K. C.; Tian, H., *Angewandte Chemie-International Edition* **2004** (43) 2661.
20. Perez, E. M.; Dryden, D. T. F.; Leigh, D. A.; Teobaldi, G.; Zerbetto, F., *J. Am. Chem. Soc.* **2004** (126) 12210.
21. Flood, A. H.; Ramirez, R. J. A.; Deng, W. Q.; Muller, R. P.; Goddard, W. A.; Stoddart, J. F., *Aust. J. Chem.* **2004** (57) 301.
22. Gatti, F. G.; Leigh, D. A.; Nepogodiev, S. A.; Slawin, A. M. Z.; Teat, S. J.; Wong, J. K. Y., *J. Am. Chem. Soc.* **2001** (123) 5983.
23. Lane, A. S.; Leigh, D. A.; Murphy, A., *J. Am. Chem. Soc.* **1997** (119) 11092.
24. Leigh, D. A.; Murphy, A.; Smart, J. P.; Slawin, A. M. Z., *Angewandte Chemie-International Edition in English* **1997** (36) 728.
25. Gatti, F. G.; Lent, S.; Wong, J. K. Y.; Bottari, G.; Altieri, A.; Morales, M. A. F.; Teat, S. J.; Frochot, C.; Leigh, D. A.; Brouwer, A. M.; Zerbetto, F., *Proc. Natl. Acad. Sci. U. S. A.* **2003** (100) 10.
26. Brancato, G.; Coutrot, F.; Leigh, D. A.; Murphy, A.; Wong, J. K. Y.; Zerbetto, F., *Proc. Natl. Acad. Sci. U. S. A.* **2002** (99) 4967.
27. Clegg, W.; Gimenez-Saiz, C.; Leigh, D. A.; Murphy, A.; Slawin, A. M. Z.; Teat, S. J., *J. Am. Chem. Soc.* **1999** (121) 4124.
28. Brouwer, A. M.; Frochot, C.; Gatti, F. G.; Leigh, D. A.; Mottier, L.; Paolucci, F.; Roffia, S.; Wurpel, G. W. H., *Science (Washington, D. C., 1883-)* **2001** (291) 2124.
29. Altieri, A.; Gatti, F. G.; Kay, E. R.; Leigh, D. A.; Martel, D.; Paolucci, F.; Slawin, A. M. Z.; Wong, J. K. Y., *J. Am. Chem. Soc.* **2003** (125) 8644.
30. Ge, Y.; Lilienthal, R. R.; Smith, D. K., *J. Am. Chem. Soc.* **1996** (118) 3976.
31. Deans, R.; Niemz, A.; Breinlinger, E. C.; Rotello, V. M., *J. Am. Chem. Soc.* **1997** (119) 10863.
32. Niemz, A.; Rotello, V. M., *Acc. Chem. Res.* **1999** (32) 44.
33. Braunschweig, A. B.; Northrop, B. H.; Stoddart, J. F., *J. Mater. Chem.* **2006** (16) 32.
34. Gase, T.; Grando, D.; Chollet, P. A.; Kajzar, F.; Murphy, A.; Leigh, D. A., *Advanced Materials* **1999** (11) 1303.
35. Service, R. F., *Science* **2001** (294) 2442.
36. Service, R. F., *Science* **2003** (302) 556.
37. Jang, Y. H.; Hwang, S. G.; Kim, Y. H.; Jang, S. S.; Goddard, W. A., *J. Am. Chem. Soc.* **2004** (126) 12636.
38. Deng, W. Q.; Muller, R. P.; Goddard, W. A., *J. Am. Chem. Soc.* **2004** (126) 13562.
39. Collier, C. P.; Jeppesen, J. O.; Luo, Y.; Perkins, J.; Wong, E. W.; Heath, J. R.; Stoddart, J. F., *J. Am. Chem. Soc.* **2001** (123) 12632.
40. Green, J. E.; Wook Choi, J.; Boukai, A.; Bunimovich, Y.; Johnston-Halperin, E.; DeIonno, E.; Luo, Y.; Sheriff, B. A.; Xu, K.; Shik Shin, Y.; Tseng, H.-R.; Stoddart, J. F.; Heath, J. R., *Nature* **2007** (445) 414.
41. Tseng, H. R.; Wu, D. M.; Fang, N. X. L.; Zhang, X.; Stoddart, J. F., *ChemPhysChem* **2004** (5) 111.
42. Huang, T. J.; Tseng, H. R.; Sha, L.; Lu, W. X.; Brough, B.; Flood, A. H.; Yu, B. D.; Celestre, P. C.; Chang, J. P.; Stoddart, J. F.; Ho, C. M., *Nano Lett.* **2004** (4) 2065.

43. Norgaard, K.; Laursen, B. W.; Nygaard, S.; Kjaer, K.; Tseng, H. R.; Flood, A. H.; Stoddart, J. F.; Bjornholm, T., *Angewandte Chemie-International Edition* **2005** (44) 7035.
44. Katz, E.; Lioubashevsky, O.; Willner, I., *J. Am. Chem. Soc.* **2004** (126) 15520.
45. Katz, E.; Baron, R.; Willner, I.; Richke, N.; Levine, R. D., *ChemPhysChem* **2005** (6) 2179.
46. Flood, A. H.; Peters, A. J.; Vignon, S. A.; Steuerman, D. W.; Tseng, H. R.; Kang, S.; Heath, J. R.; Stoddart, J. F., *Chemistry-a European Journal* **2004** (10) 6558.
47. Choi, J. W.; Flood, A. H.; Steuerman, D. W.; Nygaard, S.; Braunschweig, A. B.; Moonen, N. N. P.; Laursen, B. W.; Luo, Y.; DeIonno, E.; Peters, A. J.; Jeppesen, J. O.; Xu, K.; Stoddart, J. F.; Heath, J. R., *Chemistry-a European Journal* **2006** (12) 261.
48. Long, B.; Nikitin, K.; Fitzmaurice, D., *J. Am. Chem. Soc.* **2003** (125) 15490.
49. Nikitin, K.; Fitzmaurice, D., *J. Am. Chem. Soc.* **2005** (127) 8067.
50. Nikitin, K.; Long, B.; Fitzmaurice, D., *Chemical Communications* **2003** 282.
51. Berna, J.; Leigh, D. A.; Lubomska, M.; Mendoza, S. M.; Perez, E. M.; Rudolf, P.; Teobaldi, G.; Zerbetto, F., *Nat. Mater.* **2005** (4) 704.
52. Otero, T. F.; Grande, H.; Rodríguez, J., *J. Phys. Org. Chem.* **1996** (9) 381.
53. Jimenez, M. C.; Dietrich-Buchecker, C.; Sauvage, J. P., *Angewandte Chemie-International Edition* **2000** (39) 3284.
54. Collin, J. P.; Dietrich-Buchecker, C.; Gavina, P.; Jimenez-Molero, M. C.; Sauvage, J. P., *Acc. Chem. Res.* **2001** (34) 477.
55. Huang, T. J.; Brough, B.; Ho, C. M.; Liu, Y.; Flood, A. H.; Bonvallet, P. A.; Tseng, H. R.; Stoddart, J. F.; Baller, M.; Magonov, S., *Appl. Phys. Lett.* **2004** (85) 5391.
56. Samori, P.; Jackel, F.; Unsal, O.; Godt, A.; Rabe, J. P., *ChemPhysChem* **2001** (2) 461.
57. Miyake, K.; Yasuda, S.; Harada, A.; Sumaoka, J.; Komiyama, M.; Shigekawa, H., *J. Am. Chem. Soc.* **2003** (125) 5080.
58. Shigekawa, H.; Miyake, K.; Sumaoka, J.; Harada, A.; Komiyama, M., *J. Am. Chem. Soc.* **2000** (122) 5411.
59. Cacialli, F.; Wilson, J. S.; Michels, J. J.; Daniel, C.; Silva, C.; Friend, R. H.; Severin, N.; Samori, P.; Rabe, J. P.; O'Connell, M. J.; Taylor, P. N.; Anderson, H. L., *Nat. Mater.* **2002** (1) 160.
60. Kumaki, J.; Yashima, E.; Bollot, G.; Mareda, J.; Litvinchuk, S.; Matile, S., *Angewandte Chemie-International Edition* **2005** (44) 6154.
61. Kumaki, J.; Kawauchi, T.; Yashima, E., *Macromolecules* **2006** (39) 1209.
62. Biscarini, F.; Gebauer, W.; Di Domenico, D.; Zamboni, R.; Pascual, J. I.; Leigh, D. A.; Murphy, A.; Tetard, D., *Synth. Met.* **1999** (102) 1466.
63. Raehm, L.; Kern, J. M.; Sauvage, J. P.; Hamann, C.; Palacin, S.; Bourgoin, J. P., *Chemistry-a European Journal* **2002** (8) 2153.
64. Cavallini, M.; Biscarini, F.; Massi, M.; Farran-Morales, A.; Leigh, D. A.; Zerbetto, F., *Nano Lett.* **2002** (2) 635.
65. Moulin, J. F.; Kengne, J. C.; Kshirsagar, R.; Cavallini, M.; Biscarini, F.; Leon, S.; Zerbetto, F.; Bottari, G.; Leigh, D. A., *J. Am. Chem. Soc.* **2006** (128) 526.
66. Azehara, H.; Mizutani, W.; Suzuki, Y.; Ishida, T.; Nagawa, Y.; Tokumoto, H.; Hiratani, K., *Langmuir* **2003** (19) 2115.
67. Cavallini, M.; Lazzaroni, R.; Zamboni, R.; Biscarini, F.; Timpel, D.; Zerbetto, F.; Clarkson, G. J.; Leigh, D. A., *J. Phys. Chem. B* **2001** (105) 10826.
68. Feng, M.; Guo, X. F.; Lin, X.; He, X. B.; Ji, W.; Du, S. X.; Zhang, D. Q.; Zhu, D. B.; Gao, H. J., *J. Am. Chem. Soc.* **2005** (127) 15338.

69. Cavallini, M.; Biscarini, F.; Leon, S.; Zerbetto, F.; Bottari, G.; Leigh, D. A., *Science* **2003** (299) 531.
70. Biscarini, F.; Cavallini, M.; Leigh, D. A.; Leon, S.; Teat, S. J.; Wong, J. K. Y.; Zerbetto, F., *J. Am. Chem. Soc.* **2002** (124) 225.
71. Credi, A. Molecular-Level Machines and Logic Gates. University of Bologna, 1999.
72. Kobayashi, K.; Yamada, H.; Umeda, K.; T.Horiuchi; S.Watanabe; Fujii, T.; Hotta, S.; Matsushige, K., *Appl. Phys. A* **2001** (72) S97–S100.
73. Yamada, H.; Fukuma, T.; Umeda, K.; Kobayashi, K.; Matsushige, K., *Appl. Surf. Sci.* **2002** (188) 391.
74. Tamada, K.; Akiyama, H.; Wei, T. X.; Kim, S. A., *Langmuir* **2003** (19) 2306.
75. Wang, Z. X.; Cook, M. J.; Nygard, A. M.; Russell, D. A., *Langmuir* **2003** (19) 3779.
76. Wang, Z. X.; Nygard, A. M.; Cook, M. J.; Russell, D. A., *Langmuir* **2004** (20) 5850.
77. Critchley, K.; Jeyadevan, J. P.; Fukushima, H.; Ishida, M.; Shimoda, T.; Bushby, R. J.; Evans, S. D., *Langmuir* **2005** (21) 4554.
78. Miura, A.; De Feyter, S.; Abdel-Mottaleb, M. M. S.; Gesquiere, A.; Grim, P. C. M.; Moessner, G.; Sieffert, M.; Klapper, M.; Mullen, K.; De Schryver, F. C., *Langmuir* **2003** (19) 6474.
79. De Nadai, C.; Whelan, C. M.; Perollier, C.; Clarkson, G.; Leigh, D. A.; Caudano, R.; Rudolf, P., *Surf. Sci.* **2000** (454) 112.
80. Whelan, C. M.; Cecchet, F.; Clarkson, G. J.; Leigh, D. A.; Caudano, R.; Rudolf, P., *Surf. Sci.* **2001** (474) 71.
81. Whelan, C. M.; Cecchet, F.; Baxter, R.; Zerbetto, F.; Clarkson, G. J.; Leigh, D. A.; Rudolf, P., *J. Phys. Chem. B* **2002** (106) 8739.
82. Mendoza, S. M.; Whelan, C. M.; Jalkanen, J. P.; Zerbetto, F.; Gatti, F. G.; Kay, E. R.; Leigh, D. A.; Lubomska, M.; Rudolf, P., *J. Chem. Phys.* **2005** (123).
83. Whelan, C. M.; Gatti, F.; Leigh, D. A.; Rapino, S.; Zerbetto, F.; Rudolf, P., *J. Phys. Chem. B* **2006** (110) 17076.

Chapter 3: Experimental Techniques

3.1 Introduction

Local, nanoscale investigations of the interlocked rotaxane architectures described in chapter 2 are required to assess if these molecules can 'function' at surfaces. By 'function' I mean the rotaxane is 'switched', altering the relative binding strengths of the thread stations, and then the macrocycle should move to the more stable newly-lower-energy site. Electrical, optical or chemical properties of organic molecules can be affected by conformational changes, and most attempts to verify the functionality of rotaxanes at surfaces have relied upon measuring the averaged affect of these changes at surfaces (see section *2.5* for a thorough discussion).

AFM can allow us to locally detect conformational changes in the rotaxanes through two signals. The first signal is straightforward – molecular-scale constant-force contour images. By measuring directly, with sub-molecular resolution, the local structural information we can hope to detect structural changes. The other signal – dissipation – is essentially used as a measure of the molecular conformational freedom, and can also be measured at the molecular scale (see results presented in chapters 5 and 6, sections *5.10* and *6.8-9*). When a probe is oscillating vertically in close proximity to a sample (i.e. within the van der Waals regime), a certain amount of the vibrational energy is transferred to the sample. This energy transfer is dependent upon the local structural/conformational properties of the sample, as will be discussed in this chapter (section *3.3.3*). Thereby one can hope to detect directly the rotaxane functionality by one of these two signals. The signals are discussed thoroughly in this chapter, and the development of this technique is illustrated by experimental results throughout chapters 5 and 6.

For the case of a rotaxane film that would be part of an addressable device, the measurement of the local molecular-scale order is of course integrated into the investigations described above. AFM is also applicable at the meso-scale in this sense for accurate determination of the length-scales to which the local order extends, i.e. the effect of reconstruction lattice mismatch, the resulting domain sizes and the morphologies of the films. One of the studies in this thesis uses information about the film structure to determine the effect of the solvent used during deposition. The film

structures are found to reflect the solid-state structures measured by x-ray diffraction when the molecules are crystallised from various solvents. This work will be detailed in chapter 4.

In this chapter I discuss the experimental methods for producing well ordered rotaxane films, and details of the Atomic Force Microscopy technique, and the adaptations used in this work, by which potential rotaxane functionality may be locally clarified at the nanoscale.

3.2 Sample Preparation

The films in this study are drop-cast onto a clean HOPG surface. In the process of 'drop-casting', a solution of the molecules in question is prepared in a volatile solvent. A drop of this solution is then added to the substrate and the solvent allowed to evaporate, leaving only the molecules at the surface in a thin film. The thickness of the film depends on the volume and concentration of the drop.

3.2.1 Choice of deposition technique: drop casting

The drop-casting method is chosen because it is a straight-forward, reproducible technique, which can be repeated easily for a high throughput of samples. In chapter 4 I will describe experiments that illustrate changes in rotaxane film structure based upon the type of solvent used during film preparation. This type of comparison required that many films be made under various conditions. I required an efficient process that was not overly expensive or time-consuming, since many samples would be made. I decided to avoid vacuum deposition techniques such as molecular beam epitaxy (or vacuum sublimation) for these reasons. I instead chose this liquid-solid interface deposition method known as drop-casting.

3.2.2 Choice of substrate: HOPG

HOPG is the substrate of choice because it can be rapidly and reproducibly cleaved to give a clean and flat surface.[1] Cleaving like this has long been used because perfect lattices spanning hundreds of nanometres can be obtained.[2] The graphite structure is illustrated in Figure *3.1*. For the purposes of AFM experiments HOPG is normally cut

into blocks of approximately $10\ mm \times 10\ mm \times 1\ mm$, with the $10\ mm \times 10\ mm$ surface being the (0001) plane. The HOPG is easily cleaved on the (0001) plane because of the relatively weak π-π interactions between these crystal planes (the carbon atoms are sp2 hybridized). Simply cleaving the substrate with scotch tape or some other adhesive tape I can expose a clean substrate with large flat terraces.

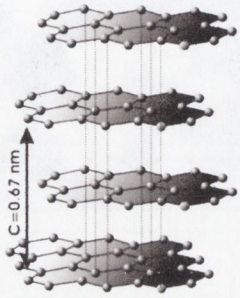


Figure 3.1: Illustration of the HOPG lattice structure. This structure is stacked sheets of graphene, and is easily cleavable because of the relatively weak bonding between the stacked sheets. Image Source: Wikipedia (http://en.wikipedia.org/wiki/Graphite - fetched July 2007).

3.1.3 Other Substrates

While developing the deposition process I did investigate other substrates to try to understand which surface conditions resulted in the best films for AFM experiments. The adsorption of exopyridyl rotaxanes on COOH-terminated thiol SAMs (on Au(111)) of 11-mercaptoundecanoic acid was demonstrated by Cecchet *et al.*,[3,4] (see section *2.5.1*). A SAM surface can be useful because the chemical properties can be tuned by varying the chemical structure of the end (exposed) group. An image of a rotaxane-functionalised SAM on Au(111) that I prepared is shown in Figure *3.2*. The rotaxane molecules are physically adsorbed via an exopyridyl moiety. The height trace (cross section) on Figure *3.2* shows that the 'white protrusions' have a thickness of the order of 1 nm, which at the same length scale as the deposited rotaxane molecules. These protrusions therefore most likely represent individual rotaxanes or clusters of rotaxanes. The molecules do not present any distinct patterns or resolution. This result somewhat mirrors the films prepared by Azehara *et al.* and the resolution achieved by them.[5] For these reasons the use of these surfaces as model substrates for the study of rotaxane surface structure and orientation was ruled out.

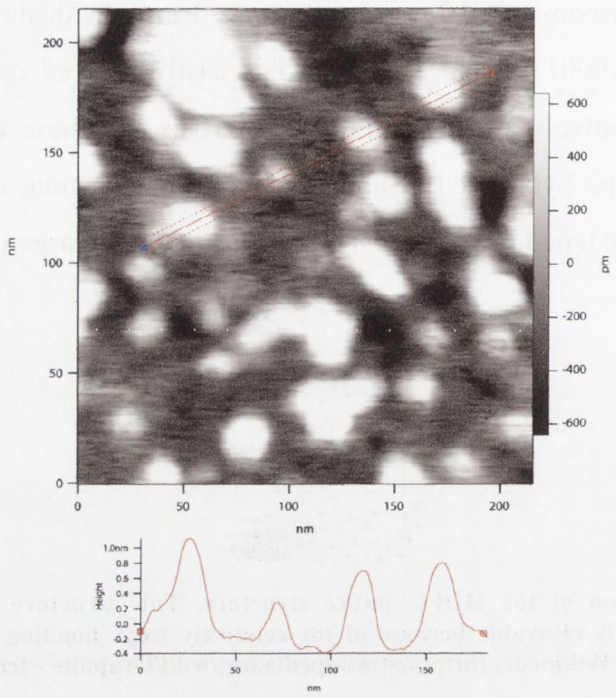


Figure 3.2: AFM image of thin film of rotaxane molecular shuttle (of the kind discussed in section 2.4.4) physisorbed on a SAM of 11-mercaptoundecanoic acid on Au(111). This film was prepared according to the method of Cecchet *et al.*[3, 4]

A Silicon Dioxide substrate can also be easily covered with a SAM formed through phosphate functionalisation. These surfaces importantly can exhibit controllable properties such as hydrophobicity based upon the end group of the molecule, just as in the case of thiol SAMS on Au. Such a controllable surface might be desirable to modulate the rotaxane-surface interaction. Upon examination of typical phosphate films as demonstrated in Figure *3.3* one can see that the roughness (RMS value 450 pm) is too high for the kinds of resolution I would like to observe.

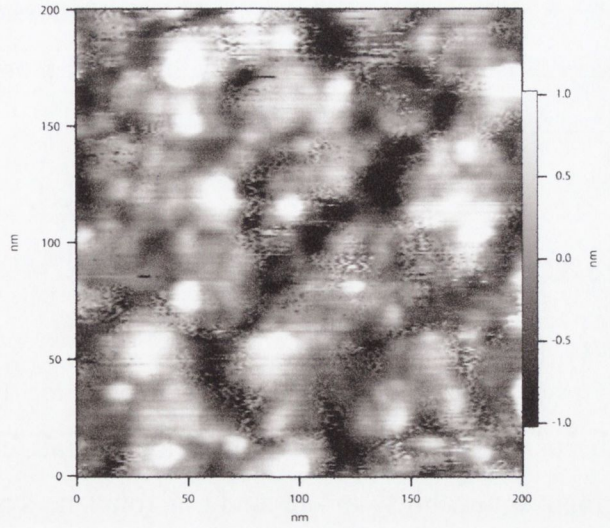


Figure 3.3: AFM image of thin film of Fumaramide rotaxane (section 2.4) physisorbed on a methylated silicon surface. This film was prepared by exposing a clean silicon 001 surface to Methylsilane vapour. The surface has an RMS roughness of 450 pm.

Another 'ideal' AFM substrate is mica in that it can be easily cleaved to prepare a clean (001) surface, however the highly charged nature of the surface groups means that the rotaxane molecules when deposited tend to aggregate rather than form a film, as shown in Figure *3.4*. This is because the non-polar rotaxane molecules have lower free energy when recrystallized than when adsorbed on a polar substrate.

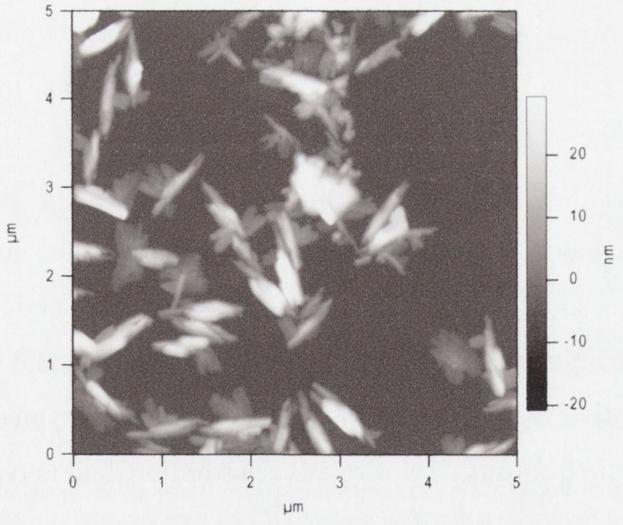


Figure 3.4: AFM image of Exo-pyridyl Fumaramide Rotaxane deposited on a freshly cleaved Mica(0001) surface. The rotaxane molecule has formed crystallites but not spread on the surface.

Graphite, not having a charged surface, having large, easily reproduced and quickly obtainable flat terraces is the best substrate for the study of organic molecules that do not have a large overall dipole moment and which will thus be physically adsorbed onto the graphite surface. The low roughness means that molecules can form flat films

where the chief corrugation will be in the molecular features (on the order of picometres) as opposed to large surface corrugations (on the order of nanometres) seen in molecular films formed on other substrates.

3.2 Atomic Force Microscopy

3.2.1 Introduction

An introduction to probe microscopies was made in chapter 1, section *1.6*. The following sections discuss the operation of AFM in closer detail, concentrating on the various modes and their applicability to the study of rotaxane systems. This section also details the concepts of Frequency Modulation AFM (FM-AFM), a dynamic AFM mode that can be used for quantitative and high-resolution studies, and the concept of Energy dissipation in dynamic AFM. Energy dissipation is an important concept for this thesis, as it is developed throughout chapters 5 and 6 as a route to detection locally of rotaxane functionality and shuttling.

3.2.2 Principle of Operation

A typical probe microscope can operate in two modes - spectroscopic mode and imaging mode. (Actually these two methods can be combined for another "Spectroscopic Mapping" mode which allows 3-dimensional measurement of an interaction).

In the spectroscopic mode the interaction between a sharp probe and the sample under investigation is measured as the distance between probe and sample is varied, resulting in a graph which will typically show the approaching and retracting "curves" as a function of relative separation. In AFM this curve would typically show the force experienced by the tip as a function of relative separation, and is typically known as a "force curve".

By "feeding-back" on one of these measured properties, (using electronics to keep a measured value constant by controlling the tip-sample separation), there can be relative lateral tip-sample displacement (i.e. scanning) and the force between tip and sample between will automatically be regulated. Typically the sample is placed on a

piezo element and the tip-sample distance controlled by the voltage applied to the piezo. The feedback loop changes the piezo voltage in order to keep the measured property at a constant value. This means that by measuring the displacement applied to the piezo by the feedback electronics, the surface can be mapped to produce a map of a region above the sample where the tip-sample force is constant. At the length-scales of a typical AFM experiment, this essentially corresponds to a topographic image. Interestingly, in AFM measurements at length-scales approaching the molecular level however (as will be shown in Chapters 5 and 6), the notion of force corresponding to topography becomes is not necessarily valid because of force variations from different chemical groups.

Figure *3.5* shows the operating principle of an AFM in contact mode, where the cantilever deflection is kept constant by a feedback loop. The force on the cantilever (F) is kept constant because the deflection (d) is linearly related to the force by Hooke's Law:

$$F = kd \qquad (3.1)$$

where k is the cantilever spring constant.

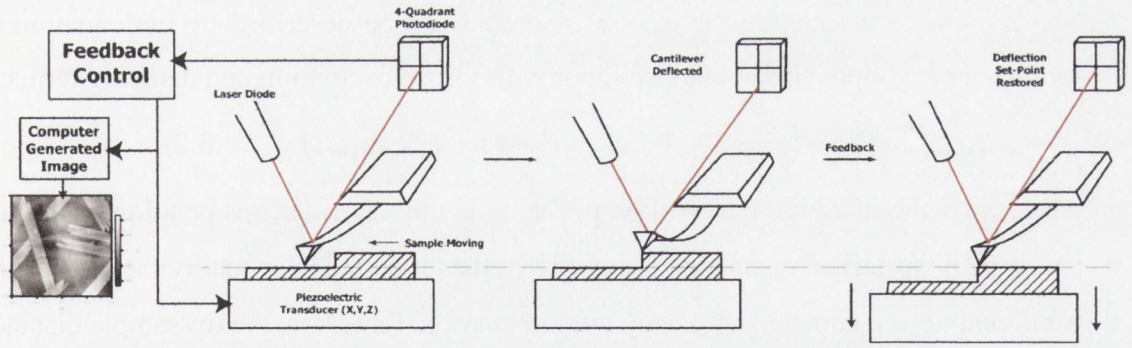


Figure 3.5: Principle of AFM operation.

3.3 Dynamic AFM

Contact or D.C. mode AFM has proven unsuitable for many applications, including imaging of soft samples, including biological samples, because of the large and constant forces typically applied during the experiment. The minimum force that can be applied between the tip and sample is limited by the spring constant of the lever combined with the tip-sample adhesion. Contact mode therefore suffers from "snap-in" – an effect which occurs when the force gradient experienced by the tip is greater than

the cantilever spring constant and the tip jumps into contact with the surface. This has partly driven the growth in use of dynamic AFM methods,[6, 7] where the AFM lever is oscillated at or around its resonance frequency and the characteristics of the vibration are altered as a result of the tip's interaction with the surface.[8, 9] Snap-in is avoided in dynamic modes because stiffer levers can be used while still retaining sensitivity, and by using large amplitudes of oscillation. Contact mode also suffers from thermal drift, which results in movement of the laser spot on the photodiode, mimicking displacement of the lever and causing inaccurate measurements and feedback. Drift of the laser spot in dynamic modes is not so impacting because the properties of the oscillation do not vary so severely with laser spot displacement (the dependence is obviously directly proportional in contact mode).

These multi-environment dynamic techniques can image cell surfaces, proteins and DNA as well as other soft molecules without sample damage. True atomic resolution in UHV is routinely possible,[10] and during the period of the undertaking of this thesis, atomic and molecular resolution in gaseous[11] and liquid[12] environments has also been reported.

The motion of the cantilever and tip ensemble can be described by the equation of motion for a Simple Harmonic Oscillator with forced oscillation and damping terms:

$$m\ddot{z}_t + \left(\frac{m\omega_0}{Q}\right)\dot{z}_t + kz_t = F_{ts}(z) + F_0\cos(\omega t) \qquad (3.2)$$

where m is the effective mass of the probe, z_t is the instantaneous position of the tip, ω_0 is the unperturbed resonance frequency of the lever, Q is the quality factor, k is the cantilever spring constant, F_{ts} is the total tip-sample force, z is the tip-sample distance and F_0 and ω are the amplitude and frequency of the driving force. By solving this equation[7] it can be shown that the dynamics of a vibrating cantilever can be expressed in terms of the phase (θ), frequency (ω) and amplitude (A) of the oscillation. The Amplitude (A) can be described by the expression:

$$A(\omega) = \frac{F_0/m}{[(\omega_0^2-\omega^2)^2+(\omega\omega_0/Q)^2]^{1/2}} \qquad (3.3)$$

and the phase (θ) by the expression:

$$\tan\theta = \frac{\omega\omega_0/Q}{\omega_0^2-\omega^2} \qquad (3.4)$$

Names for various dynamic modes of AFM come from whichever of these three properties is used as a feedback parameter for distance regulation.

3.3.1 Amplitude Modulation AFM

In Amplitude Modulation AFM (AM-AFM) the cantilever with sharp probe is oscillated at a fixed frequency on or close to the cantilever resonance, (usually, but not always the fundamental). The value of the amplitude is calculated from the signal measured at the photodiode, and is used as a feedback parameter to measure the region of constant force above the sample.

The amplitude of the oscillating system depends upon the frequency of the fixed driving oscillation relative to the resonance and upon the damping forces experienced (equation *3.3*). Any change in the amplitude of the oscillation occurs either due to a shift in the resonance peak relative to the fixed driving signal (conservative) or due to an overall reduction in the amplitude of the resonance peak (reduction in Q factor i.e. dissipation). The amplitude of an oscillating probe will thus be influenced as the tip approaches the surface by conservative tip-sample forces, dissipative tip-sample forces, and the viscous damping from the environment.

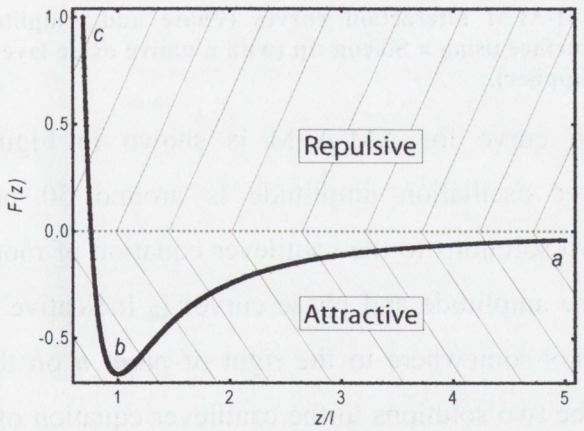


Figure 3.6: Graph of the Lennard-Jones force law (eq. 3.5).

Let us briefly consider a simple Lennard-Jones force law which describes the forces experienced by two bodies in close proximity as an approximation for the tip-sample interaction, as shown in Figure *3.6*. This consists of a long-range attraction and a short-range repulsive interaction:

$$F(z) = F_0\left(\frac{l^4}{3z^6} - \frac{1}{z^2}\right) \qquad (3.5)$$

where F_0 is a constant, z is the tip-sample separation, and l is the separation at which the attractive force is a maximum. As the tip moves towards the sample the force experienced changes from points a to c. Between points a and b the tip feels an attractive force towards the sample which perturbs the natural oscillation of the system such that the effective spring constant is altered (reduced in an attractive force). This equates to a reduction of the natural resonance frequency of the lever, via the relationship:

$$\omega = \sqrt{k/m} \qquad (3.6)$$

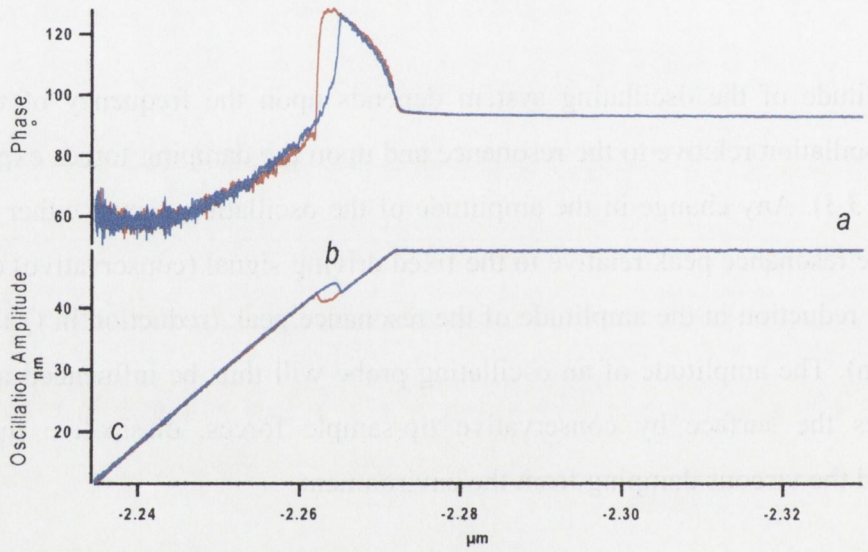


Figure 3.7: Typical AM-AFM interaction curves (Phase and Amplitude). The curve was measured on a HOPG surface using a Silicon tip (with a native oxide layer) with radius approx. 10 nm (as specified by supplier).

A typical interaction curve for AM-AFM is shown in Figure *3.7*, where the unperturbed cantilever oscillation amplitude is around 50 nm. Mathematically speaking there are two solutions to the cantilever equation of motion (Equation 3.2). The sharp jump in the amplitude and phase curves is indicative of a jump between these states, and occurs somewhere to the right of point ***b*** on the force interaction curve (Figure *3.6*). The two solutions to the cantilever equation of motion are known as the high amplitude (H) and low amplitude (L) solutions. The L-state solution dominates when the tip-sample force is a net attractive force (commonly considered as being non-contact).[7] After the discontinuity in the amplitude curve (point ***b*** in Figures *3.6* and *3.7*) the repulsive force begins to dominate the interaction and the oscillation changes to the H-state and the tip is considered to be intermittently contacting the surface. The "non-contact" mode (imaging with conditions where the

L-solution dominates) is useful for non-destructive imaging of soft samples.[13] This inherent bistability can result in unstable imaging conditions as the oscillation can seem to randomly switch between the two solutions.[14] This switching can be minimized by using small lever oscillations and imaging set-points that are close to the unperturbed oscillation amplitude of the lever.[15] This bistability actually prevents quantification of the forces measured by the technique, and is something that can be avoided by utilizing frequency-modulation AFM (FM-AFM), discussed in the next section.

"Phase imaging" involves recording the phase difference between the driving force of the lever and the actual oscillation frequency.[15] A typical variation of phase with relative tip-sample separation is also shown in Figure *3.7*. This technique could potentially allow us to chemically distinguish materials, or to detect variations in material properties such as adhesion, elasticity and viscoelasticity because of the relationship between the phase signal and the energy transferred between tip and sample during imaging.[16, 17] In Figure *3.7*, in the phase signal shows two solutions (at point b) which means there are also quantification difficulties associated with this technique.

3.3.2 Frequency Modulation AFM

In Frequency Modulation AFM (FM-AFM), the cantilever with sharp probe is oscillated at its resonance frequency. The detected cantilever oscillation signal is amplified and phase-shifted and used to drive the cantilever. To ensure that the lever is always oscillated at its resonance a constant phase difference of 90° between the driving signal and the detected signal is maintained by a phase-locked-loop (PLL).

As the tip approaches the sample the force interaction changes the effective stiffness of the oscillation system, which changes the resonance frequency. The "frequency shift" ($\Delta\omega$) as it is called can be used as a feedback parameter for the imaging of contours of constant force. The amplitude of the system is damped by viscous forces and the dissipative tip-sample interaction. The signal that drives the lever can be amplified in one of two ways. It can be multiplied by a fixed value (constant excitation) or another feedback loop can be employed to keep the value constant

(constant amplitude). The method employed in this study is Constant Amplitude FM-AFM (hereafter referred to as simply FM-AFM).

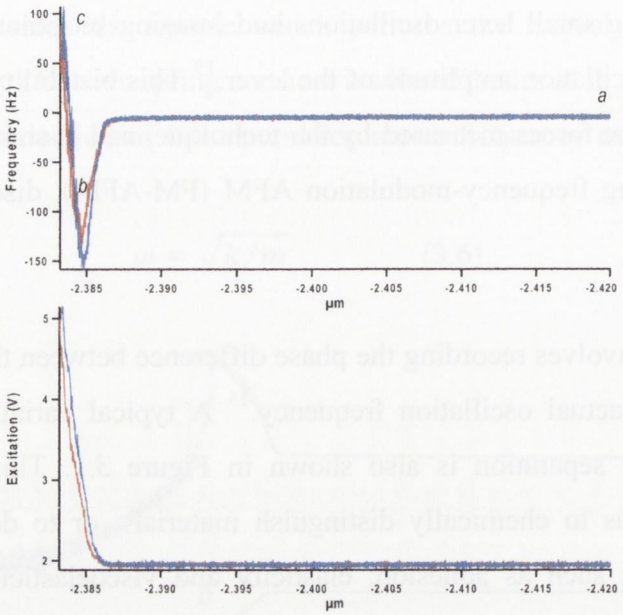


Figure 3.8: Typical FM-AFM interaction curves (Frequency and Excitation Voltage). The curve was measured on a HOPG surface using a Silicon tip (with a native oxide layer) with radius approx. 10 nm (box value). Point 'a' is a point where the tip-sample separation is large and no perturbation is experienced. Point 'b' is the point of minimum force (i.e. maximum net attractive force). At point 'c' the tip and sample are close together and repel each other.

Actually the interpretation of the frequency versus tip-sample distance curves in terms of the force is more straightforward for FM-AFM than in the case of AM-AFM. A typical interaction curve for FM-AFM is shown in Figure *3.8*, again with points of interest labelled *a-c* as in Figure *3.6*. Negative values of frequency shift correspond to a net attractive force between tip and sample.

The amplitude feedback loop forces the cantilever to oscillate at constant amplitude and the 90° phase shift between drive signal and detection signal means that the oscillation is always at resonance. Therefore the energy losses of the cantilever (whether hydrodynamic, due to the structure of the cantilever, or because of the tip-sample interaction) must be exactly matched by the cantilever excitation required to keep the amplitude constant. As such the conservative and dissipative components of the cantilever equation of motion (Equation 3.2) can be treated separately. This means that conveniently the frequency shift and excitation amplitude in Constant Amplitude FM-AFM can respectively be used to calculate the conservative and dissipative components of the force interaction. Considering only the conservative parts of the

interaction the following expression relating frequency shift to force can be derived (from reference [18]):

$$\frac{\Delta\omega}{\omega_0} = -\frac{1}{\pi Ak}\int_{-1}^{1} F_{ts}\big(z_0 + A(1+u)\big)\frac{u}{\sqrt{1-u^2}}du \qquad (3.7)$$

where $\Delta\omega$ is the change in resonance frequency, z_0 is the distance of closest approach of the tip and sample and $u = \cos(\omega t)$. Sader *et al.* successfully analytically inverted this equation such that it is valid for any value of oscillation amplitude A.[19] Therefore the conservative force can now be easily calculated from the frequency shift via the formula:

$$F(z_{ts}) = 2k\int_{z_{ts}}^{\infty}\left(1+\frac{A^{1/2}}{8\sqrt{\pi(t-z_{ts})}}\right)\Omega(t) - \frac{A^{3/2}}{\sqrt{2(t-z_{ts})}}\frac{d\Omega(t)}{dt}dt \qquad (3.8)$$

where

$$\Omega(z_{ts}) = \frac{\Delta\omega(z_{ts})}{\omega_0} \qquad (3.9)$$

Sader *et al.* also showed that separation of conservative and dissipative interactions in this manner is valid even for oscillating FM-AFM systems that are slightly detuned (and therefore not exactly on resonance),[20] which attests to the robustness of the technique.

Because the frequency shift is very sensitive to the force interaction, stiff cantilevers can be employed for imaging. This means that "snap-in" can be avoided and the full range of the force interaction can be explored. Again, as in the case of AM-AFM, the region of net attractive force implies a "non-contact" regime, and very low-force imaging can be employed. This technique has successfully been used to image semiconductor, insulator and metal surfaces with atomic resolution in UHV,[10, 21, 22] as well as individual adsorbed molecules in UHV,[23] and molecular thin films.[24] The technique has recently been extended for operation in air and liquid environments,[25-27] where atomic and molecular resolution has recently been achieved.[11, 12, 28]

3.3.3 Energy Dissipation in FM-AFM

Even in the case of "non-contact" imaging modes some energy loss of the vibrating cantilever occurs that is associated with the tip-sample interaction. This energy is dissipated as heat, phonon coupling or some other mechanism (some theories are discussed below) and the amount depends upon the tip and sample structure and

chemistry. As mentioned above, the energy dissipation in FM-AFM is proportional to the necessary excitation in the amplitude feedback circuit. This dissipation shows contrast between regions of different material properties and chemical identity, [16, 29-31] and even shows contrast at the atomic,[32] and molecular scale.[33, 34] As a result there is much interest in developing this technique for quantifiable materials property measurement, and for understanding atomic- and molecular-scale dissipation processes.

The phenomenon of a tip-sample energy transfer which can be mapped with atomic and molecular resolution is difficult to explain theoretically. One suggested source of the energy dissipation is the 'stochastic friction force', which says that random atomic vibrations at the tip-sample interface result in a friction force acting on the tip, although calculations involving this theory result in dissipated energies at least three orders of magnitude smaller than experiment.[35] The 'adhesion hysteresis' mechanism is the other main suggested method and involves relaxation of the tip or sample atoms at the interface during tip approach leading to different forces on approach and retract.[36] Although the calculated energies of this process are closer to experiment, it is still unclear whether such reconstruction could occur at the relatively large separations associated with the attractive force region and result in stable dissipation imaging.[37]

The energy dissipation contrasts found during the imaging of organic thin films suggests that disordered or loose packing commonly found in the molecular surface (and hence the stability against the tip-sample interaction force) has a strong effect on these images. Ichii *et al.* found higher dissipation on disordered dithiol monolayers than on a well ordered thiol monolayer.[38] Moreover when the tip was scanned closer to the sample, the observed dissipation increased significantly on the dithiol monolayer and only slightly increased on the thiol monolayer, which suggests that the arrangement of the dithiol monolayer was changed by the tip-sample interaction. Fukuma *et al.* showed that the dissipation is strongly correlated with the molecular packing; clear dissipation contrasts were observed for the not-so-well ordered delta-phase of a 12 Carbon chain Self Assembled Monolayer on Gold while the well ordered eta-phase showed hardly any molecular-scale contrast.[34] Further results from Fukuma *et al.* also suggest that the contrasts are probably related to the number of

molecules interacting with the tip – the more molecules interacting with the tip, the greater the dissipation; thus the dissipation image shows inverted contrast relative to the topographic image at the molecular scale. This phenomenon is illustrated in Figure *3.9*, and can be explained by the fact that the tip at position A has more energy dissipation pathways available than at position B, since at A it is interacting with more than one molecule. Fukuma *et al.* also showed that well-ordered Copper phthalocyanine (CuPc) grains showed lower dissipation than less well ordered (as shown in topography) CuPc monolayers.[33] Finally and importantly they showed direct evidence of energy transfer from the tip to the sample by showing that the sample was 'locally annealed' after a few scans – hence the vibrational energy of the cantilever was transformed into kinetic energy of molecular fluctuations through dissipative tip-sample interactions. Therefore, whatever the mechanism of energy transfer, it can be said that energy is transferred into the sample.

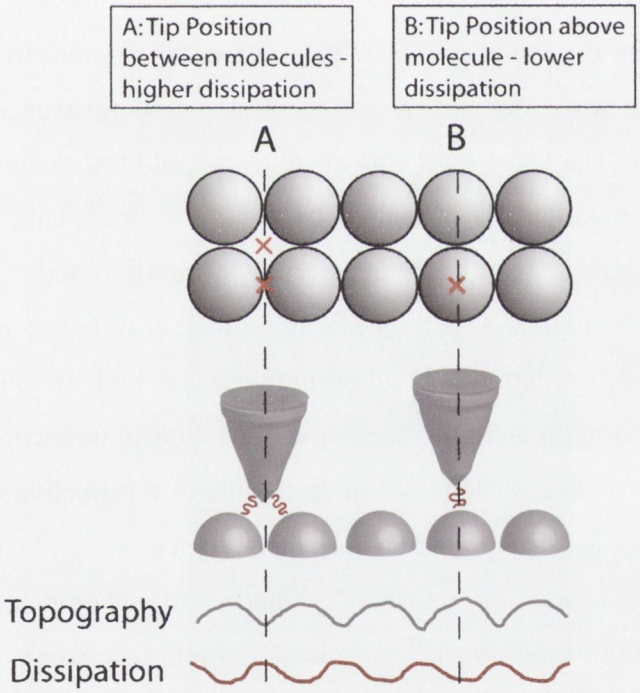


Figure 3.9: Proposed model for the inverted Topography and Dissipation signals seen during FM-AFM scanning.

Through the principle of conservation of energy the total power supplied to the cantilever ($\bar{P}_{tot}$) must equal the total dissipated power, which is comprised of the power dissipated through the natural damped motion of the cantilever ($\bar{P}_0$) and the power dissipated through the tip-sample interaction ($\bar{P}_{ts}$),[31] such that:

$$\bar{P}_{tot} = \bar{P}_0 + \bar{P}_{ts} \,. \qquad (3.10)$$

Since the cantilever is being driven at a constant amplitude, one can substitute for $\bar{P}_{tot}$, and by characterising the lever resonance properties (ω_0 and Q), one can also substitute for $\bar{P}_0$, which yields the equation for the average energy transferred to the sample per oscillation cycle (E_{ts}):

$$E_{ts} = \frac{\pi k A^2}{Q}\left(\frac{A_{exc}}{A_{exc0}} - 1\right) \qquad (3.11)$$

where A_{exc} is the excitation voltage of the Voltage Controlled Oscillator (VCO) that drives the cantilever and A_{exc0} is the excitation voltage when the tip is far from the surface. E_{ts} will be in units of $eV/cycle$.[39]

3.4 AFM probes.

3.4.1 Measurement of lever displacement

In AFM the cantilever is either deflected as a result of a tip-sample force, or if the lever is oscillating then the oscillation parameters are changed. Thus a sensitive technique for measuring the cantilever displacement is required. In the original AFM design, which was based on that of the STM, an STM tip was used to detect the motion of the lever. The lever itself was made from Gold foil, which is conducting so that its displacement might be measured by the STM tip.[40] This method was soon succeeded by optical methods such as heterodyne interferometry,[41] which were not dependent upon the roughness of the back side of the cantilever, and which allowed the cantilever to be oscillated at large amplitudes and high frequencies.[8] The most common and easy to implement method is the optical beam deflection (OBD) method, where a small laser beam is shone on the back side of a reflective cantilever and the deflection detected with a position sensitive detector, typically a segmented photodiode.[42] It was soon realised that by segmenting the photodetector laterally also, any torsional bending of the cantilever, caused by friction between the tip and sample during contact mode imaging, could also be detected.[43] An illustration of the 4-quadrant photodetector can be seen as part of Figure *3.5*.

3.4.2 Calibration of levers

In simple contact mode the total force experienced by the cantilever (F) can be calculated through Hooke's Law:

$$F = kd \qquad (3.1)$$

where d is the cantilever deflection and k is the cantilever spring constant. One must therefore have reliable methods of determining these quantities. These values are also necessary for the calculation of the tip-sample force in AM-AFM and FM-AFM.

While the interferometric methods measure the displacement of the lever directly, in the case of the OBD method it is necessary to calibrate the system for each lever by measuring the deflection sensitivity. The deflection sensitivity is a calibration constant that allows us to convert the voltage measured on the photodiode into a real displacement.

In the most straightforward measurement of this parameter the tip is pressed against the sample, which deflects the lever, and the voltage (V) measured by the photodiode is measured as a function of displacement (h). The sensitivity is therefore the slope $\frac{\partial V}{\partial h}$ and is usually quoted as its inverse in units of nm/V.

Since the optical path and lever characteristics will be different in every case this value must be calculated for every AFM experiment, or if the laser position on the cantilever changes. Although this is a very straightforward method it has some major disadvantages such as the fact that the tip will quite likely be damaged and/or become contaminated by hard contact with the sample. The method also assumes zero deformation of the tip or sample.

Now to calculate the force from equation *3.1* we need to know the cantilever spring constant as well as the displacement distance. Methods of calculating the cantilever spring constant are discussed in the following section.

3.4.3 Calibration of spring constant

An experimental determination of the spring constant (k) is also normally required. This is despite the fact that k can be calculated for a rectangular lever based upon the geometry and material properties of the lever by the equation:

$$k = M_e \rho_c b h L \omega_{vac}^2 \qquad (3.12)$$

where h, b, and L are the thickness, width, and length of the cantilever, respectively, ρ_c is the density of the cantilever, ω_{vac} the natural resonance of the cantilever in vacuum and M_e is the effective mass.[44]

This calculation is prone to errors because geometric values must be measured with a microscope (for high accuracy a scanning electron microscope (SEM) must be used). The thickness is very difficult and awkward to measure accurately and the dimensions of the lever are typically non-uniform anyway. As well as this the calculation assumes a perfectly homogenous cantilever material, when in fact there will always be some native oxide growth.

An AFM cantilever can be calibrated by measuring the displacement when pressed against a cantilever of known spring constant (the Reference Cantilever Method),[45] or by measuring resonance changes of the lever as masses are added to the end of the lever (Dynamic Added Mass Method),[46] however these methods are awkward and time-consuming.

The Thermal Noise Method [47] is a straightforward noncontact method that uses the Equipartition Theorem to calculate the *dynamic* spring constant from the measured thermal noise spectrum of the cantilever. For the fundamental resonance of a rectangular cantilever the dynamic spring constant is 1.04 the spring constant.[48] This method also required calibration of the deflection sensitivity. As discussed in the next section however, the equation from this method can be used inversely to calculate the sensitivity after the spring constant has been measured.

In this thesis the method of choice is the "Sader Method" for lever calibration as discussed in the next section.

3.4.4 Sader Method for Lever Calibration

3.4.4.1 Spring Constant

The Method of Sader *et al.* [49] (The Unloaded Resonance Method) can be used to calculate k based upon the motion of the lever through a fluid, using the formula:

$$k = 0.1906\rho b^2 LQ\Gamma_i(\omega_R)\omega_R^2 \qquad (3.13)$$

such that it is only necessary to know the length (L), width (b) resonance frequency (ω) and quality factor (Q) of the lever, as well as the fluid density (ρ) and viscosity (Γ_i). The density and viscosity of air and water are well known and the length and width of the lever can be measured in a SEM.

3.4.4.2 Sensitivity

Because we can easily measure the spring constant using the Sader method, we can use the Thermal Noise Method in the following way to calculate the sensitivity.[47]

The thermal noise spectrum of the lever can be measured and the Equipartition Theorem applied yielding the equation:

$$\text{Sensitivity} = \sqrt{\frac{2k_BT}{\pi k \omega_R P_{dc} Q}} \qquad (3.14)$$

where k_B is the Boltzmann constant, T is the temperature and P_{dc} is the measured voltage signal at the photodetector at a given frequency.

This means that by this method it is possible to calibrate the cantilever in all respects before the experiment is carried out and without tip damage. We can therefore know the exact amplitude of oscillation in-situ. Currently, force measurement calculations in FM-AFM using Equation *3.5* are carried out after the experiment; however with increasing computing power and a sophisticated algorithm it should be possible at some point in the future to know the forces in the experiment "live". This would mean for example that a value for "Force" could be used as a set-point for imaging. This is currently possible for "contact mode" imaging, however as discussed in section *3.3* this imaging method can be very detrimental to the sample. In current FM-AFM experiments an estimate of the force based on the spring constant and amplitude is used during the experiment.

3.4.5 Cantilever Hydrodynamic Considerations

When considering the method of Sader and Jarvis for recovering the force from the interaction frequency as discussed in section 3.3.2 one of the important assumptions that must hold true if the conversion is to be valid is that the resonant frequency must be independent of the tip-sample separation (it is dependent upon the tip-sample force,

not the separation). It is therefore necessary to consider the effect of hydrodynamics upon the lever resonance, especially as the lever approaches the sample to within its hydrodynamic length scale.[50] The hydrodynamic length scale is the lever-sample distance at which the inertial loading of the cantilever is significantly affected by the interfacial hydrodynamic forces – when a surface is present the flow of liquid around the cantilever is disrupted. This length-scale is typically the same as the width of the cantilever.[51]

To verify that the resonant frequency is independant of the tip-sample separation I measured the frequency shift of a cantilever as a function of separation in water (Sader *et al.*)[51]. In liquid this effect of squeezing fluid between the lever and sample would be greatly enhanced compared to in ambient conditions, where the fluid (air) is obviously less dense. Figure *3.10(a)* shows the large frequency shift over the last 14 microns of interaction due to the hydrodynamic interaction. The frequency does depend on the distance for large length-scales (approximately equal to the cantilever width). For typical tip-sample separations that are probed in AFM however, (Figure *3.10(b)* shows the frequency shift for the last 200 nm of tip-sample separation), the frequency shift due to the hydrodynamic effect of the surface is essentially constant.

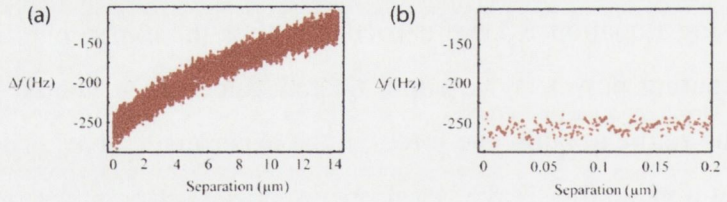


Figure 3.10: Cantilever frequency shift in liquid as the cantilever/tip ensemble approaches the surface. The long range shift (a) shows significant deviation due to hydrodynamic damping. This effect however is unimportant over the region of interest (b) (last 200 nm). This interaction was measured using a silicon tip under water as an approach to a HOPG surface was made.

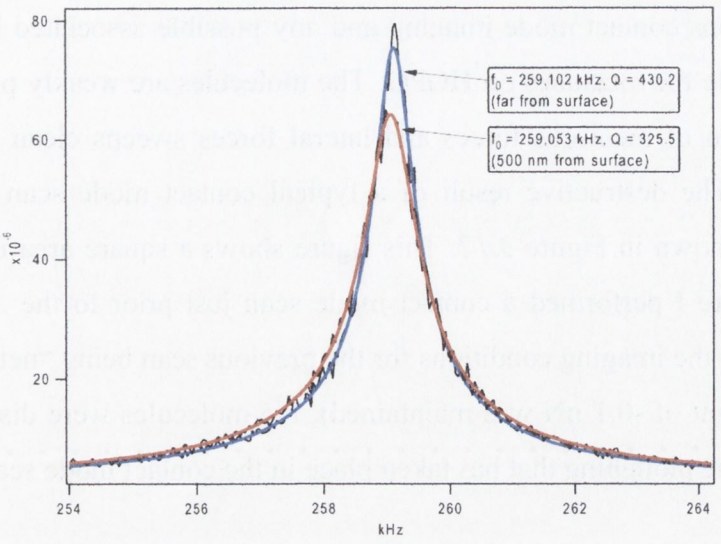


Figure 3.11: Measurement of hydrodynamic damping. This was observed in Ambient conditions.

This same effect is also present in air and is a concern for the correct calibration of the cantilever for force and dissipation calculations. A typical resonance curve for a lever is shown in Figure *3.11* at large separation (a few mm) and at 500 nm separation. When calibrating levers using the noncontact method it is tempting and more convenient to perform the calibration at very large separations. In this example I have shown that this can result in errors of in this case 32% in the measured quality factor *Q*, which would be important in quantitative measurements of the Energy Dissipation (according to Equation *3.11*).

3.5 Experimental Setup/AFM Modifications

3.5.1 Imaging modes for rotaxanes on HOPG

Many groups have in the past managed to achieve high imaging resolution in liquid environments using contact mode AFM imaging. Müller *et al.* could frequently image the lattice structure of the Bacteriorhodopsin protein.[52] These samples are typically robust and the films are very tightly packed. This means that the film can withstand any high lateral forces exerted by the tip. Also, in a liquid environment the contact forces can be balanced because there is only one interface (liquid-solid). In ambient conditions a water meniscus forms between tip and sample when in close enough proximity. As the tip drags this meniscus across the surface it can exert large forces and greatly deform soft surfaces.

For these reasons contact mode imaging and any possible associated high-resolution was not possible for rotaxanes on HOPG. The molecules are weakly physisorbed and the combination of meniscus forces and lateral forces sweeps clean the area under investigation. The destructive result of a typical contact mode scan on a rotaxane monolayer is shown in Figure *3.12*. This figure shows a square area in the centre of the image where I performed a contact mode scan just prior to the AM-AFM scan shown. Despite the imaging conditions for the previous scan being "net" attractive (an imaging set-point of -0.1 nN was maintained), the molecules were displaced. This is evidenced by the ploughing that has taken place in the contact mode scan.

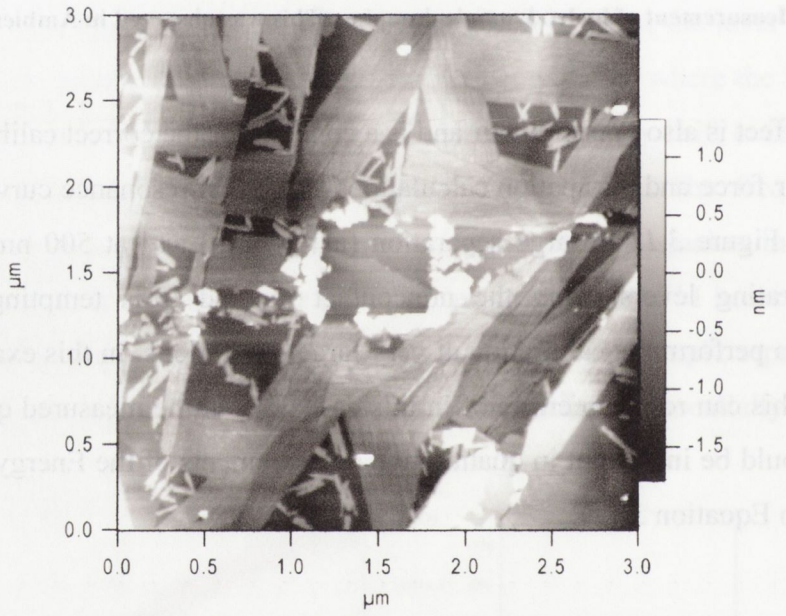


Figure 3.12: AM-AFM image of a rotaxane thin film on HOPG. The square in the centre of the image is where a Contact Mode scan (500 nm x 500 nm) was performed previously. In the Contact Mode scan no topographic details were observed. The AFM mode was changed to AM mode and the scan size was zoomed out to observe the damage done by tip ploughing.

As discussed in section *3.3.1*, an AFM operating in AM mode can have a cantilever that is oscillating in one of two solutions to the cantilever equation of motion (called the H and L solutions). In the experiments of San Paulo *et al.* they showed the damaging effects of switching between the H and L solutions to the tip-sample force.[13] They imaged the trimer structure of human serum albumin (a-HAS) while the cantilever was oscillating in the L branch and then switched to the H branch where no structure was visible. The molecular structure was destroyed by this process as evidenced by the subsequent scan in the L-branch.

In my rotaxane imaging experiments I observed film damage as a result of switching branches, which resulted in similar effects to those observed in Figure *3.12*. This switching can be minimized by using small lever oscillations and imaging set-points that are close to the unperturbed oscillation amplitude of the lever.[15] In Figure *3.7*, point b indicates the tip-sample distance (x-axis) where this switching of solutions occurs for this given free amplitude of oscillation (50 nm – the value at point a, far from the surface), and where the cantilever can randomly switch between solutions. By imaging in the attractive or "non-contact" mode I was able to maintain consistency in my measurements of rotaxane film height above the HOPG between non-contact AM-AFM and non-contact FM-AFM. This is because the imaging forces were similarly low in either case and deformation of the rotaxane film was minimized. Values of amplitude set-point higher than the value at point b in Figure *3.7* allow for non-destructive imaging to take place.

3.5.2 FM-AFM Imaging: Avoiding Instrumental Artefacts

In general, it is also important to use due consideration of the gains in the automatic gain controller (AGC), and in the z-piezo feedback circuit, in relation to the imaging speed such that the acquisition rate does not exceed the bandwidth limitation of the various elements of the system. If the feedback circuit is not adjusted correctly one will often see "edge effects" when the sample is rough, which are caused when the tip meets a feature, but the z-feedback is too slow in pulling the tip away from the surface we get an artificial increase in the observed dissipation caused by the tip being closer to the sample and/or an increase in the contact area. In the case of a very rough sample of homogeneous composition this can cause artefacts of higher dissipation to be observed which are unrelated to the mechanical properties of the sample.

3.5.3 AFM Modifications - Introduction

The Asylum Research Molecular Force Probe Three Dimensional AFM (MFP-3D) is an excellent system for an innovating nanoscience laboratory. This is chiefly because of the open-source nature of the controlling software. This allowed us to rewrite the software to incorporate FM-detection and a new scan engine for a home-built scanner. A Field-Programmable Gate Array (FPGA) chip also allows for easy signal manipulation, to do things like incorporate software controls to switch between piezo

cantilever activation and magnetic activation, or between the in-built scanner, and my home-built scanner.

For all that I could reliably measure very small differences in rotaxane film height with AM-AFM and FM-AFM using the Asylum MFP-3D AFM (this data will be presented in Chapter 4), I wished to improve its capabilities for fast feedback and lateral resolution, and for force and dissipation imaging (the limitations of the commercial system will be described below). To this end I added a new scanner and capability for Magnetically Activated Dynamic AFM (or MAD-mode).[53, 54] These modifications allowed me to achieve molecular resolution studies of rotaxane molecules in ambient conditions for the first time, and these results are discussed thoroughly in chapter 5.

3.5.4 AFM Scanner Modification

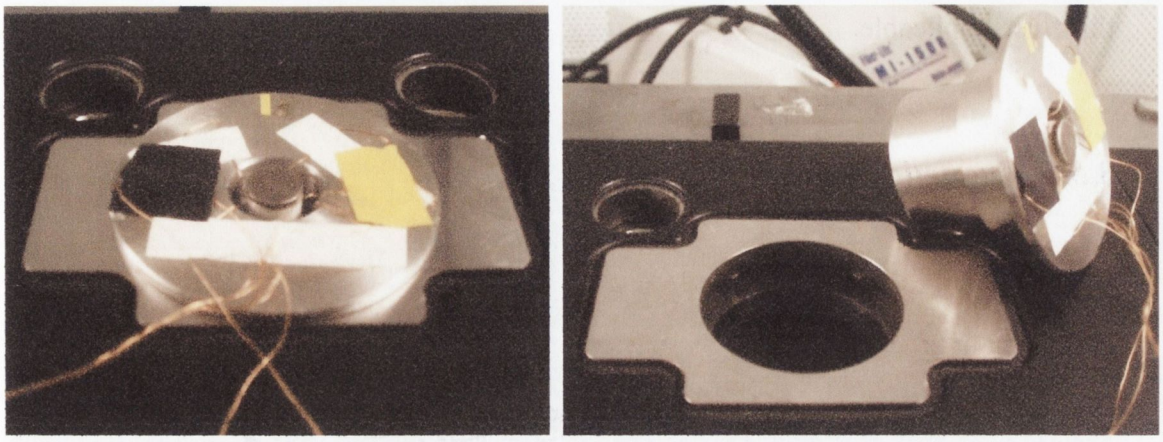


Figure 3.13: Photograph of AFM scanner modifications. The new piezo tube sits in a hole in a heavy stainless steel fitting. This fitting is carried along by the original flexure scanner. A software modification allows disable the original scanner and move the sample with the piezo tube. This allowed significant reduction of the positional noise caused by having such a large scan range on the original scanner.

The MFP-3D AFM is built with biological experiments in mind. As such the scanner has a very large maximum scan range to accommodate the imaging of large cells. The scanner also has the form of a flexure stage, a design used so that biological samples on glass slides can easily be investigated, and an objective microscope lens incorporated, and because it allows the incorporation of a lateral feedback system. This feedback system is useful for controlling thermal drift, but adds to the lateral noise of the system. As well as this the scanner moves around 500 nm for every 1 volt applied. This low sensitivity means that for small movements of the stage the motion is very sensitive to noise in the voltage signal. With an r.m.s. noise in the position of the scanner of around 1 nm, this is not conducive to high-resolution imaging. Figure *3.13* shows a piezo scanner assembly I designed and built to seamlessly integrate with the MFP-3D stage. The home-built scanner sits into the space where normally an optical microscope objective lens resides. The scanner housing is constructed so that there is space for it to "ride along" with the MFP-3D scanner. This design allows us to select between scanners for a large range of scan sizes without replacing the sample or moving the tip location above the sample. The home-built scanner has a maximum scan range of 2 μm and with a voltage range of ± 100 V, which means it is susceptible to an r.m.s. displacement noise of less than 0.2 Å. This noise level is of the order of other contributions to the total noise such as vibrational noise and deflection noise (from the Brownian motion of the lever). The ride-along scanner could be calibrated

by sequentially matching scan traces between it and the Asylum flexure stage. A calibration grating was not used because the maximum scan range was too small for this to be applicable.

3.5.5 Magnetic Activation

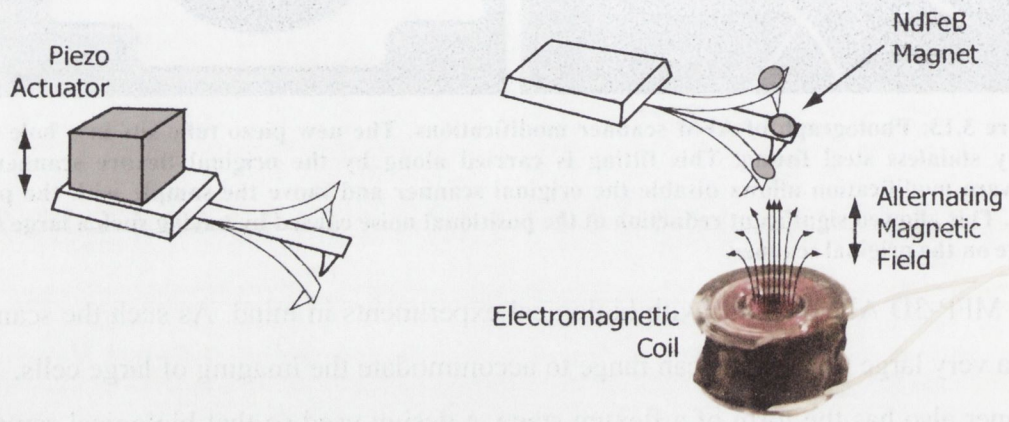


Figure 3.14: Illustrations of the main methods used for AFM cantilever activation.

Figure *3.14* illustrates the two methods most commonly used to oscillate AFM cantilevers, namely piezo activation and magnetic activation. It is also possible to activate the lever by modulating the laser power, causing local heating and expansion/contraction of the lever material at the frequency of the modulation, which oscillates the lever, but this method is far less common.[55] By attaching a small magnetic particle (with size typically on the order of the cantilever width, around 20-35 μm) to the backside of the AFM cantilever, the cantilever can be oscillated in an alternating magnetic field. In liquids the lever response spectrum can typically contain a "forest of peaks" around the cantilever resonance.[56] This is because the shaking of the piezo coupled by the surrounding liquid can activate spurious resonances of the cantilever-holder/sample system. This is avoided through directly activating the end of the lever by magnetic activation. In relation to the ambient studies performed in this work, Magnetic Activation provides a cleaner response spectrum, which makes Frequency Modulation easier to implement. This technique also has the advantage of directly activating the free end of the cantilever without any phase lag that might be associated with a delay between oscillating a piezo element at a certain frequency and the cantilever response.

3.5.6 Design of the coil assembly

It was necessary to design the magnetic cantilever activation system around the pre-existing available space of the commercial *Asylum Research* MFP-3D AFM. The AFM is designed with biological experiments in mind, so there is space for a microscope lens beneath the sample, which is generally mounted upon a standard-sized glass slide. For standard samples I could thus replace the lens with a suitable coil. My design of a "ride-along" scanner (section *3.4.2.1*) required a revised driving coil design. I decided to activate the levers using the external field of a coil (which is much weaker than the internal field I had previously been using).

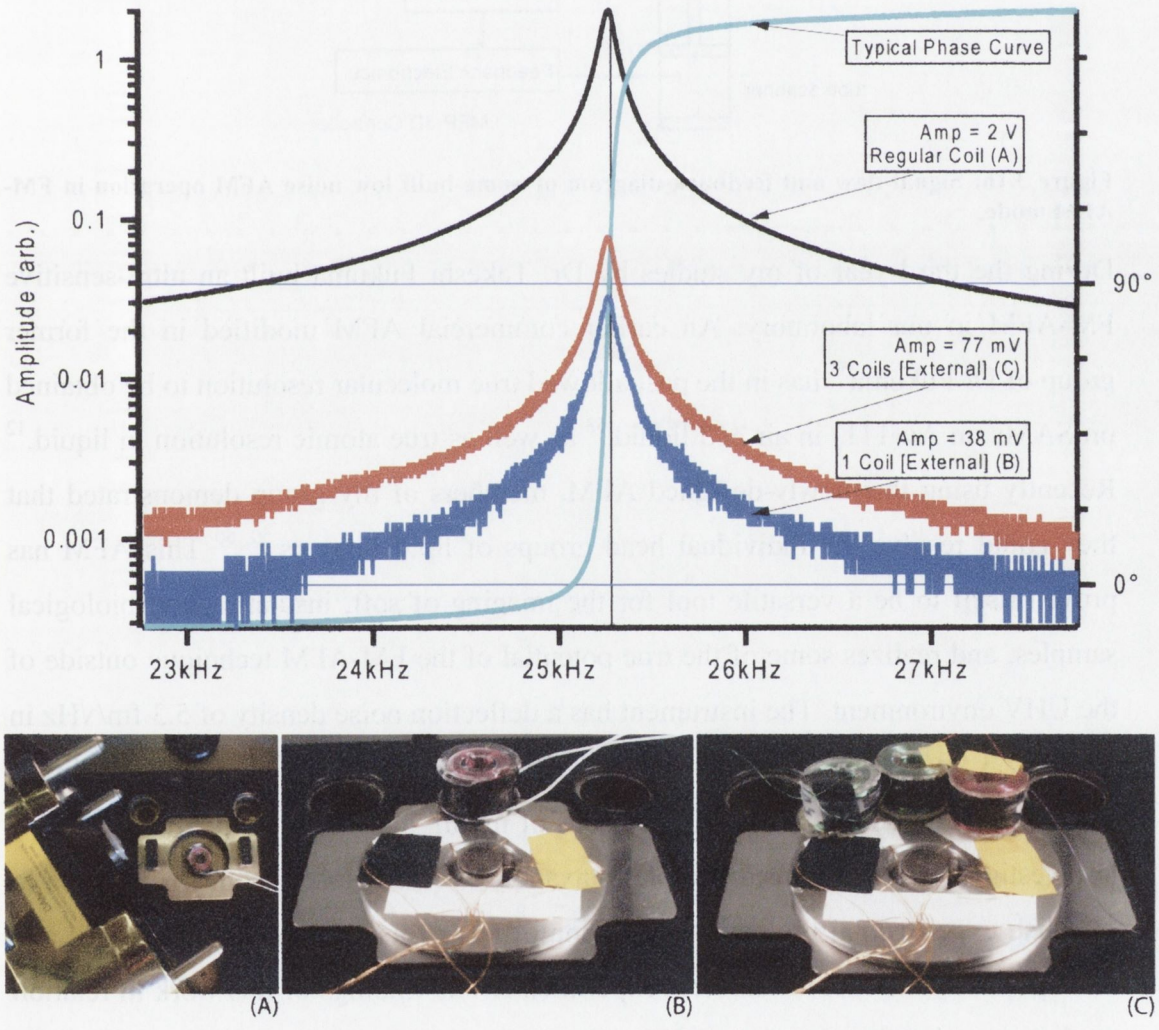


Figure 3.15: Comparison of the activation spectra for a cantilever with attached magnet for the three different coil setups. This figure also shows photographs of the Magnetic Activation modification used with the Asylum MFP-3D, and the modified scanner.

Figure *3.15* shows a comparison of the resonance response of a cantilever using different coil arrangements and piezo activation for the same lever with a driving voltage of 100 mV in each case.

3.5.7 Ultra-sensitive AFM experiments

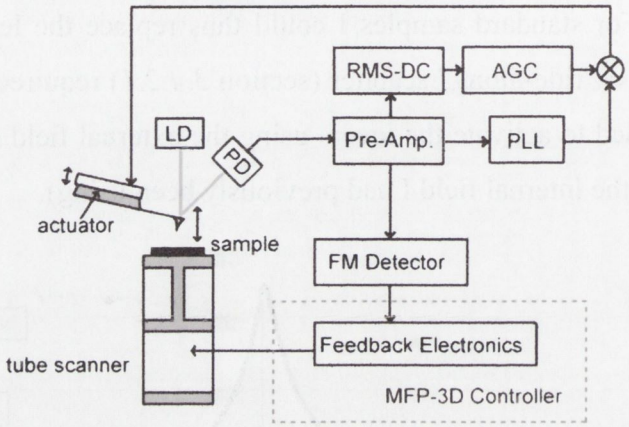


Figure 3.16: Signal flow and feedback diagram of home-built low noise AFM operation in FM-AFM mode.

During the third year of my studies by Dr. Takeshi Fukuma built an ultra-sensitive FM-AFM in our laboratory. An earlier commercial AFM modified in the former group of Dr Fukuma[57] has in the past allowed true molecular resolution to be obtained on SAMs on Au(111) in air and liquid,[58] as well as true atomic resolution in liquid.[12] Recently using this newly-designed AFM, members of my group demonstrated that they could resolve the individual head groups of lipid bilayers.[59, 60] This AFM has proven itself to be a versatile tool for the imaging of soft, insulating and biological samples, and realizes some of the true potential of the FM-AFM technique outside of the UHV environment. The instrument has a deflection noise density of 5.3 fm/√Hz in air and 7.3 fm/√Hz in water.[57, 61] The automatic gain control (AGC) and phase shifter were also home built.[62] After the successes of modifying the Asylum MFP-3D AFM to investigate ordered films of simple rotaxanes I worked closely with Dr. Fukuma to establish experimental protocol for imaging of large rotaxane molecular shuttles and to help qualify the tool for ambient experiments. The findings of this work in relation to the potential functional mobility of rotaxanes in surface-mounted devices are discussed in Chapter 6.

3.6 Conclusions

This chapter detailed experimental methods used during this work for the reproducible production of ordered rotaxane thin films. The theory behind AFM and current status of the field have been detailed with particular attention to the dynamic methods necessary for the investigation of soft and easily damaged samples such as rotaxane thin films. In particular FM-AFM, and the properties exploited in this work, such as the potential for high-resolution studies, and dissipation measurements have been explored. The particular AFM modifications I preformed to achieve molecular resolution in ambient conditions were also discussed, as well as the cantilever calibrations necessary to obtain quantitative data. Having armed myself with this most sophisticated of local nanoscale investigation tools, the following three chapters detail the experimental findings on the particular H-Bond assembled rotaxane systems studied.

3.6 References

1. Hansma, P. K., *Bull. Am. Phys. Soc.* **1985** (30) 251.
2. Binnig, G.; Fuchs, H.; Gerber, C.; Rohrer, H.; Stoll, E.; Tosatti, E., *Europhys. Lett.* **1986** (1) 31.
3. Cecchet, F.; Pilling, M.; Hevesi, L.; Schergna, S.; Wong, J. K. Y.; Clarkson, G. J.; Leigh, D. A.; Rudolf, P., *J. Phys. Chem. B* **2003** (107) 10863.
4. Cecchet, F.; Rudolf, P.; Rapino, S.; Margotti, M.; Paolucci, F.; Baggerman, J.; Brouwer, A. M.; Kay, E. R.; Wong, J. K. Y.; Leigh, D. A., *J. Phys. Chem. B* **2004** (108) 15192.
5. Azehara, H.; Mizutani, W.; Suzuki, Y.; Ishida, T.; Nagawa, Y.; Tokumoto, H.; Hiratani, K., *Langmuir* **2003** (19) 2115.
6. Giessibl, F. J., *Reviews of Modern Physics* **2003** (75) 949.
7. Garcia, R.; Perez, R., *Surf. Sci. Rep.* **2002** (47) 197.
8. Martin, Y.; Williams, C. C.; Wickramasinghe, H. K., *J. Appl. Phys.* **1987** (61) 4723.
9. Albrecht, T. R.; Grutter, P.; Horne, D.; Rugar, D., *J. Appl. Phys.* **1991** (69) 668.
10. Giessibl, F. J., *Science (Washington, D. C., 1883-)* **1995** (267) 68.
11. Sasahara, A.; Kitamura, S.; Uetsuka, H.; Onishi, H., *J. Phys. Chem. B* **2004** (108) 15735.
12. Fukuma, T.; Kobayashi, K.; Matsushige, K.; Yamada, H., *Appl. Phys. Lett.* **2005** (87).
13. San Paulo, A.; Garcia, R., *Biophys. J.* **2000** (78) 1599.
14. Garcia, R.; San Paulo, A., *Physical Review B* **2000** (61) R13381.
15. Martinez, N. F.; Garcia, R., *Nanotechnology* **2006** (17) S167.
16. Cleveland, J. P.; Anczykowski, B.; Schmid, A. E.; Elings, V. B., *Appl. Phys. Lett.* **1998** (72) 2613.
17. Tamayo, J.; Garcia, R., *Appl. Phys. Lett.* **1998** (73) 2926.
18. Giessibl, F. J., *Physical Review B* **1997** (56) 16010.
19. Sader, J. E.; Jarvis, S. P., *Appl. Phys. Lett.* **2004** (84) 1801.

20. Sader, J. E.; Jarvis, S. P., *Physical Review B* **2006** (74) 195424.
21. Bammerlin, M.; Luthi, R., *Probe Microscopy* **1997** (1) 3.
22. Loppacher, C.; Bammerlin, M.; Guggisberg, M.; Battiston, F.; Bennewitz, R.; Rast, S.; Baratoff, A.; Meyer, E.; Guntherodt, H. J., *Appl. Surf. Sci.* **1999** (140) 287.
23. Fukui, K.; Onishi, H.; Iwasawa, Y., *Appl. Surf. Sci.* **1999** (140) 259.
24. Gotsmann, B.; Schmidt, C.; Seidel, C.; Fuchs, H., *European Physical Journal B* **1998** (4) 267.
25. Kobayashi, K.; Yamada, H.; Matsushige, K., *Appl. Surf. Sci.* **2002** (188) 430.
26. Jarvis, S. P.; Ishida, T.; Uchihashi, T.; Nakayama, Y.; Tokumoto, H., *Appl. Phys. A* **2001** (72) S129–S132.
27. Nishi, R.; Houda, I.; Sugawara, Y.; Morita, S., *Appl. Phys. A* **2001** (72) S93.
28. Hoogenboom, B. W.; Hug, H. J.; Pellmont, Y.; Martin, S.; Frederix, P.; Fotiadis, D.; Engel, A., *Appl. Phys. Lett.* **2006** (88).
29. Loppacher, C.; Bennewitz, R.; Pfeiffer, O.; Guggisberg, M.; Bammerlin, M.; Schar, S.; Barwich, V.; Baratoff, A.; Meyer, E., *Physical Review B* **2000** (62) 13674.
30. Bennewitz, R.; Foster, A. S.; Kantorovich, L. N.; Bammerlin, M.; Loppacher, C.; Schar, S.; Guggisberg, M.; Meyer, E.; Shluger, A. L., *Physical Review B* **2000** (62) 2074.
31. Anczykowski, B.; Gotsmann, B.; Fuchs, H.; Cleveland, J. P.; Elings, V. B., *Appl. Surf. Sci.* **1999** (140) 376.
32. Luthi, R.; Meyer, E.; Bammerlin, M.; Baratoff, A.; Howald, L.; Gerber, C.; Guntherodt, H. J., *Surf. Rev. Lett.* **1997** (4) 1025.
33. Fukuma, T.; Kobayashi, K.; Yamada, H.; Matsushige, K., *J. Appl. Phys.* **2004** (95) 4742.
34. Fukuma, T.; Ichii, T.; Kobayashi, K.; Yamada, H.; Matsushige, K., *J. Appl. Phys.* **2004** (95) 1222.
35. Trevethan, T.; Kantorovich, L., *Nanotechnology* **2004** (15) S44.
36. Kantorovich, L. N., *Journal of Physics-Condensed Matter* **2001** (13) 945.
37. Trevethan, T.; Kantorovich, L., *Nanotechnology* **2006** (17) S205.
38. Ichii, T.; Fukuma, T.; Kobayashi, K.; Yamada, H.; Matsushige, K., *Appl. Surf. Sci.* **2003** (210) 99.
39. Gotsmann, B.; Seidel, C.; Anczykowski, B.; Fuchs, H., *Phys. Rev. B: Condens. Matter* **1999** (60) 11051.
40. Binnig, G.; Quate, C. F.; Gerber, C., *Phys. Rev. Lett.* **1986** (56) 930.
41. McClelland, G. M.; Erlandson, R.; Chiang, S., In *Review of Progress in Quantitative Non-Destructive Evaluation*, Thompson, D. O.; Chimenti, D. E., Eds. Plenum: New York, 1987; Vol. 6, p 1307.
42. Meyer, G.; Amer, N. M., *Appl. Phys. Lett.* **1988** (53) 1045.
43. Meyer, G.; Amer, N. M., *Appl. Phys. Lett.* **1990** (57) 2089.
44. Sader, J. E.; Chon, J. W. M.; Chon, J. W. M.; Mulvaney, P., *Rev. Sci. Instrum.* **1999** (70) 3967.
45. Torii, A.; Sasaki, M.; Hane, K.; Okuma, S., *Meas. Sci. Technol.* **1996** (7) 179.
46. Cleveland, J. P.; Manne, S.; Bocek, D.; Hansma, P. K., *Rev. Sci. Instrum.* **1993** (64) 403.
47. Hutter, J. L.; Bechhoefer, J., *Rev. Sci. Instrum.* **1993** (64) 1868.
48. Burnham, N. A.; Chen, X.; Hodges, C. S.; Matei, G. A.; Thorenson, E. J.; Roberts, C. J.; Davies, M. C.; Tendler, S. J. B., *Nanotechnology* **2003** (14) 1.
49. Sader, J. E.; Chon, J. W. M.; Mulvaney, P., *Rev. Sci. Instrum.* **1999** (70) 3967.
50. Sader, J. E., *J. Appl. Phys.* **1998** (84) 64.

51. Sader, J. E.; Uchihashi, T.; Higgins, M. J.; Farrell, A.; Nakayama, Y.; Jarvis, S. P., *Nanotechnology* **2005** (16) S94.
52. Müller, D. J.; Sass, H.; Müller, S.; Büldt, G.; Engel, A., *J. Mol. Biol.* **1999** (301) 869.
53. Jarvis, S. P.; Tokumoto, H.; Yamada, H.; Kobayashi, K.; Toda, A., *Appl. Phys. Lett.* **1999** (75) 3883.
54. Jarvis, S. P.; Dürig, U.; Lantz, M. A.; Yamada, H.; Tokumoto, H., *Appl. Phys. A* **1998** (66) S211.
55. Ratcliff, G. C.; Erie, D. A.; Superfine, R., *Appl. Phys. Lett.* **1998** (72).
56. Revenko, I.; Proksch, R., *J. Appl. Phys.* **2000** (87) 526.
57. Fukuma, T.; Kimura, M.; Kobayashi, K.; Matsushige, K.; Yamada, H., *Rev. Sci. Instrum.* **2005** (76).
58. Fukuma, T.; Ichii, T.; Kobayashi, K.; Yamada, H.; Matsushige, K., *Appl. Phys. Lett.* **2005** (86) 034103.
59. Fukuma, T.; Kobayashi, K.; Matsushige, K.; Yamada, H., *Appl. Phys. Lett.* **2005** (86).
60. Higgins, M. J.; Polcik, M.; Fukuma, T.; Sader, J. E.; Nakayama, Y.; Jarvis, S. P., *Biophys. J.* **2006** (91) 2532.
61. Fukuma, T.; Jarvis, S. P., *Rev. Sci. Instrum.* **2006** (77).
62. Kobayashi, K.; Yamada, H.; Itoh, H.; Horiuchi, T.; Matsushige, K., *Rev. Sci. Instrum.* **2001** (72) 4383.

Chapter 4: The Effect of Solvent upon Molecularly Thin Rotaxane Film Formation

4.1 Introduction

In this chapter I discuss experiments on the growth and characterization of thin films of rotaxanes via the evaporation of a solvent. I explore the effects of the film deposition conditions upon rotaxane film formation and how the resulting film structures will impact potential rotaxane mobility. Specifically, I explore the effect on the molecular reconstruction of the solvent hydrogen bonding ability (section *4.5*) and of the surface concentration (i.e. molecular packing density - and in particular how this relates to the type of solvent used) (section *4.6*). The molecular type is varied to investigate the sensitivity of the self-assembly to changes in the molecular composition section *4.4*.

It has been discussed extensively in chapter *2*, section *2.3*, that many rotaxane types are known to be switchable in the solution phase.[1-4] Of course the breadth of possible applications is extended greatly if these molecules can also function at a solid interface. This chapter attempts to understand how the potential functionality of such interlocked molecules will be altered or inhibited by the interaction with the surface and by the conditions during film formation. As discussed in section *2.6*, there is existing evidence that solvent dependant co-conformational changes in interlocked molecules at surfaces have also been observed, illustrating the importance of the environment during deposition.[5]

It will be seen in section *4.5* that the distinct hydrogen-bonding networks seen in crystal structures of rotaxanes from certain solvents are reflected in the surface structure of films from these solvents as observed by AFM. Also tailoring the molecular type can be used to control the domain size and order – this will be seen to be inter-related to the information in chapter 6 where molecular-scale details will be discussed.

All of these parameters will strongly affect the potential functionality of rotaxanes. H-Bonding of neighbouring rotaxane molecules to each other would not be good for mobility of the rotaxane components. The molecules should be arranged into films

where the hydrogen-bonding interactions between neighbouring molecules are minimized so that they are not conformationally locked. The varying degree of order found by varying the molecular type is also discussed, in terms of a potential device and the order and addressability that would thus be required.

For the work described in this chapter I have focussed primarily upon simple non-shuttling rotaxanes, which are starting point for the study of more complicated and functional rotaxanes. In the solid state such molecules are usually immobilised by inter-molecular hydrogen bonding[6] and the knowledge gained here provides insight into whether or not the extra degrees of freedom associated with the molecules being at a surface may allow the occurrence of sub-molecular motion. The work described in this chapter has also been published in the Journal "Applied Surface Science".[7]

4.2 Sample preparation

4.2.1 Materials

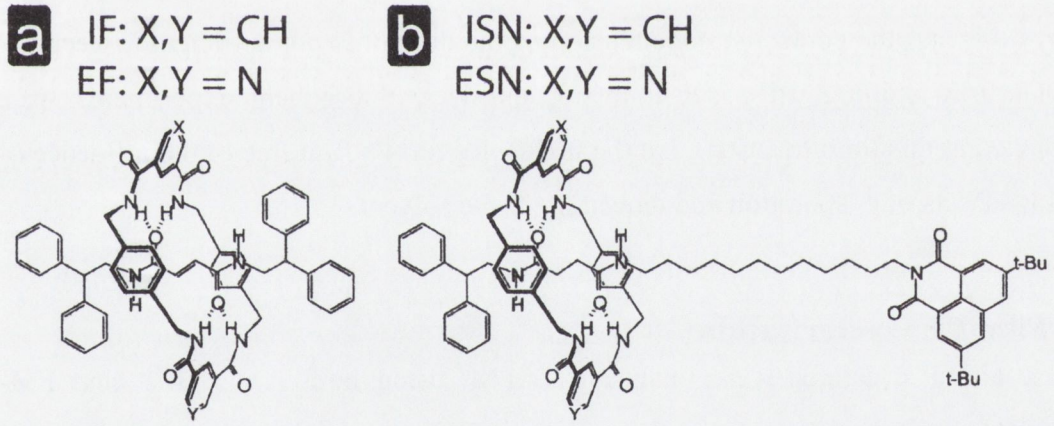


Figure 4.1: Rotaxane molecular structures of IF (Isophthalyl Fumaramide rotaxane), EF (Exo-pyridyl Fumaramide), ISN (Isophthalyl Succinamide-Naphthalimide Shuttle) and ESN (Exo-pyridyl Succinamide-Naphthalimide Shuttle).

In these experiments I investigated four related rotaxane molecules. The fumaramide rotaxanes (IF and EF) (Figure *4.1(a)*) have only one fumaramide station and a short chain length; the molecules are identical except for an (exo-)pyridyl group in the macrocycle of EF.[8] The remaining two molecules (ISN and ESN) (Figure *4.1(b)*) are rotaxane molecules, where the thread portion has two stations, in this case succinamide and naphthalimide stations, and similarly the molecules are distinguished by an (exo-)pyridyl feature on the macrocycle.[9, 10] These [2]rotaxanes are

electrochemically switchable. Acetone, Chloroform, Tetrahydrofuran (THF), Methanol and Dimethyl sulfoxide (DMSO), were used as solvents for the preparation of dilute rotaxane solutions. All solvents were HPLC grade.

4.2.2 Solvent evaporation times

To prepare the films on a freshly cleaved 10 mm x 10 mm HOPG substrate, a single drop of solution (rotaxanes in acetone, concentration approximately 1 μM) was deposited and the acetone solvent was allowed to evaporate slowly in a 500 cm^3 container with an atmosphere saturated with acetone vapour. The area per rotaxane at the surface was estimated to be around 2.1 nm^2 by using the rotaxane molecular dimensions.[11] These dimensions of the rotaxane reconstruction will be illustrated in chapter *5*, section *5.5.1*. A drop volume of 14 μL provided an even solvent distribution to the whole sample and with this volume any concentration less than $5x10^{-6}$ M gave sub-monolayer coverage of rotaxanes, as verified by AFM measurements. Optimisation of the method showed that a drop of 14 μL of acetone on a square 10 mm x 10 mm HOPG sample is at the upper limit of a stable droplet (above this and the contact surface tension of the droplet is not sufficient to keep the droplet from spilling off a substrate of this size). Subsequent experiments were conducted at this limit to ensure that the molecules form a film free of the influence of pulling effects of evaporation and dewetting of the solvent.

4.3 Film Characterisation

The resulting structures were imaged by AFM, using both AM-AFM[12] and FM-AFM[11, 13] for tip-sample distance regulation. By maintaining a consistent set of experimental parameters I was able to compare film height data from many different tip-sample combinations. In AM mode the phase between cantilever excitation and deflection detection was monitored to ensure that the tip-sample interaction was always in the attractive regime. Similarly in FM mode the tip-sample force was always attractive. Dynamic AFM techniques were employed exclusively in this study and a net attractive force between tip and sample was always maintained, to ensure that the weakly-physisorbed and flexible rotaxanes were not deformed by a strong tip-sample interaction or displaced by meniscus forces between tip and sample. Film heights of the imaged rotaxanes were consistent between the two modes.

Typical experimental parameters for all of the images in this chapter are as follows: (AM mode: Amplitude (A) = 16 nm, Set Point (S.P.) = 95%; FM mode: A = 10 nm, Frequency Shift (Δf) = -50 Hz). The AFM probes used in this experiment were Nanosensors PPP-EFM levers (typical characteristics: spring constant (k): 0.1 N/m, Resonance Frequency (f_0): 69 KHz, tip radius: 10 nm). An Asylum Research MFP-3D SA AFM was used for all images.

4.3.1 Surface coverage calculation

The surface coverage percentage was calculated by printing the image with a 200-point grid superimposed and counting the number of points intersecting with the rotaxane film.

4.4 Rotaxane Film morphology

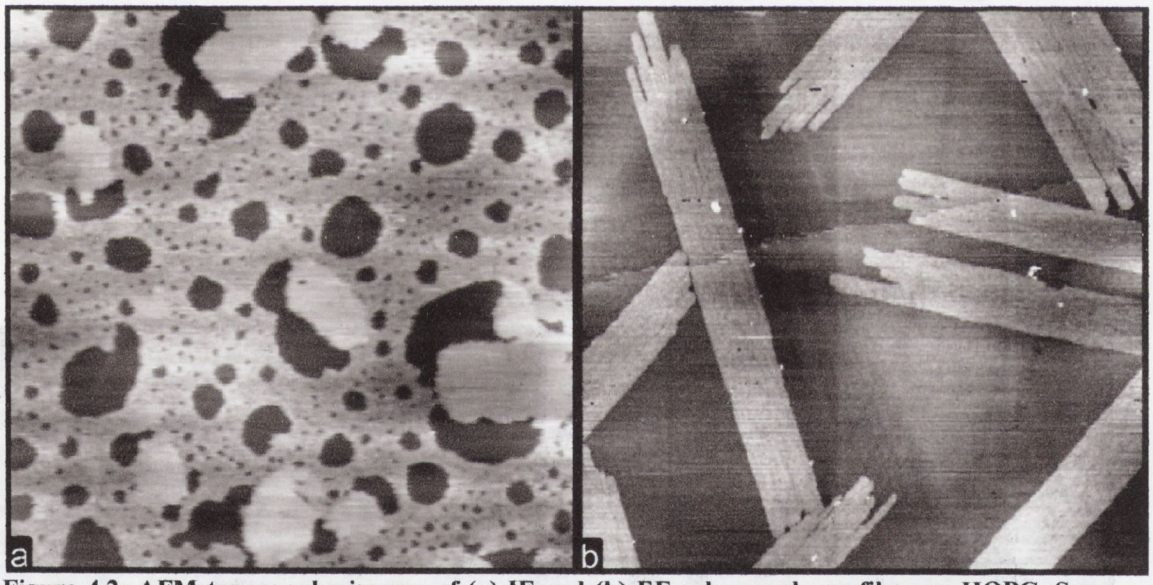


Figure 4.2: AFM topography images of (a) IF and (b) EF sub-monolayer films on HOPG. Scan sizes 2 µm.

The images in Figure *4.2* show typical film structures for sub-monolayer films of rotaxane molecules IF and EF respectively as deposited from acetone. Comparing the film structures of IF to its exo-pyridyl equivalent it can be seen that in the case of EF the angle between neighbouring domains is approximately 60° and from this result it can be said that the domains are preferentially oriented relative to each other according to the symmetry directions of the underlying graphite lattice. The only difference between the IF and EF molecules is the presence of the two external pyridyl groups on the macrocycle of EF, which are isophthaloyl groups in the case of

IF. The difference in film characteristics of the two molecules suggests that it is the presence of the external pyridyl group on the EF that causes the molecules to sit at preferred sites in a preferred orientation on the graphite surface. This could occur either by interaction of the exopyridyl group with the surface directly, or by the interaction of neighbouring exopyridyl groups thus aligning the molecules and favouring their interaction with the surface in a specific manner. The crystal structure for both molecules is almost identical, and there is a π-π interaction between neighbouring isophthaloyl/exopyridyl groups. The relevant distances are very similar and there is nothing in the solid-state geometries to suggest any significant difference in intermolecular interactions as a result of this difference in the neighbouring group type. Therefore it would seem that the dominant interaction is not between neighbouring exopyridyl groups, but between the exopyridyl group and the graphite surface. The nature of this interaction could be π/π stacking or a lone-pair/π interaction. Since it is preferential that the rotaxane be attached to a surface via the macrocycle (as discussed in section *2.6.1*), it is an important result that in this case registry with the surface occurs because of a slight change in the chemical composition of the macrocycle.

4.4.1 Morphology of other rotaxane functionalities

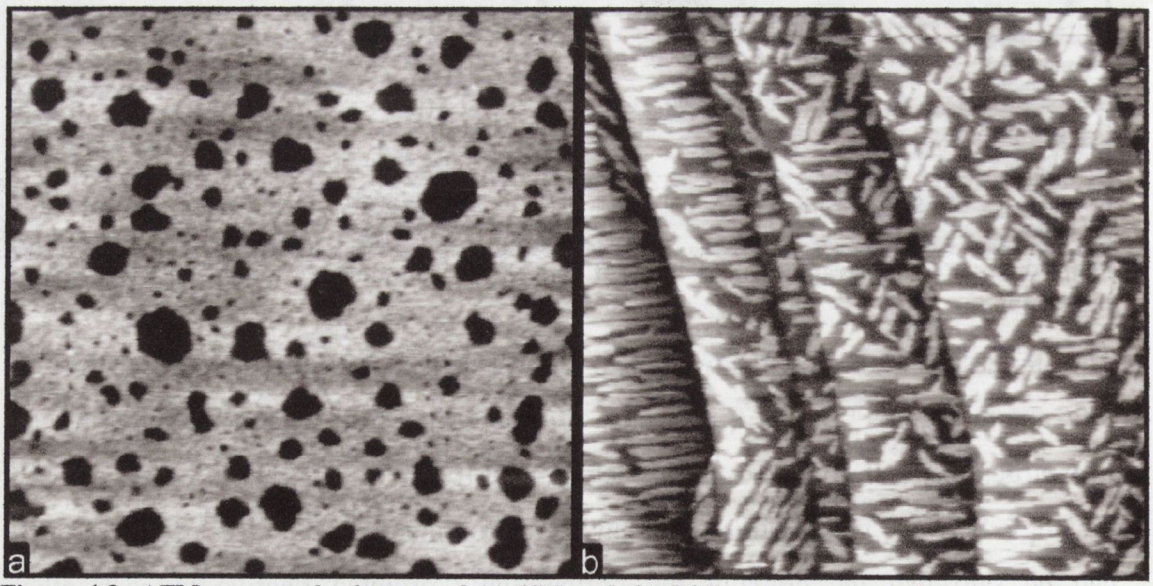


Figure 4.3: AFM topography images of (a) ISN and (b) ESN sub-monolayer films on HOPG. Scan sizes 1 μm.

The images in Figure *4.3* show typical film structures for ISN and ESN as deposited from acetone. The differences between the morphologies of the ISN and ESN are

analogous to those between IF and EF. This means that the pridyl group is directing the alignment of ESN in the same manner as the EF molecule. It is clear that the long thread of the ESN molecule and the rotaxane's resulting decrease in symmetry and increase in size has resulted in a greater lattice mismatch between the film and the graphite surface since the molecular domains are so much smaller in the case of ESN.

4.5 Effect of solvent basicity on rotaxane film structure

To investigate the effect of the solvent used during rotaxane deposition I measured the height of the sub-monolayer films formed for each solvent, focussing on the EF molecule because of the large and uniform domain size and the fact that the molecule is anchored to the surface via its exo-pyridyl moiety. This film quality allows the best chance of observing film structure differences between samples.

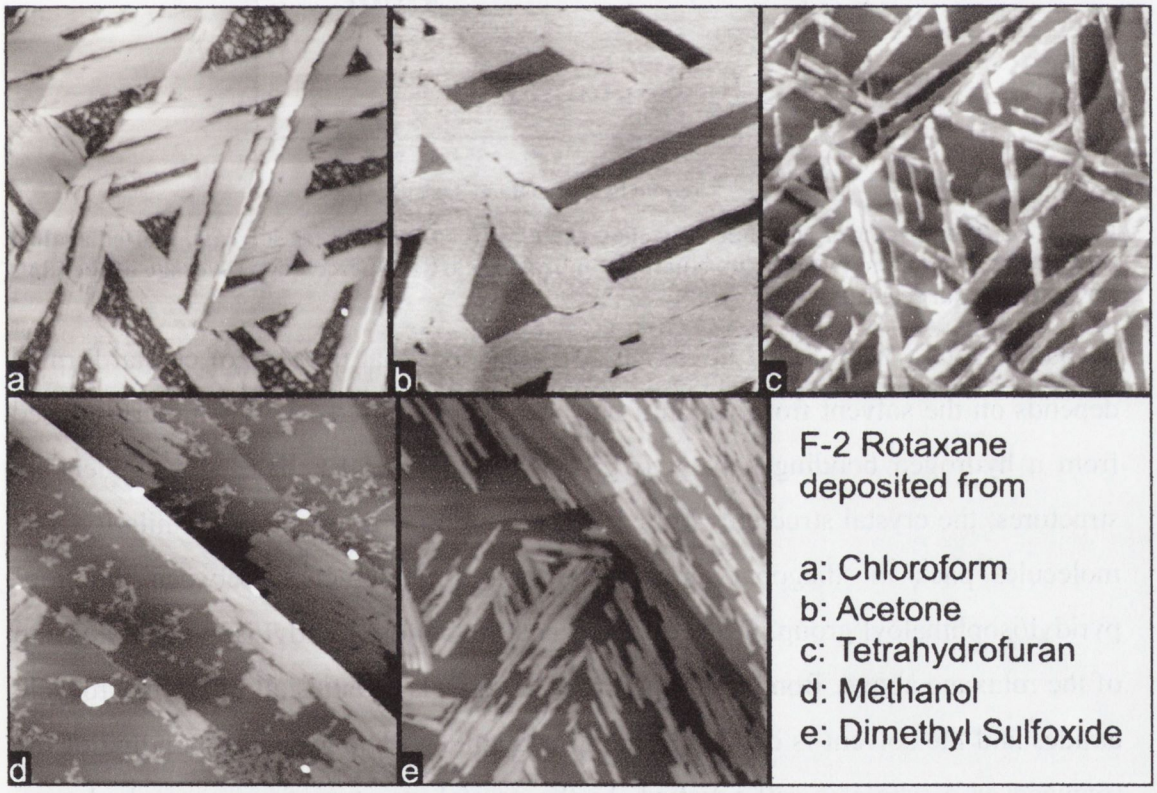


Figure 4.4: AFM topography images of EF sub-monolayer films on HOPG as deposited from a range of solvents. Scan sizes 1 μm.

In Figure *4.4* are typical images of sub-monolayer films of the EF Rotaxane as deposited from five different solvents with a range of hydrogen-bond basicity (ß), which is a measure of the ability of the solvent to accept hydrogen bonds, with solvents of high ß being better hydrogen-bond acceptors. Irrespective of the solvent used molecular assembly with substrate registry was observed. To measure the height

of the rotaxane films, cross-sections of the images were taken. The sections were locally plane-fitted to subtract the slope evident in most AFM images to ensure correct measurement of the height. On average 10 measurements of the height were taken per solvent of deposition. Figure *4.5* shows the average height measured by AFM, plotted with the ß-value of each solvent of deposition. There is a clear change in the height of the sub-monolayer film with increasing hydrogen-bond basicity of the solvent. This difference in height suggests that for low-ß value solvents the molecules adopt a different arrangement to the molecules deposited from higher-ß solvents.

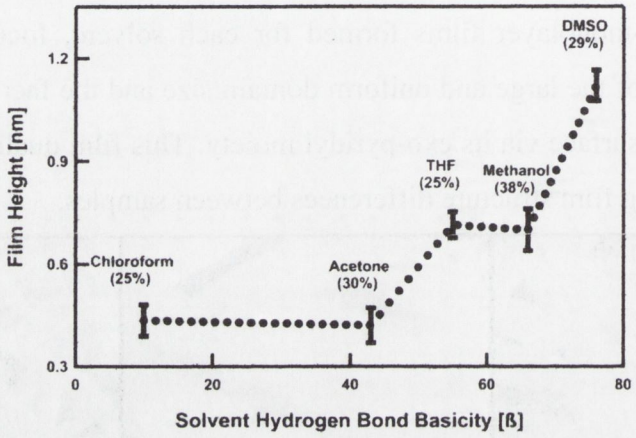


Figure 4.5: Film height of rotaxane IF monolayer films for five different solvents, plotted against solvent hydrogen-bond basicity (β). Numbers in brackets are the percentage coverage of the films for those measurements.

It has previously been found in the case of Rotaxanes that the type of crystal formed depends on the solvent from which it has been recrystallised.[6, 14] When recrystallised from a hydrogen bonding solvent (e.g. DMSO), IF and EF have almost identical structures; the crystal structures in Figure *4.6(a)* and *(b)* illustrate this similarity. The molecules pack in 'diagonal' columns with a π-π interaction between the 'top' pyridyl/isophthaloyl group of one rotaxane and the bottom pyridyl/isophthaloyl group of the rotaxane above. Bonding to the thread carbonyls satisfies all of the macrocycle amides and the solvent is bonded to the thread amides. The hydrogen bonding of the rotaxane as a whole is self-satisfied. In the crystal structure from a non-hydrogen bonding solvent, as shown in Figure *4.6(c)*, the IF molecule has two out of four macrocycle amides bonding to the thread and the other two bonding to the next rotaxane. In this manner the crystal consists of rows of molecules connected by hydrogen bonding. The molecule has a distorted shape especially along the rows of inter-molecular hydrogen-bonding. In the case of the EF molecule, as adsorbed to the HOPG surface, the pyridyl groups are interacting with the surface. The inter-

molecular hydrogen-bonding leads to a significant change in the film height since the plane of the macrocycle will be closer to being parallel to the HOPG plane in order to hydrogen-bond to its neighbouring rotaxane.

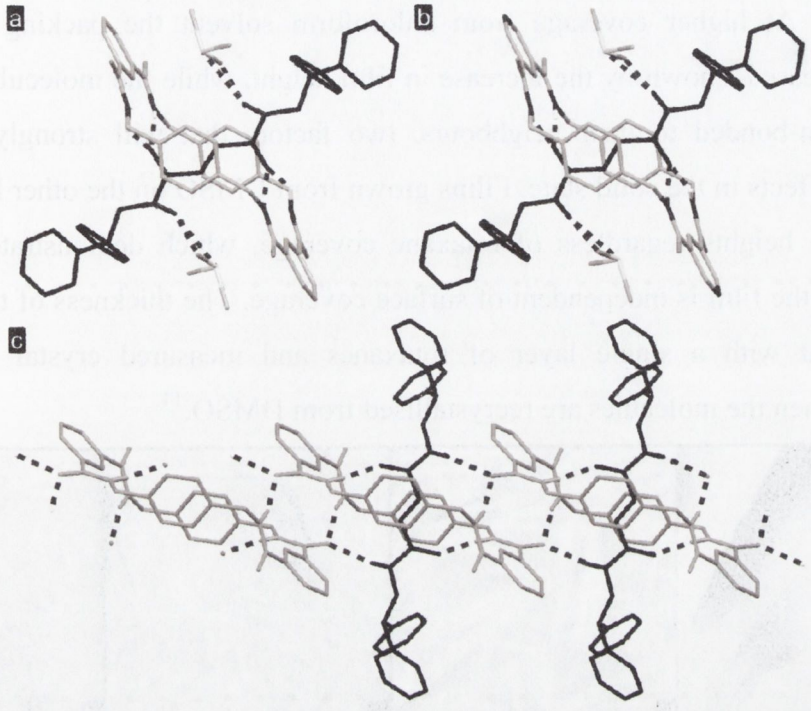


Figure 4.6: Rotaxane crystal structures; (a) IF as recrystallised from DMSO, (b) EF as recrystallised from DMSO , (c) IF as recrystallised from CHCl3/MeCN (non hydrogen-bonding solvent).

The observed differences in height are direct evidence that the solvent used in the rotaxane deposition influences the final orientation and hydrogen-bonding state of the rotaxane thin film. A rotaxane that is not hydrogen-bonded to neighbouring molecules will have increased mobility of its sub-molecular components (thread and macrocycle) relative to each other. Analysis of the energetics of a Fumaramide rotaxane system in the solid state by Biscarini *et al.* has also demonstrated this to be true.[6]

4.6 Effect of surface coverage on rotaxane film structure

Figure *4.7* shows a rotaxane thin film as deposited from chloroform solution at surface coverages of 20% (a), 50% (b), 78% (c) and 95% (d). Figure *4.8* shows a rotaxane thin film as deposited from DMSO solution at surface coverages of 14% (a), 29% (b), 55% (c) and 88% (d). Figure *4.9* shows the film heights for the different surface coverages. Clearly another variable in the film height observed by AFM is the packing density of the rotaxanes. Rotaxanes are large and flexible molecules and as a result of these characteristics a large lattice mismatch can be accommodated in these

epitaxial films. This was apparent from the fact that substrate registry occurred for all solvents and is further demonstrated here by the dramatic difference in film structure between high and low coverages, from chloroform solution, while substrate registry is maintained. At higher coverage from chloroform solvent the packing density is greatly increased, shown by the increase in film height, while the molecules will still be hydrogen-bonded to their neighbours, two factors that will strongly disfavour switching effects in the solid state. Films grown from DMSO on the other hand, show similar film heights regardless of rotaxane coverage, which demonstrates that the structure of the film is independent of surface coverage. The thickness of these layers is consistent with a single layer of rotaxanes and measured crystal interplanar distances when the molecules are recrystallised from DMSO.[14]

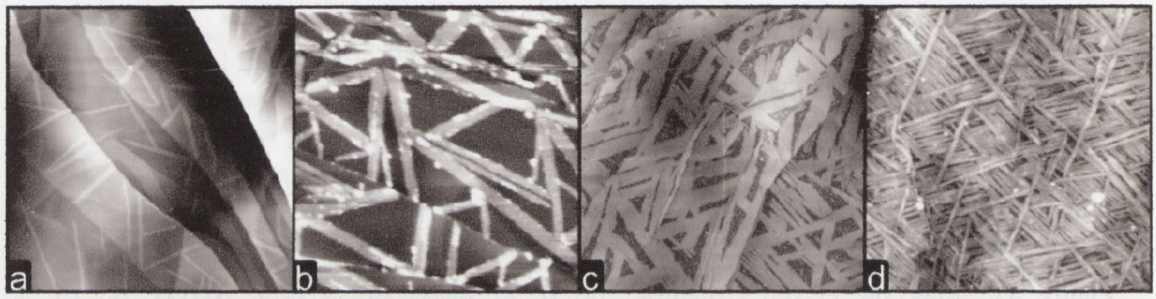


Figure 4.7: AFM topography images of EF sub-monolayer films on HOPG as deposited from chloroform for a range of surface coverages; (a) 20%, (b) 50%, (c) 78% and (d) 95%. Scan sizes: (a), (c), (d) 2 μm, (b) 1 μm.

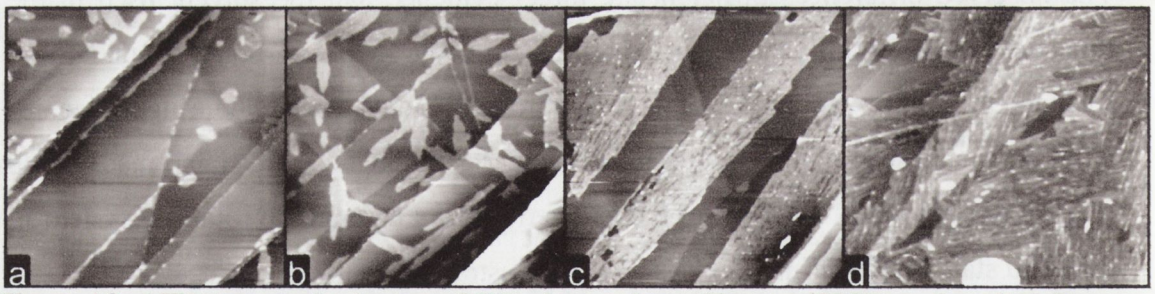


Figure 4.8: AFM topography images of EF sub-monolayer films on HOPG as deposited from DMSO for a range of surface coverages; (a) 14%, (b) 29%, (c) 55% and (d) 88%. Scan sizes 2 μm.

It is clear that one cannot ignore the solvent of deposition. Actually it can be said that to favour the occurrence of switching effects in such rotaxane thin films it would be best to use a solvent with high hydrogen-bond basicity such as DMSO. A commonly-used solvent in rotaxane surface experiments, where the method of deposition has been drop-casting, is acetone.[6, 11, 15, 16] In hindsight this solvent may not have been the best choice because I have shown that its use results in thin films with rows of rotaxanes that are hydrogen-bonded in a way not conducive to sub-molecular motion. This inter-molecular hydrogen-bonding may even have been an important factor in the

concerted motion of rotaxanes under the influence of an AFM tip, which resulted in the formation of periodically spaced dots and which is being exploited as a molecular nano-recording device.[15] These experiments have illustrated the importance of solvent choice for the drop-casting technique, and I have directly observed with AFM controlled conformational differences in rotaxane structure based upon the deposition solvent.

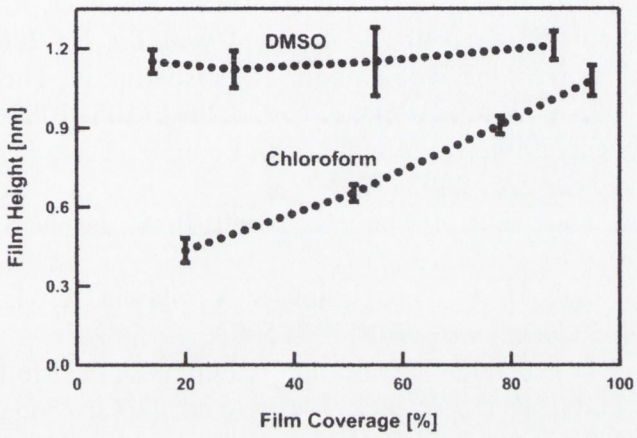


Figure 4.9: Film height of rotaxane IF monolayer films for chloroform and DMSO, plotted as a function of surface coverage.

4.7 Conclusions

I have investigated differences in the structure of molecularly-thin rotaxane films deposited by solvent evaporation as a result of small changes in the molecular structure, as a function of hydrogen-bond basicity of the deposition solvent and as a function of the surface coverage. The addition of exopyridyl moieties to the rotaxanes resulted in uniform domains having orientation corresponding to the underlying substrate lattice while a larger, less symmetric molecule resulted in a greater lattice mismatch and smaller domain sizes. When a solvent is a poor hydrogen-bond acceptor (has low hydrogen-bond basicity (ß)) the rotaxane film will be greatly different in structure when compared to a film formed from a good hydrogen-bond acceptor, since molecules in the former will be hydrogen-bonded to their neighbours rather than self-satisfied. I have demonstrated the importance of solvent choice in the 'wet' formation of rotaxane thin films because of the effect of the solvent on the thread-macrocycle interaction, and that a good hydrogen-bond accepting solvent such as DMSO will result in films more likely to favour the occurrence of sub-molecular switching events in rotaxanes.

4.8 References

1. Sauvage, J. P.; DietrichBuchecker, C.; Eds., *Molecular Catenanes, Rotaxanes and Knots*. Wiley-VCH: Weinheim, 1999.
2. Balzani, V.; Credi, A.; Raymo, F. M.; Stoddart, J. F., *Angewandte Chemie-International Edition* **2000** (39) 3349.
3. Altieri, A.; Bottari, G.; Dehez, F.; Leigh, D. A.; Wong, J. K. Y.; Zerbetto, F., *Angewandte Chemie-International Edition* **2003** (42) 2296.
4. Leigh, D. A.; Morales, M. Á. F.; Pérez, E. M.; Wong, J. K. Y.; Saiz, C. G.; Slawin, A. M. Z.; Carmichael, A. J.; Haddleton, D. M.; Brouwer, A. M.; Buma, W. J.; Wurpel, G. W. H.; León, S.; Zerbetto, F., *Angew. Chem. Int. Ed.* **2005** (44) 3062.
5. Cavallini, M.; Lazzaroni, R.; Zamboni, R.; Biscarini, F.; Timpel, D.; Zerbetto, F.; Clarkson, G. J.; Leigh, D. A., *J. Phys. Chem. B* **2001** (105) 10826.
6. Biscarini, F.; Cavallini, M.; Leigh, D. A.; Leon, S.; Teat, S. J.; Wong, J. K. Y.; Zerbetto, F., *J. Am. Chem. Soc.* **2002** (124) 225.
7. Farrell, A. A.; Kay, E. R.; Bottari, G.; Leigh, D. A.; Jarvis, S. P., *Appl. Surf. Sci.* **2007** (253) 6090.
8. Gatti, F. G.; Leigh, D. A.; Nepogodiev, S. A.; Slawin, A. M. Z.; Teat, S. J.; Wong, J. K. Y., *J. Am. Chem. Soc.* **2001** (123) 5983.
9. Brouwer, A. M.; Frochot, C.; Gatti, F. G.; Leigh, D. A.; Mottier, L.; Paolucci, F.; Roffia, S.; Wurpel, G. W. H., *Science (Washington, D. C., 1883-)* **2001** (291) 2124.
10. Altieri, A.; Gatti, F. G.; Kay, E. R.; Leigh, D. A.; Martel, D.; Paolucci, F.; Slawin, A. M. Z.; Wong, J. K. Y., *J. Am. Chem. Soc.* **2003** (125) 8644.
11. Farrell, A. A.; Fukuma, T.; Uchihashi, T.; Kay, E. R.; Bottari, G.; Leigh, D. A.; Yamada, H.; Jarvis, S. P., *Physical Review B* **2005** (72).
12. Garcia, R.; Perez, R., *Surf. Sci. Rep.* **2002** (47) 197.
13. Albrecht, T. R.; Grutter, P.; Horne, D.; Rugar, D., *J. Appl. Phys.* **1991** (69) 668.
14. *Crystallographic data (excluding structural factors) for FR as crystallized from DMSO and MeCN can be found in the Cambridge Crystallographic Database, supplementary publication numbers CCDC-157383 and CCDC-160650 respectively.*
15. Cavallini, M.; Biscarini, F.; Leon, S.; Zerbetto, F.; Bottari, G.; Leigh, D. A., *Science* **2003** (299) 531.
16. Moulin, J. F.; Kengne, J. C.; Kshirsagar, R.; Cavallini, M.; Biscarini, F.; Leon, S.; Zerbetto, F.; Bottari, G.; Leigh, D. A., *J. Am. Chem. Soc.* **2006** (128) 526.

Chapter 5: Quantitative conservative and dissipative force imaging of rotaxanes at the meso and molecular scale

5.1 Introduction

This chapter discusses the first molecular-scale investigation of an ordered rotaxane thin film. In Chapter 4 the importance of film preparation parameters in producing films with properties conducive to surface functionality was discussed. As part of that work I showed how simple variations in the molecular structure vastly affect the morphology of the resulting domains in the film. One of these film types – the exopyridyl fumaramide molecule, had the highest degree of meso-scale order of the set, from which it would follow that the order at the molecular scale would be good also. Molecular-scale investigation of rotaxanes was desirable to help assess potential functionality and order, and the EF molecule seemed to be the most promising candidate for such experiments.

The importance of ordering and addressability in device formation has been discussed throughout this thesis. Interestingly in this case the order is of use because it enables easier molecular-scale investigations. The specific results in this chapter, the measured reconstruction (section *5.5.1*), tell us that at the molecular level the films are ordered, and this order can be increased by adding energy to the system, i.e. annealing. The EF molecule is in fact switchable by UV light (although no shuttling takes place, only increased rates of rotation; as discussed in section *2.4.1*). Other similar benzylic amide rotaxanes can have different kinds of switching behavior (section *2.4.4*),[1-3] and from the results of the simple molecule used in this chapter we may predict some aspects of their behaviour on a surface. In fact some of the data in this chapter is used to help calculate the reconstruction of a more complicated rotaxane shuttle studied in chapter 6 (the reconstruction is illustrated in Figure *6.3*, section *6.6*). In the solid-state such molecules are usually immobilised in a fixed conformation due to intermolecular hydrogen bonding.[4] These measurements help determine if the potential switching effects will be restricted at a surface also despite the extra degrees of freedom relative to the solid state.

The molecular-scale information is first measured in UHV conditions (section *5.5*) by FM-AFM and I later extend this technique for use in ambient conditions (sections *5.6-5.10*). FM-AFM is shown to be a powerful tool for ambient exploration of organic films. The molecular-scale dissipation signal that was also measured for the first time in ambient conditions is promising as a potential technique for switching detection. This idea is further developed in chapter 6 (sections *6.8-6.9*). The dissipation (as discussed in section *3.3.3*) is a barometer for molecular flexibility (i.e. degrees of freedom) at surfaces. The development of dissipation imaging in ambient conditions on this model rotaxane system provides the opportunity to study externally stimulated sub-molecular motion at the local molecular level simultaneously with topography in this practical environment.

At the time of obtaining the UHV high-resolution experiments discussed in this chapter the only means of accessing such resolution of soft organic molecules was in a UHV FM-AFM system. This is unless the molecules are small enough that a thin film can be investigated with STM (i.e. thin enough that a current can pass through a film), which is not the case for these rotaxanes. The problems associated with ambient AFM (discussed in section *3.3*, and *5.2* below) had not yet been addressed sufficiently. The modification and qualification of an AFM for high-resolution observations of rotaxanes, including FM mode and Magnetic activation, were obviously not to be under taken blindly. It was unclear at the offset of this work if the high-resolution structure of the EF molecule would actually be observable at all. This is why the need was there for UHV experiments – so as not to test a developing technique on an unknown system. So the rotaxane films at this time had the double purpose of measuring the effectiveness of the ambient AFM setup, while being used to test the rotaxane functionality with AFM. The work described in this chapter has also been published in the Physical Review.[5]

5.2 Imaging in ambient vs UHV conditions – challenges overcome during this work

This chapter also considers the use of Ambient AFM in the sense of evaluating its worth as a tool for quantitatively measuring interaction forces and energy transfer (i.e.

degrees of freedom), as well as discussing the potential for use as an investigative tool for fragile biological and other soft samples.

Real world chemical and biological applications require operation in air or liquid environments. In the liquid environment, where meniscus forces are not present, the FM-AFM technique is being adopted.[6-9] In ambient conditions the presence of any native water layer limits the imaging resolution and resolution of the full range of the force interaction, although some FM-AFM experiments in air have been presented.[10, 11]

Recently Sasahara *et al.* imaged oxygen-atom vacancies as depressions in oxygen atom rows in a controlled dry N_2 environment after back-filling of a UHV chamber.[12] Fukuma *et al.* also imaged a hydrophobic alkanethiol SAM with true-molecular resolution.[13] Hölscher *et al.* used the constant excitation FM-AFM method to quantify the force in ambient conditions valid for large cantilever oscillation amplitudes.[14, 15] Using the related dynamic technique of AM-AFM with ~ 1 nm cantilever oscillation amplitudes in the attractive force regime, Anselmetti *et al.* reported single molecular resolution of a hexagonal packed intermediate protein layer.[16] By monitoring the Q-factor of the cantilever as a function of tip-sample distance an indication of the energy dissipation was provided. These other works listed here represent the only other high resolution FM-AFM and dynamic AFM studies carried out in ambient conditions to this date to the best of my knowledge.

I show that an FM-AFM experiment carried out in ambient conditions can achieve comparable results to an FM-AFM experiment carried out in UHV. I discuss the important information that can be obtained with the technique in relation to the specific system of rotaxane molecules. This information includes qualitative imaging, high-resolution imaging, exact determination of the force irrespective of the oscillation amplitude and quantitative energy dissipation imaging at different length scales.

5.3 Experiment

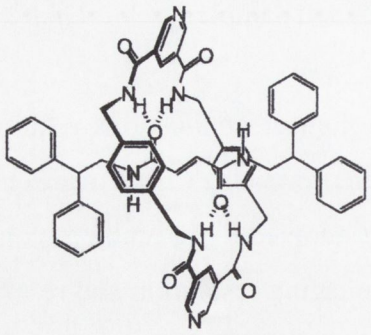


Figure 5.1: Molecular structure of exopyridyl fumaramide rotaxane (EF).

The synthesis of fumaramide rotaxane molecules has been described in Chapter *2*, section *2.4*, and the exopyridyl version used in this study (EF - as shown in figure *5.1*) was prepared by an analogous method.[17] Samples were prepared by dropping from acetone solution (HPLC grade, Aldrich). 0.005 mM solutions of exopyridyl fumaramide rotaxane were dropped (14 $\mu l/cm^2$) onto a freshly cleaved HOPG surface (ZYA quality, NT-MDT) to give approximately one monolayer surface coverage. As discussed in Chapter *4*, section *4.2.2*, the acetone solvent was allowed to evaporate slowly in a 500 cm^3 container with an atmosphere saturated with acetone vapour.

A commercially available FM-AFM (JEOL JSPM-4500) was used for UHV imaging (base pressure: about 1 x 10^{-7} Pa). It was modified so that the original frequency shift detector was replaced with a newly-developed frequency modulation detector.[18] A highly-doped *n*-Si cantilever (Nanosensors: NCH) with a resonance frequency of about 300 kHz and a nominal spring constant of 40 N/m was used for FM-AFM imaging. The *Q* factor measured under UHV conditions was about 30,000. After preparation the sample was immediately placed into the UHV chamber. For annealing the sample was removed and annealed in air at 150° C for two hours and re-introduced to the UHV chamber.

The modified Asylum MFP-3D AFM, as discussed in section *3.5* was used for imaging in ambient conditions, operated in FM-AFM mode with piezo activation, or in the case of the high-resolution imaging magnetically activated cantilevers (MAD-Mode).[19] Magnetic activation is discussed in section *3.4.2*, and is implemented here for the cleaner cantilever oscillation response compared to piezo activation, which makes FM-AFM easier to implement. Using the same Nanosensors NCH cantilevers

as above a magnetic particle of NdFeB (with dimensions around 20 microns) was attached with epoxy to the end of the backside of the cantilever. After attachment the resonance of the lever was typically reduced to about 50 kHz. The Q-factor in ambient conditions was around 500. The home-built piezo tube scanner discussed in section *3.4.4* was also used for high resolution imaging.

All FM-AFM measurements were performed in the constant frequency shift mode, where the negative frequency shift of the cantilever resonance frequency (Δf) induced by the tip sample interaction was kept constant during FM-AFM imaging. The cantilever is vibrated at constant amplitude, where the vibration amplitude of the cantilever (a) was kept constant by adjusting the amplitude of a cantilever excitation signal A_{exc}. In this excitation mode, energy dissipation caused by the tip-sample interaction can be calculated from the additional increase of A_{exc}.[20] Thus, the dissipation image was obtained as a two-dimensional map of A_{exc}.

5.4 Meso-scale imaging in UHV and ambient conditions

Figure *5.2(a)* shows an FM-AFM image of a thin film of expyridyl fumaramide rotaxane on HOPG. The orientation of the domains according to the lattice direction of the substrate again shows that the molecule grows epitaxially on graphite. After annealing (Figure *5.2(b)* it can be seen that the domain edges are straight and that domains are more clearly defined. The increased uniformity of the surface indicates that the energy provided by the annealing process has resulted in rearrangement of the molecules in a lower energy configuration. Figure *5.2(c)* demonstrates that the shape of the domains can also be evaluated by FM-AFM imaging in air.

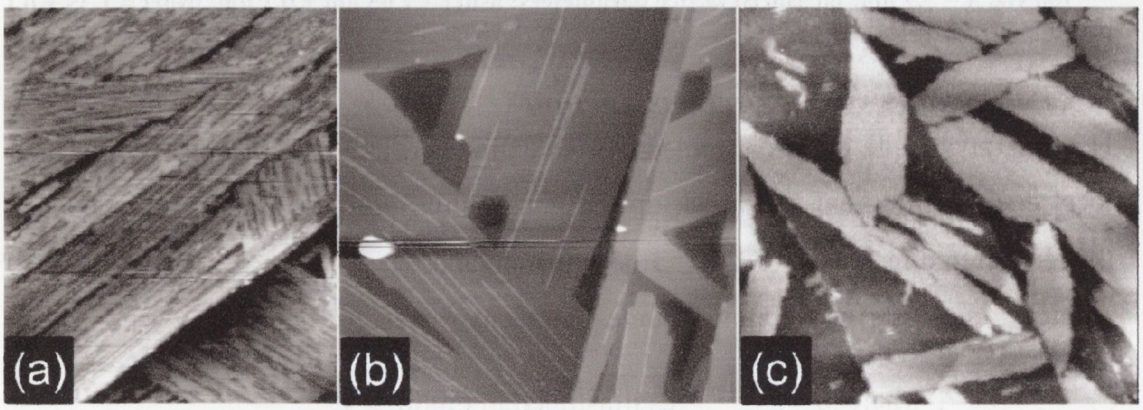


Figure 5.2 Meso-scale FM-AFM images of an EF thin film on HOPG (a) in UHV before annealing (464 nm x 558 nm, cantilever: Nanosensors NCH, Δf = - 15 Hz, a = 8 nm), (b) in UHV

after annealing (500 nm x 500 nm, cantilever: NCH, Δf = - 20 Hz, a = 8 nm), (c) in ambient conditions no annealing (500 nm x 500 nm, cantilever: Nanosensors EFM, Δf = - 25 Hz, a = 9.6 nm, Q = 154).

5.5 Molecular-scale imaging in UHV conditions

Molecular-scale topographic images of the un-annealed sample are shown in Figures *5.3(a)-(c)*. Individual molecules in the rows can often be resolved, however no periodic intermolecular distance is found along the rows (stripes in the image) and the rows are also unevenly spaced. The molecules are in a somewhat disordered non-equilibrium arrangement. In the case of the annealed sample (Figure *5.3(d)*), there is strong periodicity in both directions. This increase in long and short-range order is typical of the annealing process.

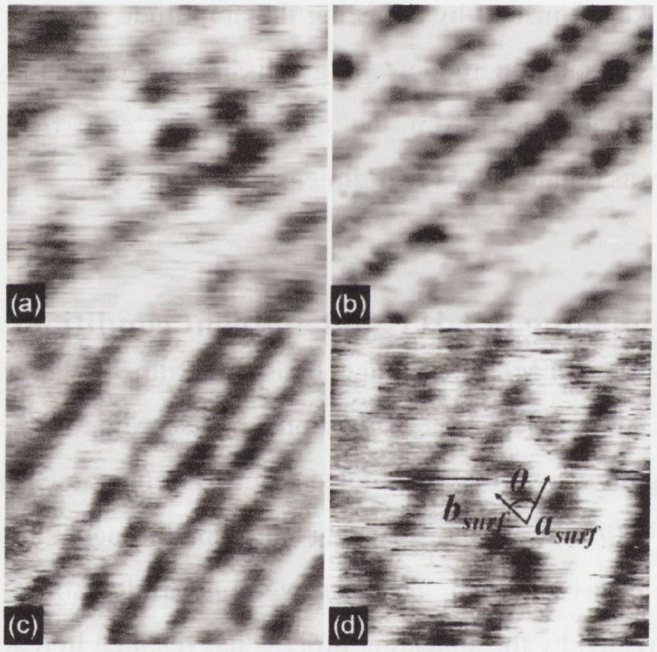


Figure 5.3: Molecular-scale UHV FM-AFM images of an EF thin film on HOPG. (a), (b), (c) Before annealing and (d) annealed sample, [(a): 9 nm x 9 nm, Δf = - 150 Hz, a = 6.5 nm, (b): 9 nm x 9 nm, Δf = - 150 Hz, a = 6.5 nm, (c): 9 nm x 9 nm, Δf = - 170 Hz, a = 6.5 nm, (d): 9 nm x 9 nm, Δf = - 180 Hz, a = 5.9 nm; measured lattice parameters: asurf = 1.65 nm ± 0.1 nm, bsurf = 1.35 ± 0.1 nm, θ = 70° ± 2°].

5.5.1 Rotaxane surface reconstruction

Heating the sample gives the molecules the extra energy required to move from their local energy minimum and break up the non-equilibrium packing structure. In fact, the measured dimensions of $a_{surf} = 1.65 \pm 0.1$ nm and $b_{surf} = 1.35 \pm 0.1$ nm with $\theta = 70°$ strongly suggests a commensurate molecular reconstruction of the form: $\begin{bmatrix} a_{surf} \\ b_{surf} \end{bmatrix} = M \begin{bmatrix} a \\ b \end{bmatrix}$, where $M = \begin{bmatrix} 7 & 0 \\ -1 & 6 \end{bmatrix}$ as illustrated in Figure *5.4*.

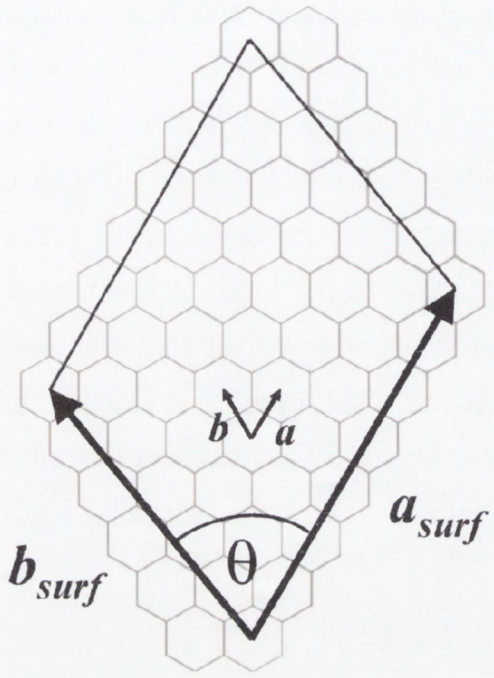


Figure 5.4: Apparent equilibrium reconstruction of the EF film on HOPG after annealing with parameters: a_{surf} = 1.65 nm, b_{surf} = 1.37, θ = 68°.

Strong intermolecular interactions in a closely packed film are restrictive to sub-molecular motion so it is not necessarily a good thing that the film be so well ordered and it is useful that we are able to access the many non-equilibrium film-structures shown in *5.3(a)-(c)*. The reconstructions measured in this work do not correspond to any of the crystal planes measured by X-Ray diffraction in bulk crystals.[21]

5.6 Molecular-scale imaging in air



Figure 5.5: Molecular-scale ambient FM-AFM topography image of EF thin film on HOPG (70 nm x 70 nm, cantilever: Nanosensors NCHR + magnet, a = 10.8 nm, Δf = - 35 Hz).

Figure *5.5* is a 70 x 70 nm image taken in ambient conditions, which shows clear molecular-scale features and has been chosen because it shows two neighbouring domains and therefore true structure, as opposed to periodic noise. The film structure dimensions are consistent with those measured in UHV for the un-annealed sample. Despite the lower Q-factor of the cantilever in air (500) compared to vacuum (~30,000), the presence of a liquid layer and contamination from long-chain hydrocarbons always present in ambient conditions, the resolution is still very high. The tip can move through the liquid layer while imaging the film, and any surface contamination must only be loosely bound and does not affect the imaging. The FM-AFM technique should thus be useful for the many kinds of study where high resolution is desirable.

5.7 Quantitative force measurements in ambient conditions

In ambient conditions the native layer of water adsorbates is often a problem for AFM techniques. "Contact mode", while allowing exact determination of the force, suffers from "jump-to-contact" instabilities (caused when the force gradient is higher than the cantilever stiffness) and adhesion instabilities (caused by a water meniscus between the tip and the local sample area). Dynamic AFM systems, as discussed in section *3.3*, can be used to overcome these instabilities. "Intermittent-contact mode" can overcome these obstacles with large amplitudes and stiffer cantilevers, however unambiguous determination of the force is difficult with this technique.[22] The FM method with constant amplitude has the same advantages but allows recovery of the force, as has been demonstrated in liquid and UHV environments, and discussed in section *3.3.2*.[23, 24] Furthermore, in the FM method the attractive and repulsive force regions are easily distinguished which allows for exact control of the force. A portion of the attractive part of the force vs. distance curve for a tip with a magnetically activated cantilever in ambient conditions is shown in Figure *5.6*. The force has been calculated from the frequency shift using the method of Sader and Jarvis,[25] (section *3.3.2*). The dissipation is also calculated to give quantitave values, using the method discussed in (section *3.3.3*). The force curve clearly shows that jump-to-contact instabilities do not occur and the retract curve (not shown for clarity) follows the approach exactly (i.e. no adhesion from the water layer occurs) and therefore we have shown that with this technique we can stably measure the force even in ambient conditions.

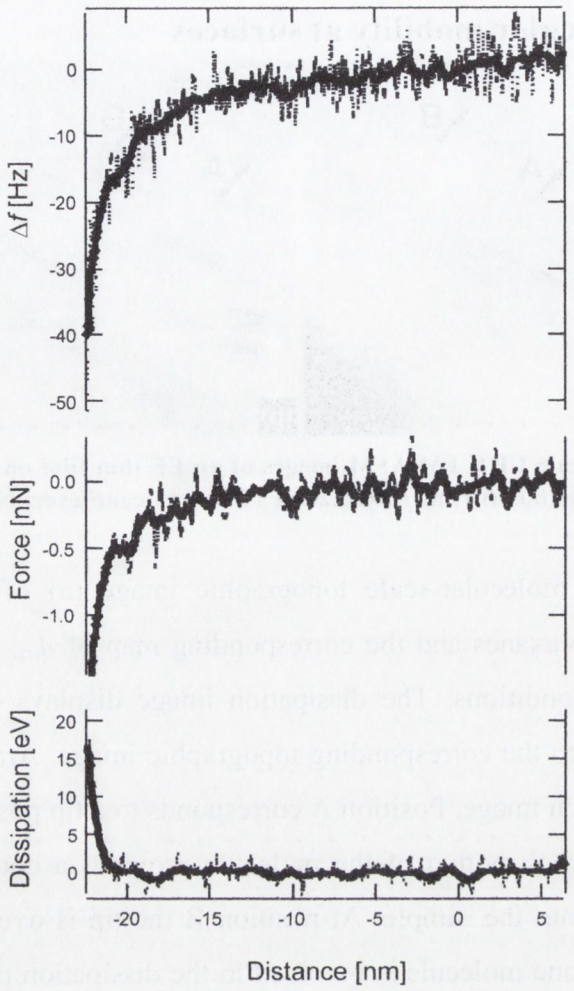


Figure 5.6: Typical frequency, force and dissipation vs. tip-sample distance curves in ambient conditions, dots: raw data, line: smoothed data (Cantilever: NCHR + magnet, Q = 510, a = 8.9 nm).

5.8 Energy dissipation in FM-AFM

It is extensively discussed in section *3.3.3* how the disordered or loose packing commonly found in organic thin films (and hence their stability against the tip-sample interaction force) has a strong influence on the contrast formation in energy dissipation images. Dissipation is increased on less ordered, less well-packed surfaces, both at the molecular scale and the meso scale.[26, 27] Fukuma *et al.* showed that the contrasts are probably related to the number of molecules interacting with the tip – the more molecules interacting with the tip the greater the energy transfer; thus at the molecular scale the dissipation image shows inverted contrast relative to the topographic image.[28]

5.9 Imaging molecular mobility at surfaces

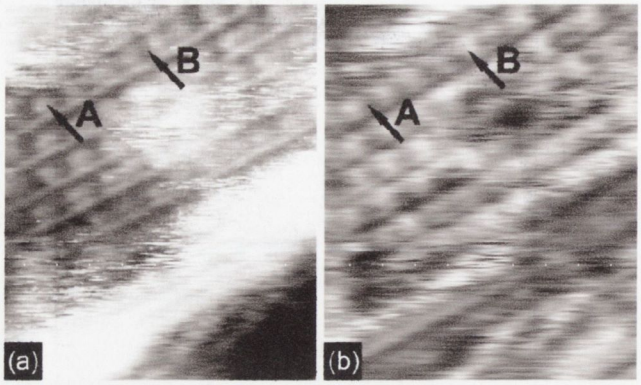


Figure 5.7: Molecular-scale UHV FM-AFM images of an EF thin film on HOPG. Simultaneous topography (a) and dissipation (b) images (23.2 nm x 27.9 nm, cantilever: NCH, Δf = - 100 Hz, a = 8.9 nm).

Figure *5.7* shows a molecular-scale topographic image (a) of a non-equilibrium arrangement of the rotaxanes and the corresponding map of A_{exc} (dissipation image) (b), taken in UHV conditions. The dissipation image displays essentially inverted contrast with respect to the corresponding topographic image. Arrows A and B mark the same points on each image. Position A corresponds to a tip position directly above a molecule. The internal motion of the molecule provides a coupling pathway and energy is dissipated into the sample. At position B the tip is over an intermolecular space and more than one molecule is involved in the dissipation process and thus the relative contrast is increased in these places. An illustration of this effect is shown in Figure *3.9*, section *3.3.3*. This model explains the contrast inversion between the two image types. Images of A_{exc} such as these are easily converted to quantitative images of the average dissipated energy per oscillation.[20]

5.10 Energy dissipation maps

5.10.1 Meso-scale

Figure *3.8(a)* shows a 500 nm scan with the same cantilever with corresponding quantified dissipation image *(b)* in units of eV per oscillation. The dissipated energy is greater on the rotaxane monolayer. The contrast in this large-scale image is essentially the same as in the height trace, the sub-molecular motion of the film providing more dissipation channels than the graphite.

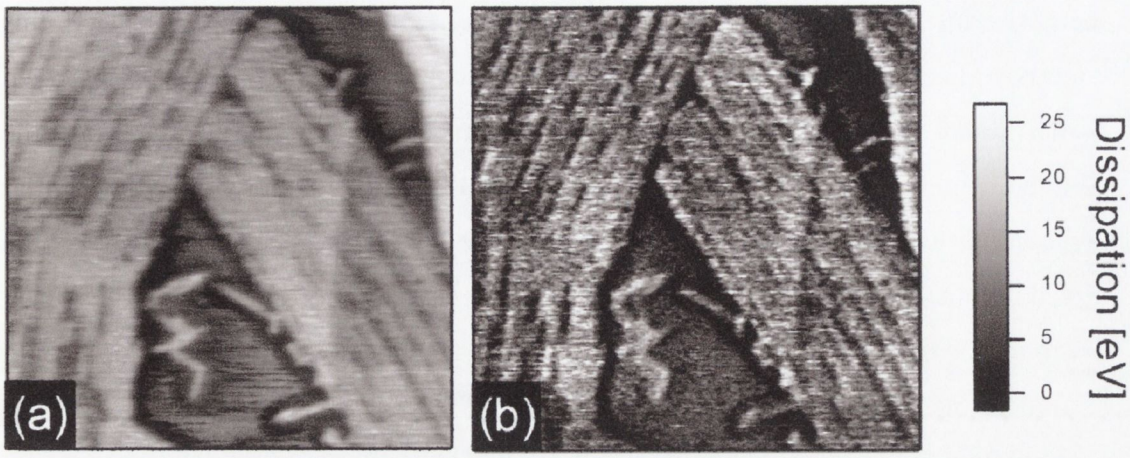


Figure 5.8: Meso-scale ambient FM-AFM simultaneous topography (a) and dissipation (b) images of an EF thin film on HOPG (500 nm x 500 nm, Δf = - 26 Hz, a = 11.8 nm).

5.10.2 Molecular-scale

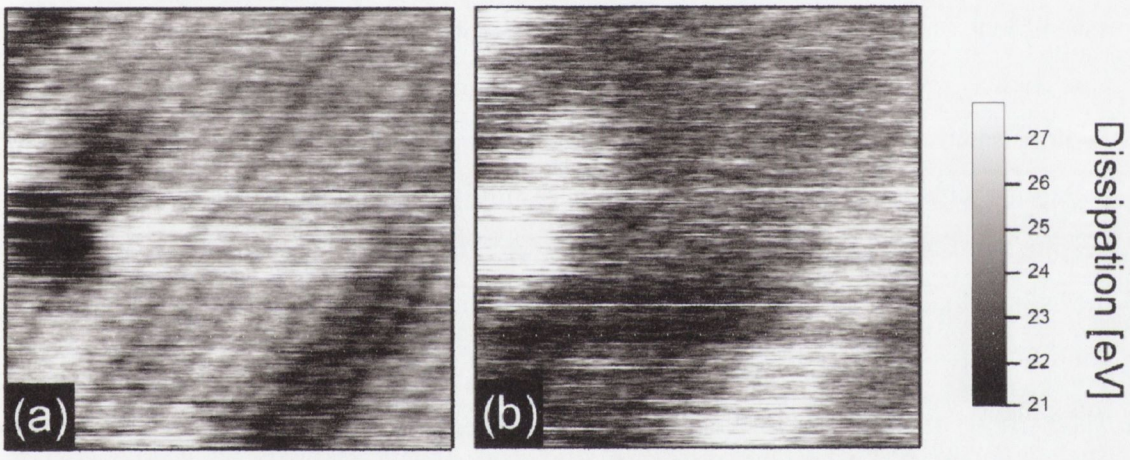


Figure 5.9: Molecular-scale ambient FM-AFM simultaneous topography (a) and dissipation (b) images of an EF thin film on HOPG (30 nm x 30 nm, Δf = - 52 Hz, a = 8.9 nm).

The molecular-scale dissipation contrast however (Figure *9(b)*), captured using the same tip is, by contrast, inverted with respect to the height trace (Figure *9(a)*). In this image the presence of a defect in the film indicates that the image shows true structure. For the higher resolution image a smaller amplitude, but also a greater frequency shift set point (-52 Hz) is used. The optimum force is probably similar in both cases. Unstable imaging conditions occur if this force is exceeded, presumably because the tip enters the force region where the feedback polarity is reversed. In Figure *3.8*, section *3.3.2* this point in the frequency vs. separation curve is the minimum indicated by the point 'b'. This is because the frequency curve mirrors a typical force interaction potential (Figure *3.6*, section *3.3.1*). The inversion of the dissipation image at the molecular scale compared to the meso-scale supports the proposed mechanism of increased dissipation when the number of energy transfer pathways is increased (by

increased internal molecular motion), as opposed to a simple tip artefact. If this contrast difference were for example due to contact potential differences between graphite and the molecules, then this would imply that at a molecular scale the contrast would not be inverted as in Figure *5.6* and Figure *5.9*, but would show similar contrast to topography – i.e. higher above the molecules and lower above the molecular spaces. Observation of increased molecular motion (and hence increased dissipation) as a result of externally induced rotaxane molecular switching would seem possible therefore by dissipation imaging.

5.11 Conclusions

In this chapter, by applying the FM-AFM technique to the study of a simple H-Bond assembled rotaxane, I have for the first time demonstrated the molecular-scale order and hence potential addressability possible in such thin films. I have also demonstrated the stable imaging capabilities of the constant amplitude FM-AFM technique outside of UHV and the high resolution imaging of a soft organic film despite low Q-factor and the native water layer. The studies of rotaxanes made in this thesis have been in a systematic fashion, i.e. with multiple variations in the deposition conditions (as in Chapter 3) or with multiple film composition investigations (i.e. the rotaxane type is varied as in Chapter 6). For investigations of this type the UHV environment is not an option due to the excessive setup time, maintenance and cost. Most UHV STM/AFM experimentalists in fact will try to avoid the introduction of organics into their system at all costs because of the potential for contamination. In relation to the dissipation contrast observed at the molecular scale for the first time, the observation of switching of material properties of organic films, especially rotaxane films, is a specific potential usefulness of the FM-AFM technique in ambient conditions.

This chapter showed the evaluation of the FM-AFM technique in ambient conditions. Accurate determination of the interaction force was achieved, and the energy dissipation was quantitatively measured even at the molecular level, by which means induced sub-molecular motion may be observed in the future. These experiments help to demonstrate the increasing applicability of the FM-AFM technique outside of UHV and the potential usefulness of the technique for the development of practical

chemical and biological applications, which should help make this important technique even more widely applicable.

5.12 References

1. Altieri, A.; Bottari, G.; Dehez, F.; Leigh, D. A.; Wong, J. K. Y.; Zerbetto, F., *Angewandte Chemie-International Edition* **2003** (42) 2296.
2. Altieri, A.; Gatti, F. G.; Kay, E. R.; Leigh, D. A.; Martel, D.; Paolucci, F.; Slawin, A. M. Z.; Wong, J. K. Y., *J. Am. Chem. Soc.* **2003** (125) 8644.
3. Leigh, D. A.; Perez, E. M., *Chemical Communications* **2004** 2262.
4. Biscarini, F.; Cavallini, M.; Leigh, D. A.; Leon, S.; Teat, S. J.; Wong, J. K. Y.; Zerbetto, F., *J. Am. Chem. Soc.* **2002** (124) 225.
5. Farrell, A. A.; Fukuma, T.; Uchihashi, T.; Kay, E. R.; Bottari, G.; Leigh, D. A.; Yamada, H.; Jarvis, S. P., *Physical Review B* **2005** (72).
6. Jarvis, S. P.; Uchihashi, T.; Ishida, T.; Tokumoto, H.; Nakayama, Y., *J. Phys. Chem. B* **2000** (104) 6091.
7. Kageshima, M.; Jensenius, H.; Dienwiebel, M.; Nakayama, Y.; Tokumoto, H.; Jarvis, S. P.; Oosterkamp, T. H., *Appl. Surf. Sci.* **2002** (188) 440.
8. Sekiguchi, H.; Okajima, T.; Arakawa, H.; Maeda, S.; Takashima, A.; Ikai, A., *Appl. Surf. Sci.* **2003** (210) 61.
9. Okajima, T.; Tokumoto, H., *Japanese Journal of Applied Physics Part 1-Regular Papers Short Notes & Review Papers* **2004** (43) 4634.
10. Nishi, R.; Houda, I.; Sugawara, Y.; Morita, S., *Appl. Phys. A* **2001** (72) S93.
11. Kobayashi, K.; Yamada, H.; Matsushige, K., *Appl. Surf. Sci.* **2002** (188) 430.
12. Sasahara, A.; Kitamura, S.; Uetsuka, H.; Onishi, H., *J. Phys. Chem. B* **2004** (108) 15735.
13. Fukuma, T.; Ichii, T.; Kobayashi, K.; Yamada, H.; Matsushige, K., *Appl. Phys. Lett.* **2005** (86) 034103.
14. Holscher, H.; Gotsmann, B.; Schirmeisen, A., *Physical Review B* **2003** (68) 153401.
15. Holscher, H.; Anczykowski, B., *Surf. Sci.* **2005** (579) 21.
16. Anselmetti, D.; Dreier, M.; Luthi, R.; Richmond, T.; Meyer, E.; Frommer, J.; Guntherodt, H. J., *Journal of Vacuum Science & Technology B* **1994** (12) 1500.
17. Gatti, F. G.; Leigh, D. A.; Nepogodiev, S. A.; Slawin, A. M. Z.; Teat, S. J.; Wong, J. K. Y., *J. Am. Chem. Soc.* **2001** (123) 5983.
18. Kobayashi, K.; Yamada, H.; Itoh, H.; Horiuchi, T.; Matsushige, K., *Rev. Sci. Instrum.* **2001** (72) 4383.
19. Jarvis, S. P.; Ishida, T.; Uchihashi, T.; Nakayama, Y.; Tokumoto, H., *Appl. Phys. A* **2001** (72) S129–S132.
20. Gotsmann, B.; Seidel, C.; Anczykowski, B.; Fuchs, H., *Phys. Rev. B: Condens. Matter* **1999** (60) 11051.
21. *Crystallographic data (excluding structural factors) for FR as crystallized from DMSO and MeCN can be found in the Cambridge Crystallographic Database, supplementary publication numbers CCDC-157383 and CCDC-160650 respectively.*
22. Garcia, R.; Perez, R., *Surf. Sci. Rep.* **2002** (47) 197.
23. Lantz, M. A.; Hug, H. J.; Hoffmann, R.; van Schendel, P. J. A.; Kappenberger, P.; Martin, S.; Baratoff, A.; Guntherodt, H. J., *Science* **2001** (291) 2580.

24. Uchihashi, T.; Higgins, M. J.; Yasuda, S.; Jarvis, S. P.; Akita, S.; Nakayama, Y.; Sader, J. E., *Appl. Phys. Lett.* **2004** (85) 3575.
25. Sader, J. E.; Jarvis, S. P., *Appl. Phys. Lett.* **2004** (84) 1801.
26. Ichii, T.; Fukuma, T.; Kobayashi, K.; Yamada, H.; Matsushige, K., *Appl. Surf. Sci.* **2003** (210) 99.
27. Fukuma, T.; Ichii, T.; Kobayashi, K.; Yamada, H.; Matsushige, K., *J. Appl. Phys.* **2004** (95) 1222.
28. Fukuma, T.; Kobayashi, K.; Yamada, H.; Matsushige, K., *J. Appl. Phys.* **2004** (95) 4742.

Chapter 6: Using mixed rotaxane thin films to investigate the effects of rotaxane structure on mechanical and morphological properties of rotaxane thin films

6.1 Introduction

While knowledge of the simplest rotaxanes' behaviour at surfaces is important, applications of these molecules often involve the more complex, less symmetric rotaxane types such as molecular shuttles.[1-3] Rotaxanes were initially regarded as molecular curiosities,[4-7] but in recent times the publication output of the field has increased significantly, and some rotaxanes are beginning to show promise for applications as surface mounted devices. As discussed in chapter 2 it has been demonstrated that the functionality of these molecules is maintained, as measured by averaging techniques such as surface pressure measurements of Langmuir-Blodgett films,[8] and cyclic voltammetry.[9] Interesting behaviour of rotaxanes at surfaces has already been demonstrated in the case of a hydrogen-bond assembled rotaxane (the kind used in this study) that, when irradiated with UV light, underwent translational sub-molecular motion, exposing a fluorinated group in the molecules that altered the wettability of the surface.[10] In another example, the exposure of a film of polymerised hydrogen-bond assembled rotaxanes to solvent vapour resulted in a switching of the molecules and their subsequent sub-molecular rearrangement caused change in the fluorescence properties of the molecules. By masking the surface an optically viewable pattern could be produced through selective exposure; one might easily imaging lithographic applications for such a technique.[11]

The question, however, of what happens at the molecular scale when rotaxanes are switched at a surface still remains open. Little or no local or molecular-scale characterization has been carried out, and a direct observation of externally-induced sub-molecular motion is required such that we might understand the specific switching characteristics. These parameters include the time-scale of the response (i.e. switching rates), the percentage of molecules that are switched, the uniformity of the motion, the stability of the switched molecules, and the effects of the surface interactions and molecular packing.

In this chapter, characterization of some of the promising molecular-shuttle type rotaxanes in close-packed molecularly-thin film environments on a HOPG surface is presented. Using a highly-sensitive AFM technique the surface reconstruction of these molecules could be determined. It is demonstrated how single and multi-component films can be precisely controlled in their surface concentration and built up step-by-step. In this way, one can characterise the reorganization of complex molecular shuttles in terms of surface concentration. Furthermore, by means of a direct comparison with model rotaxanes, the effects that the long thread has on the surface behaviour of these complicated molecules is shown. Thereby, the challenges faced by the surface chemists who would use them as surface devices or sensors are better understood. It is also demonstrated how film structure changes, as a result of changes in molecular composition, by directly comparing complex shuttles with simpler, non-shuttling, but closely related molecules in multi-component monolayers. Finally in these mixed films it is shown how the FM-AFM technique may be applied to monitor switching events via changes in molecular structure or the relative energy dissipation signatures. An example of a switching experiment based upon this technique is also illustrated.

6.2 Mixed monolayers

Mixed monolayers could be employed such that a surface can perform more than one function. For example, a chemical sensor that was based upon complexation of a surface species with a species under investigation could contain more than one chemical receptor,[12] or a surface could be made with multiple functionalities to promote the adsorption of proteins and cell proliferation.[13] On the other hand, one might simply want to precisely tune the behaviour of these surfaces, since depending on the relative ratios of components in surface-attached monolayers, surfaces can exhibit varying interfacial properties such as hydrophobicity/hydrophilicity.[14] Or for device manufacture one might be interested in "monolayers with controllable in-plane molecular organization".[15] Overall the use of mixed monolayers allows a greater flexibility in surface design.

In this chapter, mixed monolayers of different rotaxane molecules were used in an effort to make direct measurements of induced sub-molecular motion. This would be

done through the observation of local contrast, in structural and dynamic properties, (or conservative and dissipative interactions), by FM-AFM as discussed in chapters 3 and 5. This technique is extended in this chapter to observations on contrast in these signals between regions of active rotaxanes and regions of inactive rotaxanes before, during, and after switching events, where both rotaxanes are part of a mixed monolayer with discrete domains. The method of creating the mixed monolayers uses successive drop-casting events of different chemical species on the same surface, and is used to elucidate molecular and film properties as well as the possibility of observing switching. Since in this method the formation of the mixed monolayer is done in a two step process, it is similar to the two-step mixed-monolayer formation technique of Morgenthaler *et al.*.[16] In their work, they prepared gradients of one type of molecule by drawing the substrate from the solvent at a constant rate during film formation. The method described in this chapter differs in that the films have no gradient and are formed by successive drop-casting events. The resulting films share similarities in that they both demonstrate that structures formed during the first deposition propagate into the final film, as will be shown in section 6.7.

At the simplest level, this method for creating mixed monolayers can be used in conjunction with AFM measurements to reliably characterize the spatial distribution of phase-separated molecules on the 1-100 nm scale in these monolayers, and importantly the layers need not necessarily be very thin, nor conducting (as is the case in STM measurements). These molecules are observed with extremely high-resolution in ambient conditions and the films are created under solvent in a very simple process. On the other hand, the cleanliness and purity of the separated domains is an interesting avenue to explore, in itself, in terms of cost-effective self-assembly processes. If there is potential for rotaxanes as functional electronic devices then viable bottom-up self assembly of functional, multi-component, ordered surfaces will be required.

6.3 Energy Dissipation in FM-AFM

The concept of energy dissipation in FM-AFM has been discussed in-depth in sections *3.3* and *5.8*. The energy dissipation signal is used in this chapter as a possible means for the observation of induced rotaxane switching. The technique is to contrast

the energy dissipation signals of active and inactive rotaxane molecules in a mixed monolayer. In doing this a second signal is gained for direct observation of rotaxane switching - the other signal is the local molecular structure, and the observation of local topographical changes in the film.

Interestingly, other parties have investigated mixed monolayers using FM-AFM. Ichii *et al.* showed that they could detect differences in energy dissipation in mixed SAMs based on the end functional group type,[17, 18] and upon the length/flexibility of the molecule.[19, 20] Fujii *et al.* showed that they could differentiate thiol molecules with different head groups in a heterogeneously mixed SAM by controlling the chemical species on the tip apex.[21] The energy dissipation due to the tip-sample interaction is dependent upon the atomic-scale tip chemistry and structure (for the interaction area). Some authors have suggested that a carbon nanotube tip might be useful in this regard as a reusable and chemically stable tip.[22] In the experiments by Fujii *et al.* (molecular surface in UHV) the atomic-scale tip structure was controlled using a reference crystalline surface that has been extensively characterised. The tip was scanned across the surface resulting in the addition of some surface atoms, thereby altering the imaging contrast seen. They then proceeded to image the SAM, and the tip was checked on the crystal surface afterwards.[21] These experiments are also complimentary to theoretical work by Martinez *et al.*[23] because compositional contrast may soon be transformed into quantitative information about the materials properties.

On a chemically inert molecular surface in ambient conditions it is difficult to control the exact structure of the tip, and if a tip change occurs it is impossible to predict the chemical structure.[24] The chemical differentiation in the experiments presented here is done on a morphological basis. A key feature of the measured dissipation images [*Section 6.8.2 – 6.8.4*] is that they are stable and consistent. Knowing the relationship between materials properties and the energy dissipation,[25] we can directly compare rotaxane species in mixed monolayers (using the same tip), and potentially use such measurements to examine the occurrence of sub-molecular motion in rotaxane shuttles.

6.4 Experimental

6.4.1 Materials

The method used in these experiments was to contrast complex molecular shuttles with the simpler non-shuttling rotaxane (EF) that we had already extensively studied [*Chapters 4 and 5*]. The four molecules investigated in this chapter are shown in Figure *6.1* (over); the simple naming scheme is according to the type of station species present on each molecule, and according to whether or not the molecule has an exopyridyl group. The molecules IFS (isophthalyl fumaramide-succinamide C12 molecular shuttle) and EFS (exo-pyridyl fumaramide-succinamide C12 molecular shuttle) are distinguished by an exopyidyl group on the macrocycle. These molecules are light-switchable molecular shuttles, as were discussed in section *2.4.1*.[26, 27] The ESN molecule (exopyridyl-succinamide-naphthalimide) is an electrochemically switchable shuttle as discussed in section *2.4.2*.[28, 29] Since all shuttles share a common thread length between stations of 12 carbons, there is no need for further distinction.

6.4.2 Rotaxane Film Preparation

To prepare the films on a freshly cleaved 10 mm x 10 mm HOPG substrate, a single drop of solution (rotaxanes in acetone, concentration approximately 1 μM) was deposited and the solvent was allowed to evaporate slowly in a 500 cm^3 container with an atmosphere saturated with acetone vapour. Mixed monolayers were prepared by first adding one drop of solution containing the first molecule to the sample and when this had evaporated the second type of molecule was dropped. In these experiments, discretely controlling the surface coverage is achieved by controlling the concentration of the solution and the amount deposited. Optimisation of the method showed that a drop of 14 μL of acetone on a square 10 mm x 10 mm HOPG sample is at the upper limit of a stable droplet (above this and the contact surface tension of the droplet is not sufficient to keep the droplet from spilling off a substrate of this size. Subsequent experiments were conducted at this limit to ensure that the molecules form a film free of the influence of pulling effects of evaporation and dewetting of the solvent. This volume is used to calculate the concentration required to ensure complete surface coverage.

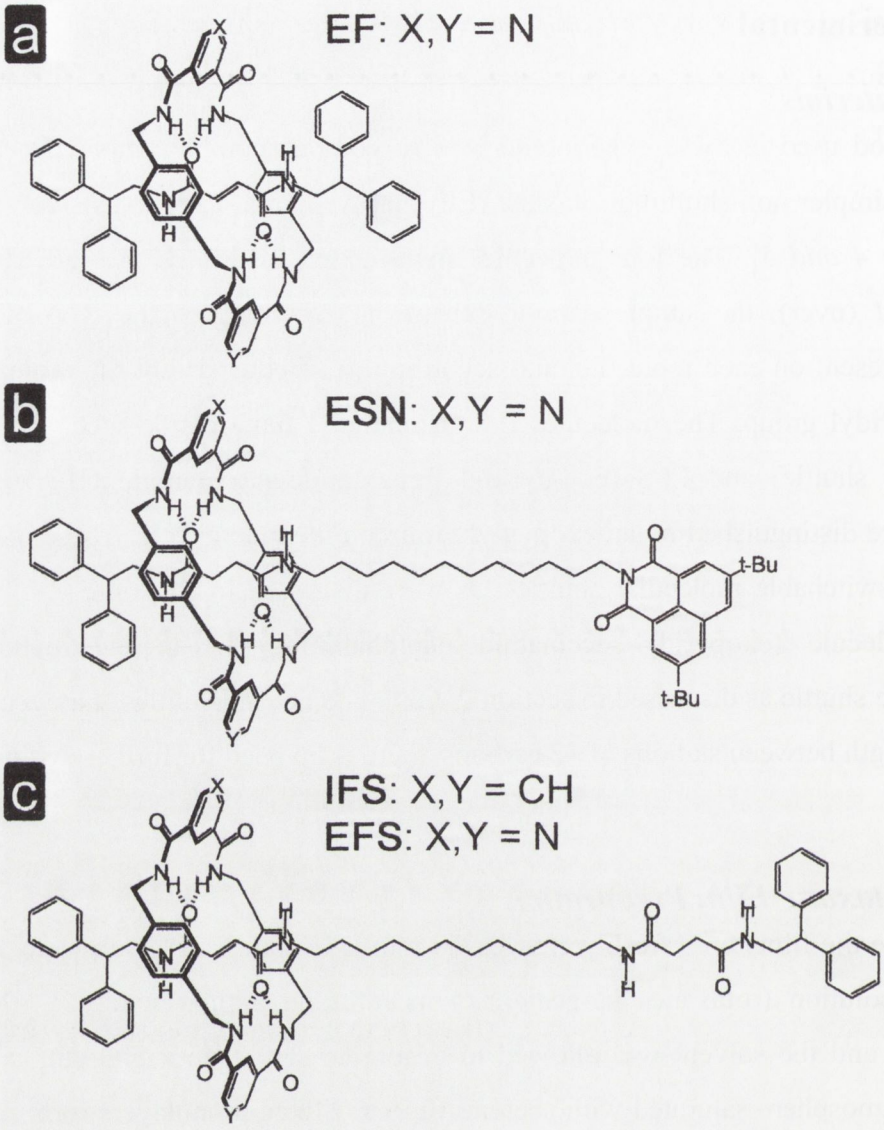


Figure 6.1: Molecular structures and nomenclature for the rotaxane molecules used in the experiments presented in this chapter. The macrocycles are distinguished by being Isophthalyl (X, Y = CH) and Exopyridyl (X, Y = N). The various "stations" (areas of the rotaxane thread where the thread-macrocycle interaction energy is locally minimized) are Fumaramide, Succinamide and Naphthalimide. A C*X* prefix corresponds to the number of carbon atoms in the thread backbone (e.g. C12 for a 12 Carbon chain). Hence the name in (a) is EF, a rotaxane with an exopyridyl-functionalised macrocycle and a single fumaramide station; (b) is a C12-ESN, which would correspond to an exopyridyl succinamide naphthalimide benzylic amide hydrogen-bond-assembled rotaxane molecular shuttle; (c) corresponds to an isophthalyl/exopyridyl macrocycle with fumaramide-succinamide stations and a 12 carbon thread

6.4.3 FM-AFM Imaging

To obtain high-resolution information about the rotaxanes an ultra-sensitive AFM built in our laboratory was used. The FM-AFM imaging technique and the construction of this AFM are discussed in-depth in section *3.3* and section *3.5.6*. The resolution achieved in these experiments cannot be achieved on any current

commercial instrument in ambient conditions without considerable modification of the instrument. All measurements were performed in the constant frequency shift mode where the frequency shift of the cantilever resonance frequency, Δf, induced by the tip-sample interaction is kept constant during FM-AFM imaging by using a feedback loop to modulate the tip-sample separation. The cantilever is vibrated at constant amplitude, where the vibration amplitude of the cantilever was kept constant by using a second feedback loop to modulate the amplitude of a cantilever excitation signal, A_{exc}. In this constant amplitude mode, energy dissipation caused by the tip-sample interaction for a given Δf can be estimated from A_{exc}.[30] Thus, the dissipation image is obtained as a two-dimensional map of A_{exc}.

6.5 Controlling the surface concentration of rotaxane thin films / The effect of packing on the observed molecular-scale structure

In Figure *6.2(a)* and *(b)* a sub-monolayer coverage film of IFS shows molecular-scale details that reveal a random morphology; the surface concentration in this case is not known exactly but will be called γ. The dark regions of the image are the bare HOPG surface. Figure *6.2(c)* shows the same rotaxane-covered HOPG surface with a surface concentration of 3γ. This is known exactly because the same droplet size was used to add additional material to the original film. It is immediately apparent that in order to minimise the energy of the surface the molecules have packed much more closely and the order of the film has been greatly increased. Adding more material to give a surface concentration of 4γ (Figure *6.2(d)*) we can see that the first monolayer has reached saturation. There are some bare patches of graphite still remaining, yet the second layer has started to grow. As the first monolayer becomes more ordered with increasing rotaxane concentration it begins to present a lower energy surface for subsequent molecules to reside upon. The first layer of rotaxanes is, at this stage, composed of domains where the molecules are in a striped reconstruction. Taking the width of a domain as the distance from edge to edge normal to the stripe direction, widths of between 90 and 180 nm are observed.

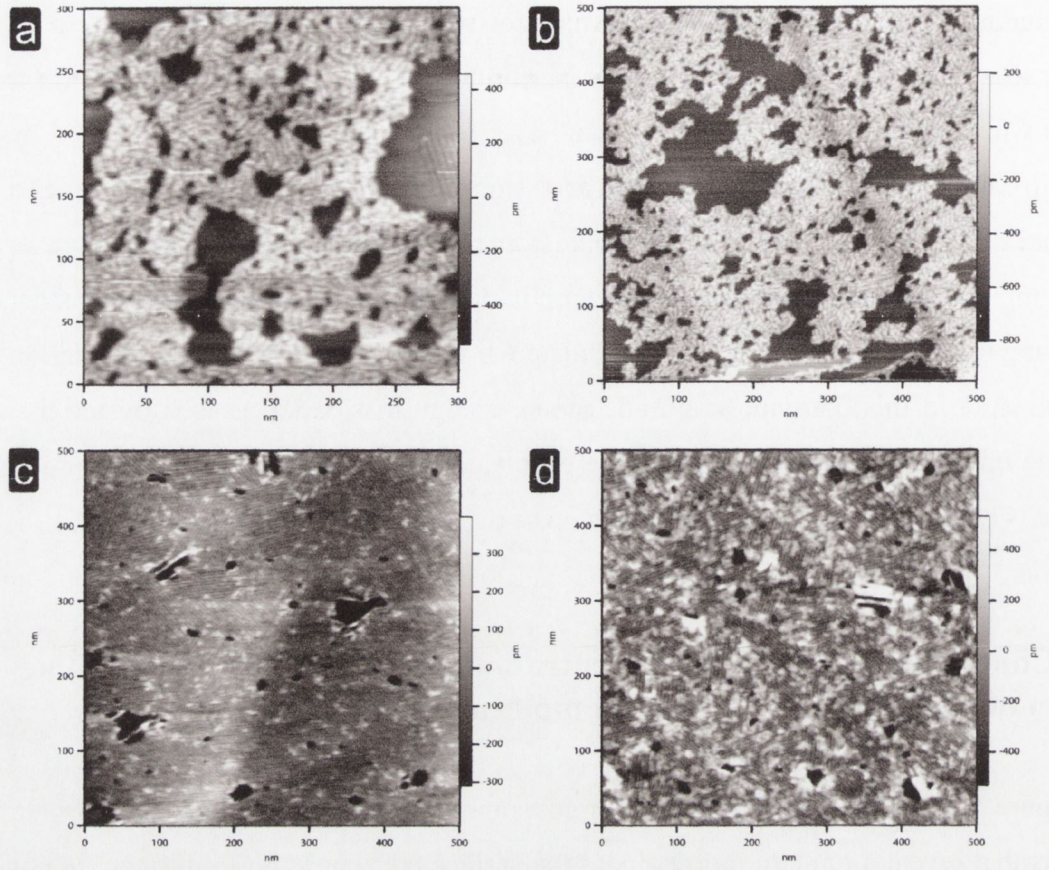


Figure 6.2: FM-AFM (ambient conditions) topography images showing molecular-scale details of C12-IFS on HOPG as deposited from acetone. The surface concentration in (a) and (b) is arbitrarily γ, and the surface concentration of (c) is 3γ and that of (d) is 4γ. The films in (c) and (d) were made by adding molecules to (a) and (c) respectively by repeating the film deposition process. Thus the sequence of images shows the gradual completion of a rotaxane monolayer.

6.6 High-resolution structure in a closely-packed film of unsymmetric rotaxanes

The images in Figure *6.3(a)* and *(b)*, trace and retrace, showing that the observations show true structure and are not an instrumental artefact, show fine structure at the molecular scale. (Periodic electrical or mechanical noise can appear in AFM scans as stripes, but in a forward and backward scan a characteristic of the stripes will be that they are at opposing angles). Specifically, we can observe a double feature on the molecular-scale stripes as indicated by the arrow in Figure *6.3(a)*. The periodic distance between stripes as calculated by FFT (inset, Figure *6.3(a)*) is 5.3 nm, a value significantly greater than the molecular length.

I have created a model for the molecular reconstruction using this information by imposing three conditions upon the molecular film: (1) The molecules are

unsymmetric and as such form a like-with-like structure, (such as is typically seen with unsymmetric molecules on HOPG);[31] In this case (2) The molecular reconstruction has a perpendicular row to row distance of 5.3 nm; (3) The macrocycle-containing fumaramide end of the molecules (region I of the IFS molecule shown in (d)) has the same unit cell that was calculated in Figure *5.4*.

This reconstruction is illustrated in image (c) where the rotaxane molecules are drawn exactly to scale and overlaid on the AFM image. The rotaxanes are 'interdigited' (i.e. the threads of neighbouring molecules form a structure like interlocked fingers) and we can use some simple trigonometry to extrapolate a surface reconstruction unit cell. The smaller box drawn on the figure is the unit cell of the EF molecules calculated in section *5.5*. The extrapolated dimensions of $a_{surf} = 1.65\ nm$ and $b_{surf} = 5.31\ nm$ with $\theta = 86.4°$ give us a commensurate molecular reconstruction of the form:

$$\begin{bmatrix} a_{surf} \\ b_{surf} \end{bmatrix} = M \begin{bmatrix} a \\ b \end{bmatrix}$$

where

$$M = \begin{bmatrix} 7 & 0 \\ -12 & 26 \end{bmatrix}$$

and where a and b are the graphite surface lattice vectors.[32]

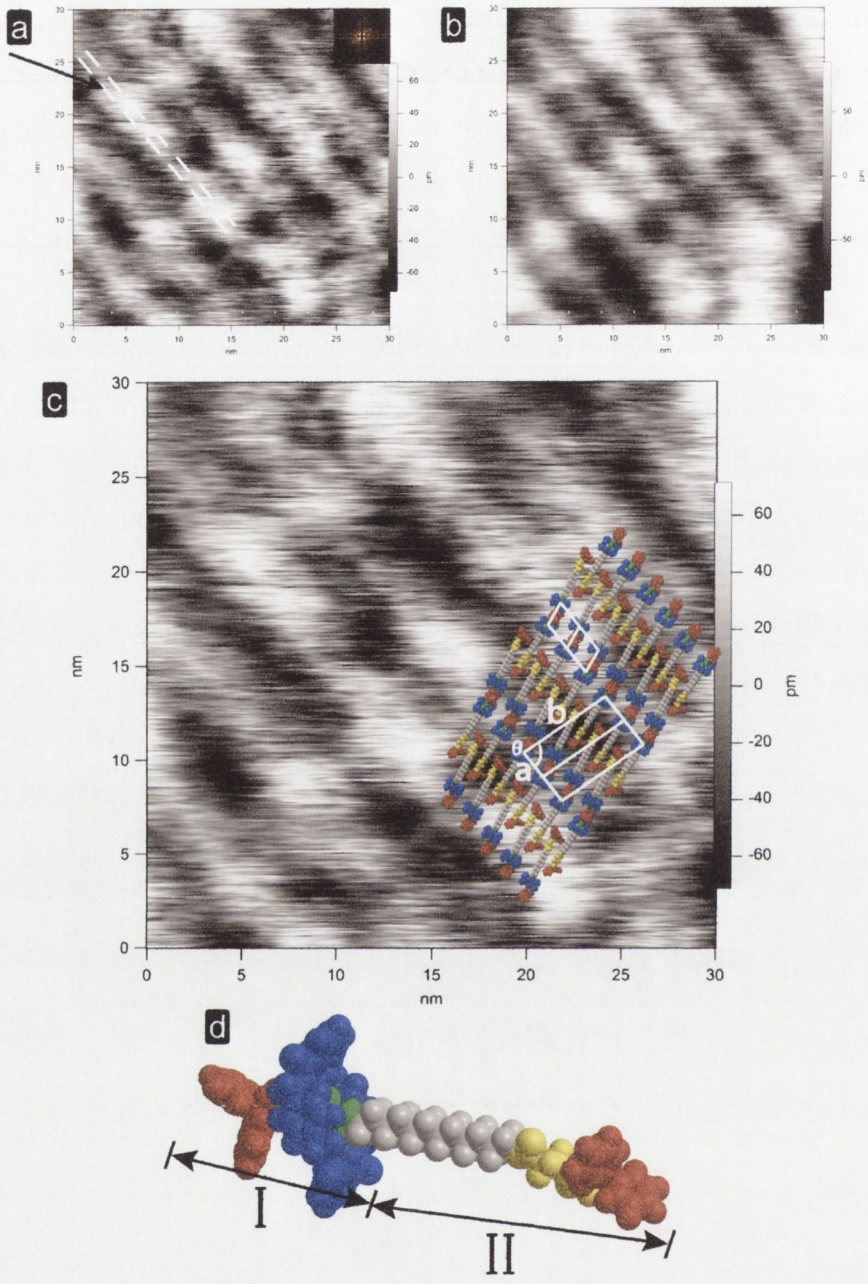


Figure 6.3: FM-AFM (ambient conditions) topography images showing high-resolution molecular-scale details of C12-IFS on HOPG deposited from acetone. The molecules are part of a compressed film as in Figure 6.2 (c). In image (a) it can be seen that the main rows actually have a fine double-row structure (indicated by the arrow); image (b) is the retrace topography image, which also shows the double-row structure, indicating that this is a true structure and not noise. The FFT of image (a) (inset) reveals a periodic distance of 5.3 nm between the double-rows.

Topographically the reconstruction is logical since region I of the IFS molecule (Figure *6.3(d)*) corresponds to the white (higher) areas of the stripes in the image, and the double feature in the stripes should therefore correspond to two macrocycles while the exposed threads are situated in the lower parts of the scan (the darker regions between stripes). When an unsymmetrical molecule forms a film the reconstruction formed is almost always a like-with-like structure, and since the macrocycle is going

to be the most prominent feature in a topography scan we can logically assign these double features, having greater prominence in the molecular rows, to rows of macrocycles. Such soft molecules as the rotaxanes are very difficult to image with high resolution. The "surface pressure" of molecules at the surface must be sufficient that the molecules are not easily fluctuated by the tip-sample interaction, because the imaging of these double rows was only possible when the first layer of rotaxanes on HOPG had been filled. This is because when close-packed the molecules are resilient to lateral motion under the influence of the tip.

The 'inter-digitation' and close-packing seen in the rotaxane reconstruction model is another barrier (in addition to the molecule substrate interactions) to the potential switching of rotaxanes. This interaction would impede motion of rotaxane macrocycle and thread components relative to each other. It is important to note that we have shown here that the surface reconstruction of varied and more complicated rotaxanes (i.e. molecular shuttles) can be better understood (from a molecular motion at surfaces standpoint) using this AFM technique. Typically high molecular-resolution imaging, especially outside of UHV conditions, is limited to STM observations, however STM measurements are precluded in this case due to the large thickness of the film (and the ease with which the molecules can be displaced by static imaging methods, as was demonstrated in section *3.5*).

6.7 Multi-component rotaxane thin films

The advantage of the step-by-step nature of the film formation process shown in Figure *6.2* is that it can be used to directly compare molecular surface reconstructions if a film with two components is made. Thus one can determine the effects of small changes in molecular structure on rotaxane film formation. Figure *6.4* dramatically shows the clear formation of domains of two types of molecule (EF followed by IFS). The different molecular types are easily identified by the morphology of the different domains, the EF forming substrate-oriented domains that are quite closely-packed (These correspond to the features seen earlier in Figures *4.2* and *5.2*, and the IFS film having a less ordered morphology. The darkest areas on the image are again the remaining bare HOPG substrate.

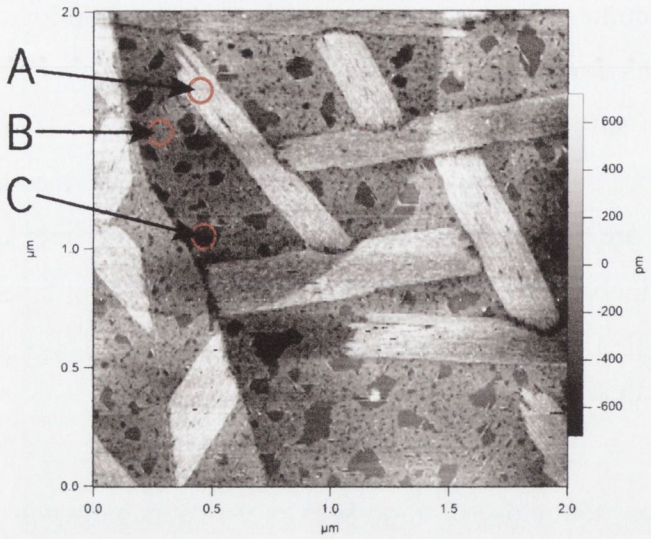


Figure 6.4: FM-AFM topography image of a two-component rotaxane film on HOPG, formed using EF and IFS partial components deposited in the order EF then IFS. The meso-scale image shows that the mixed films retain the morphological characteristics of the individual components' films. The brighter, more ordered regions are the EF molecule (region A) (which can be compared to the image in Figure *4.2(b)* and the molecules in region B are IFS molecules (which can be compared to the image in Figure *6.2(a)*). Region C is the HOPG surface.

In Figure *6.5(a)* and *(b)* are images of a mixed monolayer of EF and EFS. The EF domains in each case are easily identifiable by the film structure that has been previously established at these concentrations –in Figure *4.2 (b)*. The EFS molecule forms domains with a similar morphology to the IFS molecule at this surface concentration. In Figure *6.5(a)* the order of deposition was EF then EFS, while in Figure *6.5(b)* the order of deposition was reversed (the exact same concentrations were used in each experiment). By comparing these two images it can be seen that when the EFS molecule is deposited after the smaller EF molecule there seems to be a build up of a second layer of molecules on top of the EF molecules as well as on the HOPG surface. This second layer of molecules is not present in Figure *6.5(b)*. It would seem that the second layer on top of the EF molecules in Figure *6.5(b)* is in fact composed of EFS molecules. The EF molecules present a well-ordered surface for the EFS molecules to form a film upon. The fact that the EFS molecules have an exo-pyridyl group and the fact that both molecular types have this group should also lead to a stronger interaction between the two layers. The EF domains in Figure 6.*5(b)* are smaller than those in 5 (a) since the already-present EFS molecules disrupt the long-range packing of the EF because they are using the available space. In Figure *6.6* a film is formed with EF followed by IFS and it is clear that no secondary layers have formed on top of the EF domains, the only difference between the films in 5 (a) and 6 (a) being the exo-pyridyl moieties on the EFS molecules.

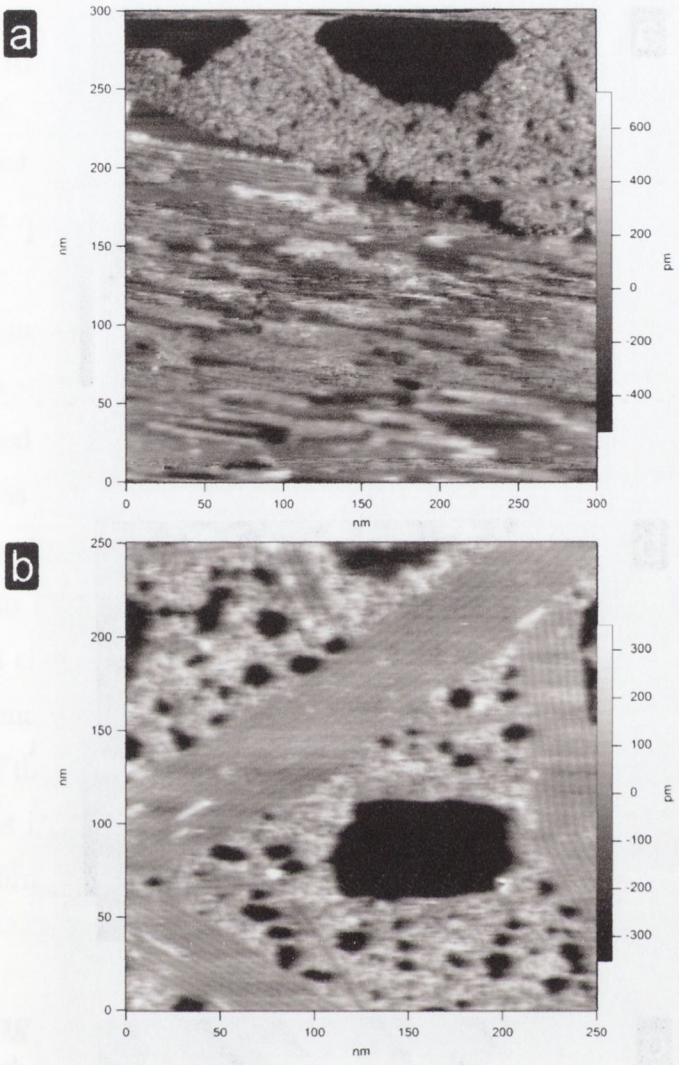


Figure 6.5: FM-AFM (ambient conditions) topography images of multi-component rotaxane films on HOPG formed using EF and EFS molecules. The images show clearly the distinct morphologies of the individual component molecular films. The film in image (a) was formed by depositing sub-monolayer coverage of the shorter EF molecule to form a partial film, followed by sub-monolayer coverage of the EFS molecule. There appears to be a build-up of the EFS molecule on the already-formed EF portion of the film. The film in image (b) was formed in the reverse order to (a), i.e. a partial monolayer coverage of EFS followed by a partial coverage of EF. The film characteristics in (b) are different to (a); the film in (b) has smaller EF domains relative to (a) and the EF portion does not have any apparent coverage of EFS molecules.

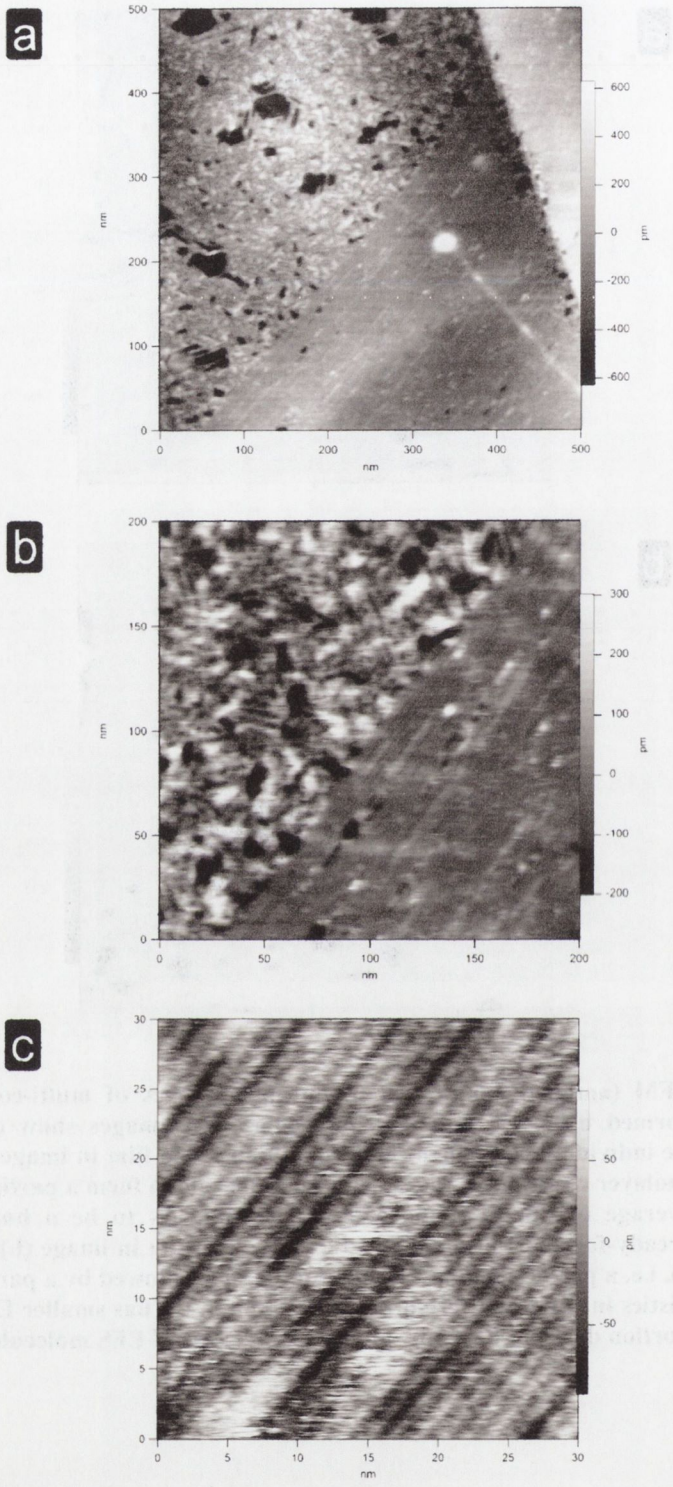


Figure 6.6: FM-AFM (ambient conditions) topography images of a multi-component rotaxane film on HOPG, formed using EF and IFS partial components deposited in the order EF then IFS. The images clearly show the molecular-scale details of both film components. These molecular-scale characteristics correspond to those of the individual components seen in Figure *4.2(b)* (EF) and Figure *6.2(a)* (IFS).

6.8 Obsevation of film characteristics useful for the detection of molecular switching events

The fundamental ways in which AFM can be useful for investigation of rotaxane molecules are that it; (i) is useful for the investigation of the structures of thin films and to determine molecular orientation, and that (ii) it might be used to locally detect a change in the chemical and/or mechanical properties of the film, i.e. it might confirm the occurrence of switching events. In the latter case we wish to show whether or not a sub-molecular rearrangement can occur as a result of stimulus. This might be detected as a change in the observed molecular reconstruction, but also would manifest as a change in the sub-molecular mobility of the film which could be detected through changes in the dissipation signal during FM-AFM imaging. In either of these cases, to test switching properties, the preparation of mixed monolayers is useful because a change would be more easily detected in an active rotaxane if there were, for reference, an inactive or "control" rotaxane. In terms of fundamental investigations of the rotaxane monolayers, by preparing a mixed monolayer with only slight differences in the molecular structures of the components, a dictionary of the effects on film formation of such small changes could be developed.

6.8.1 Observing molecular-scale structures in mixed monolayers

In Figure *6.6(a)* the topography of a mixed film of EF and IFS, deposited in that order, is shown. While distinct differences in the overall morphology of the film are readily apparent, further examination of Figure *6.6(b)* demonstrates that we can detect molecular-scale details in two components of a film simultaneously. The molecules on the right-hand side are EF, while those on the left-hand side are IFS. The IFS component of the film has a molecular rearrangement consistent with that observed in a single-component film of IFS at a similarly low surface concentration (Figure *6.2(a)*). We can also estimate that from the large size of the twisting rows of rotaxanes seen at this surface concentration (the scale of the rows is larger than the size of an IFS molecule) that these rows should be composed of the same double-rows of rotaxanes that can be detected at higher film concentrations, (Figure *6.3(c)*).

We can examine a smaller region on the EF side and detect very fine details as shown in Figure *6.6(c)*. One thing that is immediately apparent is that the rotaxane rows are

grouped together in groups of 2, 3, 4 or 5, between which we can see darker lines that correspond to a larger gap between the molecules. This reconstruction is a part of what allows the film to accommodate a lattice mismatch between the molecules and the HOPG surface. Furthermore, there is not necessarily a corresponding lattice mismatch-induced disparity in the row gap width at the molecule-substrate interface, because the molecules are quite large (the films are 0.5 to 1.1 nm thick – see sections *4.6 and 4.7*) and very flexible; molecules in different rows of the film might have a slightly different tilt angle relative to the surface. Flexible molecules are ideal for forming large domains in surface reconstructions because of their ability to absorb even severe lattice mismatches.[32]

6.8.2 Dissipation contrast

Considering the observations of Fukuma *et al.* in the case of mixed self-assembled monolayers, and the observations in Chapter 5 (5.3) of rotaxane dissipation contrast, it is feasible that differing energy dissipation signatures could be observed for the components of a mixed rotaxane film. Since one component of the dissipation is related to the internal structure and hence sub-molecular mobility of the molecule, we would expect switched and unswitched molecules in a film to show differing contrast. Again, an inactive control molecule can be used as a reference.

Figure *6.7* shows the topography *(a)* and dissipation *(b)* images for a mixed film of EF and EFS. In the dissipation image (Figure *6.7(b)*) there are three distinct regions of contrast that correspond to the bare HOPG (darkest) the EF domain and the EFS domain (brightest). Both types of molecule are exo-pyridyl, so the contrast difference between the two domains is most likely due to the fact that the EFS molecules are more loosely packed and less well-ordered, as can be seen in the image in Figure *6.7(a)*. This therefore is the expected contrast type between the domains, in a similar fashion to the observations of Ichii *et al.*, who demonstrated that in a mixed monolayer of similar molecules with different lengths, and hence packing efficiency and flexibility, the reconstruction of the longer molecules, which have formed a less ordered film than the shorter molecules, show higher dissipation.[20]

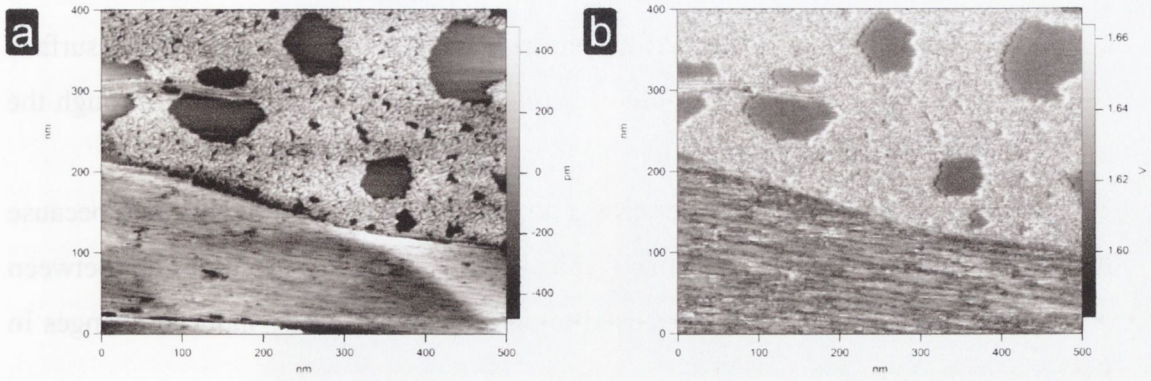


Figure 6.7: FM-AFM (ambient conditions) topography (a) and excitation voltage (proportional to dissipation) images of a multi-component rotaxane film on HOPG, formed using EF and EFS partial components deposited in the order EF then EFS. The dissipation image shows three clear regions of contrast corresponding to the EFS molecules (brightest), EF molecules and HOPG (smooth dark regions).

6.8.3 Effect of chemical structure on observed contrast

In Figure *6.8(a)*, the film of EF and IFS demonstrates distinct morphological differences between the domain types in the topography image. In Figure *6.8(b)* we can see a clear dissipation contrast between the molecular domains, however, in this case the relative contrast levels are different between EF and IFS than those that were observed between EF and EFS in Figure *6.7*. As seen in the dissipation image once again this contrast type is quite stable over long periods of time. By comparing Figure *6.7* with Figure *6.8* we can see that the surface concentrations of the films are similar and the morphology displays similarly random molecular orientations. Despite this, the IFS molecule in this Figure *6.8* has a higher energy dissipation signature than the EF molecule, while than the corresponding EFS molecule in Figure *6.7* has a higher energy dissipation signature than the EF molecule.

The difference between the molecular types is once again only a simple exo-pyridyl group and therefore the observed difference is caused by one of two things. These are either:

(i) The chemical attraction between the tip and exopyridyl molecule is causing a damping of the cantilever oscillation. This damping (in addition to the energy dissipated by the cantilever through hydrodynamic damping and the energy dissipated because of sample adhesion) must be

compensated by the feedback electronics, as explained by Fujii *et al.* and Ichii *et al.*,[17, 18, 21]

(ii) The coupling of the pyridyl group to specific sites on the HOPG surface means that energy is more effectively channelled from the tip through the molecule into the sample.

The important thing is that in either case a noticeable contrast is obvious and, because it is constant for long periods of time (typical AFM image capture times are between 30 seconds and 5 minutes), may be used to detect any externally-induced changes in the layer construction.

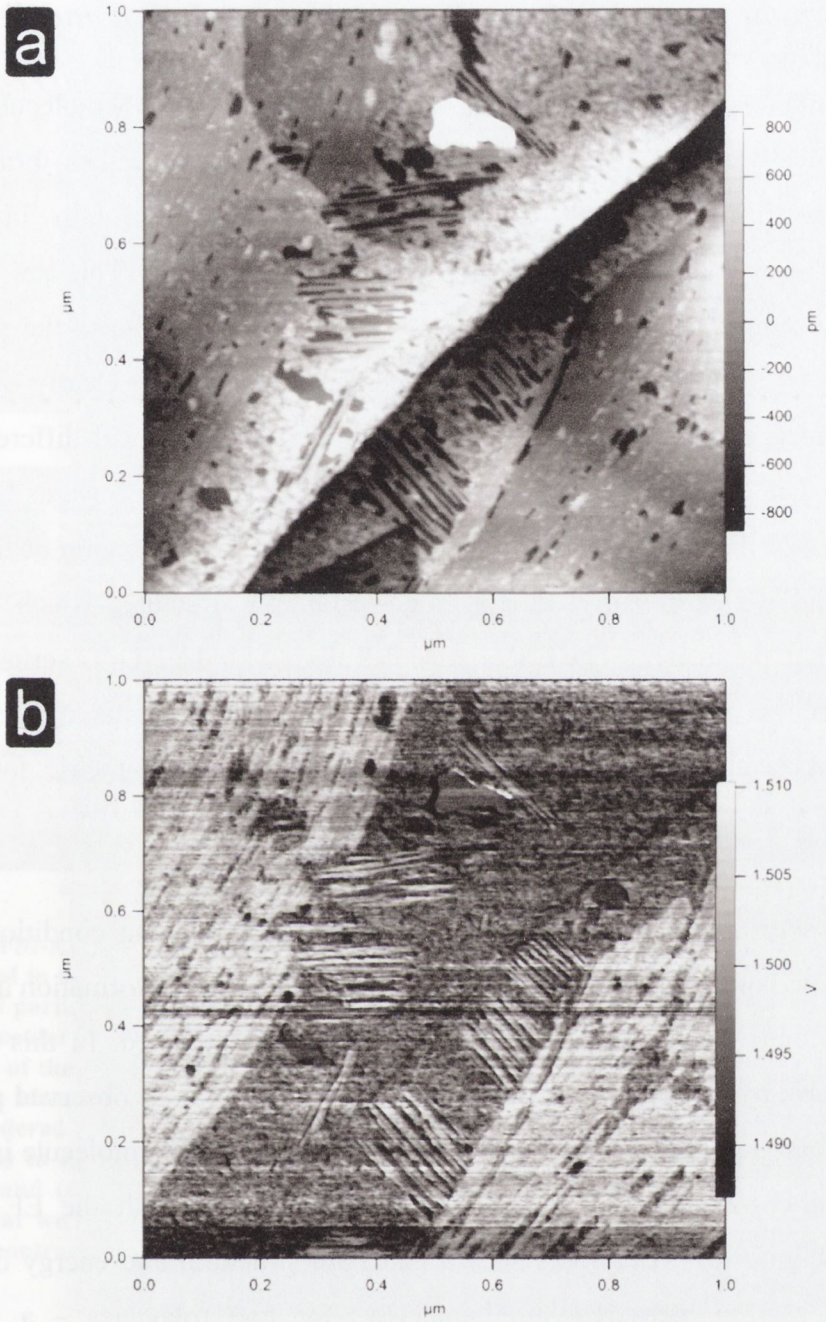


Figure 6.8: FM-AFM (ambient conditions) topography (a) and excitation voltage (proportional to dissipation) images of a multi-component rotaxane film on HOPG, formed using EF and IFS partial components deposited in the order EF then IFS. The dissipation image shows three clear regions of contrast corresponding to the EF molecules (brightest), IFS molecules and HOPG (smooth dark regions). The contrast between EF and IFS regions is inverted with respect to the contrast seen in Figure 7.

6.8.4 Optimum scan conditions for molecular resolution and dissipation contrast observation

The mixed monolayer EF and ESN was also investigated, the ESN molecule being an electrochemically switchable molecular shuttle. The ESN molecules form domains similar to the EF molecules as has been previously discussed in *4.5.1*, however the ESN domains are typically much smaller than the EF domains. (This can be seen in section *4.4*, comparing Figure *4.2(b)* to *4.3(b)*. Figure *6.9(a)* shows the meso-scale morphology of a mixed film of these components, and we can clearly observe the domain boundary between two regions through the morphological differences with the ESN molecules at the top of the image and the EF molecules towards the bottom. In Figure *6.9(b)* the scan size has been reduced to focus on the region of the domain boundary and we can clearly see two high-resolution structures which have very different lattice parameters. The ESN molecules align with the HOPG surface (section *4.5.1)* but are less uniform than the EF. However; this part of the mixed film has many more defects because of the greater lattice mismatch of the unsymmetric, longer, ESN molecules.

In Figure *6.9(c)* and *(d)* I am able to demonstrate that imaging conditions can be selected where both types of information (molecular structural information and energy dissipation contrast differences) can simultaneously be obtained. In this case both molecules have pyridyl groups and both are substrate-aligned. As observed previously, the longer, less-well packed molecular-shuttle rotaxane, the ESN molecule in this case, shows a higher relative energy dissipation (in agreement with the EF and EFS molecules; Figure *6.7*). Here it is shown that both structural and energy dissipation information can be measured simultaneously (for two rotaxanes – a functional molecular type and an inactive control), under ambient conditions, using this technique. This enhanced parameter access facilitates observation of the expected effects of switching such molecular shuttles.

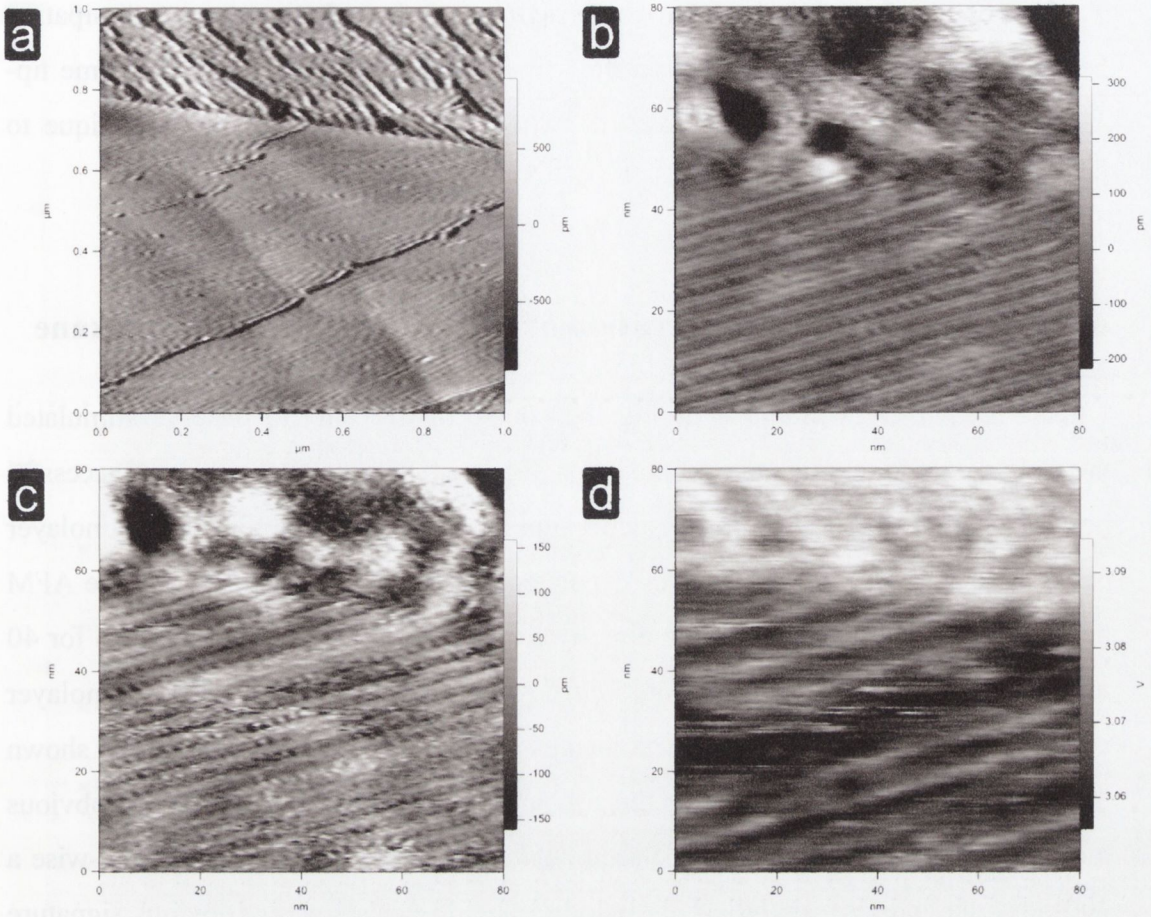


Figure 6.9: FM-AFM (ambient conditions) topography (a), (b) and (c) and excitation voltage (d) (proportional to dissipation) images of a two-component rotaxane film on HOPG, formed using EF and ESN partial components deposited in the order EF then ESN. Image (a) shows clearly the distinct molecular reconstructions of the EF film (bottom part of the image) and ESN molecules (upper part of the image). Image (b) is a zoomed image of the same region where the molecular types can be identified by the morphologies of the partial components of the film (the EF being the more ordered component of the film in the lower part of the image); section 4.4, comparing Figure *4.2(b)* to *4.3(b)* the morphologies films of the individual components can be compared. Images (c) and (d) are corresponding topography and dissipation images respectively which illustrate that we can simultaneously observe and compare the molecular reconstruction and dissipation contrast of the individual film components.

In these images the tip structure is stable for long periods of time, however, it must be pointed out that tip changes can frequently occur in FM-AFM imaging in ambient conditions. Care should be taken when interpreting dissipation images because of this. The contrast can easily appear differently from that which is presented. When this is the case the tip is unstable and rarely remains the same for an entire image. When the tip is unstable like imaging conditions can be unstable for long periods of time, but eventually the imaging and the tip can be stabilized. It is only this type of stable image that is presented.

The important point is that I am interested in comparing directly the dissipation between two molecular types within the same image and hence under the same tip-sample conditions, and, in the case of switchable rotaxanes, use the technique to detect switching events.

6.9 Attempts at direct observation of externally stimulated rotaxane motion at a surface

I made a number of attempts during the course of my PhD to observe stimulated switching events in rotaxane monolayers. None of these attempts were successful however. Figure *6.10* shows one such example. In this experiment half-monolayer coverage of C12-IFS molecules was deposited on HOPG (Figure *6.10(a)*). The AFM head was removed and the sample directly exposed to UV radiation (254 nm) for 40 minutes, with a light intensity of 5 mW/cm^2. To this sample, half-monolayer coverage of un-switched C12-IFS molecules was added. The resulting film is shown in Figure *6.10(b)*, *(c)* and *(d)*. In the topographic image (Figure *10(b)* no obvious morphological differences could be seen between any adjacent domains. Like-wise a 100 nm scan and corresponding dissipation trace do not show any obvious signature differences between any regions.

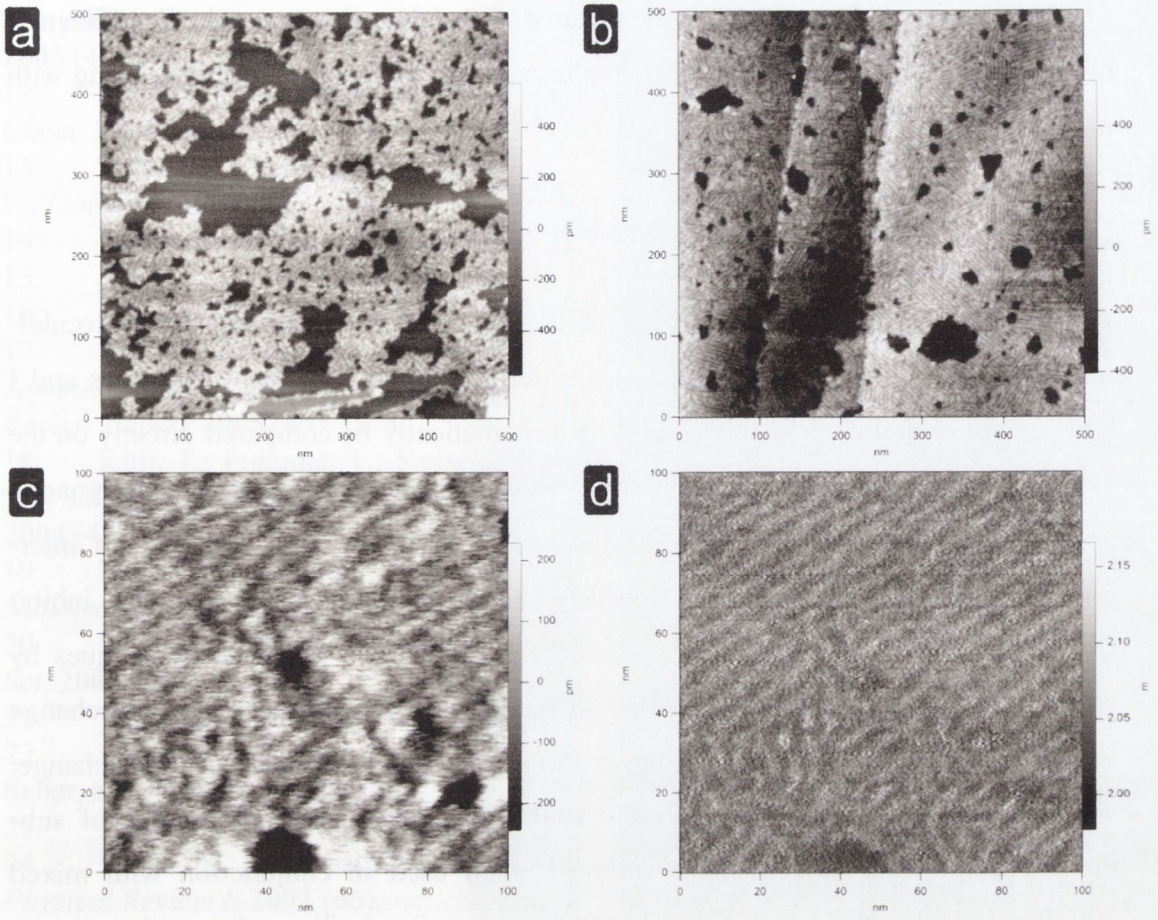


Figure 6.10: FM-AFM (ambient conditions) topography (a), (b) and (c) and excitation voltage (d) (proportional to dissipation) images of a C12-IFS monolayer on HOPG. (a) is a half-monolayer; this half-monolayer was then irradiated to switch some of the Fumaramide groups to Succinamide, hence altering the thread-macrocycle interaction strength. (b) Shows that same half-monolayer after irradiation plus another half-monolayer of unswitched C12-IFS. Higher-resolution topography and dissipation images of the mixed switched/unswitched monolayer are shown in (c) and (d) respectively.

The molecules in this experiment were stimulated by UV when the film was in a sub-monolayer state deliberately so that packing interactions would be minimized at the time of irradiation. The experiment suggests that the molecules in this case did not in fact switch. In Figure *6.10(a)* the molecules (pre-stimulus) still show a randomly oriented, disordered, row structure. The structure of the film in *6.10(b)* has been illustrated in section *6.6* to be rows of like-with-like oriented rotaxanes. The stripes in Figure *6.10(a)* therefore suggest that the rotaxanes are already oriented in like-with-like formation at low surface coverage. This kind of orientation would prohibit relative motion of the sub-molecular components. The tentative conclusion from this data is therefore that the molecules do not switch in this state. This rotaxane however is but one of many possible structure permutations, so this negative result does not rule out switching for all other rotaxanes. Clever design of a molecule could preclude

overlap of like-with-like threads in adjacent molecules. For example a sufficiently bulky stopper group might sterically hinder adjacent molecules from interfering with motion.

6.10 Conclusions

To the best of my knowledge, this is the first reported example of molecular-resolution images of these delicate, easily deformed and functional rotaxanes and I have demonstrated that the molecules can systematically be compared directly on the same substrate in terms of their local molecular scale structural and dynamic properties. The proposed model of the surface reconstruction suggests an inter-digitation of the long rotaxane threads. This behaviour would sterically inhibit rotaxane sub-molecular shuttling at a surface. I have also presented techniques by which switching of these molecules could be detected, i.e. through structural change visualised by high-resolution imaging, or through an energy dissipation signal change. These techniques should be extremely useful to elucidate the occurrence of sub-molecular rotaxane movement at surfaces when used in conjunction with mixed rotaxane monolayers of functional and non-functional (i.e. reference) rotaxane material.

6.11 References

1. Saha, S.; Stoddart, J. F., *Chem. Soc. Rev.* **2007** (36) 77.
2. Browne, W. R.; Feringa, B. L., *Nature Nanotechnology* **2006** (1) 25.
3. Kay, E. R.; Leigh, D. A.; Zerbetto, F., *Angewandte Chemie-International Edition* **2007** (46) 72.
4. Harrison, I. T.; Harrison, S., *J. Am. Chem. Soc.* **1967** (89) 5723.
5. Schill, G.; Henschel, R., *Annalen Der Chemie-Justus Liebig* **1970** (731) 113.
6. Schill, G.; Zollenko.H, *Annalen Der Chemie-Justus Liebig* **1969** (721) 53.
7. Bissell, R. A.; Cordova, E.; Kaifer, A. E.; Stoddart, J. F., *Nature* **1994** (369) 133.
8. Clemente-Leon, M.; Credi, A.; Martinez-Diaz, M. V.; Mingotaud, C.; Stoddart, J. F., *Advanced Materials* **2006** (18) 1291.
9. Flood, A. H.; Peters, A. J.; Vignon, S. A.; Steuerman, D. W.; Tseng, H. R.; Kang, S.; Heath, J. R.; Stoddart, J. F., *Chemistry-a European Journal* **2004** (10) 6558.
10. Berna, J.; Leigh, D. A.; Lubomska, M.; Mendoza, S. M.; Perez, E. M.; Rudolf, P.; Teobaldi, G.; Zerbetto, F., *Nat. Mater.* **2005** (4) 704.
11. Leigh, D. A.; Morales, M. A. F.; Perez, E. M.; Wong, J. K. Y.; Saiz, C. G.; Slawin, A. M. Z.; Carmichael, A. J.; Haddleton, D. M.; Brouwer, A. M.; Buma, W. J.;

Wurpel, G. W. H.; Leon, S.; Zerbetto, F., *Angewandte Chemie-International Edition* **2005** (44) 3062.
12. Stranick, S. J.; Parikh, A. N.; Tao, Y. T.; Allara, D. L.; Weiss, P. S., *J. Phys. Chem.* **1994** (98) 7636.
13. Tidwell, C. D.; Ertel, S. I.; Ratner, B. D.; Tarasevich, B. J.; Atre, S.; Allara, D. L., *Langmuir* **1997** (13) 3404.
14. McNamee, C. E.; Yamamoto, S.; Higashitani, K., *Langmuir* **2007** (23) 4389.
15. Sagiv, J., *J. Am. Chem. Soc.* **1980** (102) 92.
16. Morgenthaler, S. M.; Lee, S.; Spencer, N. D., *Langmuir* **2006** (22) 2706.
17. Ichii, T.; Urabe, M.; Fukuma, T.; Kobayashi, K.; Matsushige, K.; Yamada, H., *Japanese Journal of Applied Physics Part 1-Regular Papers Brief Communications & Review Papers* **2005** (44) 5378.
18. Ichii, T.; Fukuma, T.; Kobayashi, K.; Yamada, H.; Matsushige, K., *Japanese Journal of Applied Physics Part 1-Regular Papers Short Notes & Review Papers* **2004** (43) 4545.
19. Ichii, T.; Fukuma, T.; Kobayashi, K.; Yamada, H.; Matsushige, K., *Nanotechnology* **2004** (15) S30.
20. Ichii, T.; Fukuma, T.; Kobayashi, K.; Yamada, H.; Matsushige, K., *Appl. Surf. Sci.* **2003** (210) 99.
21. Fujii, S.; Fujihira, M., *Nanotechnology* **2006** (17) S112.
22. Loppacher, C.; Bennewitz, R.; Pfeiffer, O.; Guggisberg, M.; Bammerlin, M.; Schar, S.; Barwich, V.; Baratoff, A.; Meyer, E., *Physical Review B* **2000** (62) 13674.
23. Martinez, N. F.; Garcia, R., *Nanotechnology* **2006** (17) S167.
24. Foster, A. S.; Barth, C.; Shluger, A. L.; Nieminen, R. M.; Reichling, M., *Physical Review B* **2002** (66).
25. Garcia, R.; Gomez, C. J.; Martinez, N. F.; Patil, S.; Dietz, C.; Magerle, R., *Phys. Rev. Lett.* **2006** (97).
26. Altieri, A.; Bottari, G.; Dehez, F.; Leigh, D. A.; Wong, J. K. Y.; Zerbetto, F., *Angewandte Chemie-International Edition* **2003** (42) 2296.
27. Perez, E. M.; Dryden, D. T. F.; Leigh, D. A.; Teobaldi, G.; Zerbetto, F., *J. Am. Chem. Soc.* **2004** (126) 12210.
28. Brouwer, A. M.; Frochot, C.; Gatti, F. G.; Leigh, D. A.; Mottier, L.; Paolucci, F.; Roffia, S.; Wurpel, G. W. H., *Science (Washington, D. C., 1883-)* **2001** (291) 2124.
29. Altieri, A.; Gatti, F. G.; Kay, E. R.; Leigh, D. A.; Martel, D.; Paolucci, F.; Slawin, A. M. Z.; Wong, J. K. Y., *J. Am. Chem. Soc.* **2003** (125) 8644.
30. Gotsmann, B.; Seidel, C.; Anczykowski, B.; Fuchs, H., *Phys. Rev. B: Condens. Matter* **1999** (60) 11051.
31. De Feyter, S.; De Schryver, F. C., *J. Phys. Chem. B* **2005** (109) 4290.
32. Hillier, A. C.; Ward, M. D., *Physical Review B* **1996** (54) 14037.

Chapter 7: Conclusions and Outlook

7.1 Introduction

The main purpose of this thesis has been to clarify the potential for rotaxane-based applications. A rotaxane type that would be used in this fashion should of course function when deposited on a surface, preferably the molecule should assemble into a film (to better enable addressability) (although a simple functional surface would be less constrained in terms of addressability), and the film or device itself must be robust. The most important of these factors is of course the rotaxane function. The results in this thesis illustrate the importance of film deposition conditions and molecular type in this regard and illustrate the potential of AFM (particularly FM-AFM) in establishing the existence of surface functionality.

7.2 Conclusions

In this thesis I have investigated H-Bond assembled rotaxanes from the perspective of discovering if sub-molecular motion at surfaces might be possible. The film preparation conditions have a key role in potential functionality. The results in Chapter 4 show that the solvent of deposition and surface concentration can be chosen to minimise the likelihood of nearest neighbour inter-molecule hydrogen bonding.

When a solvent is a poor hydrogen-bond acceptor (has low hydrogen-bond basicity (β)) the molecules in a film deposited from the solvent will be hydrogen-bonded to their neighbours rather than self-satisfied. This is because such a solvent does not hydrogen-bond with the thread-macrocycle system, and a film deposited from a good hydrogen-bond accepting solvent such as DMSO will result in films where the molecules are self-satisfied. This reflects the x-ray crystal structures of rotaxanes recrystallised from both solvent types. Nearest neighbour binding would hinder any switching/shuttling of single molecules. In a film where neighbouring molecules were bonded, a collective reconstruction such as discussed in the work of Biscarini, Cavallini *et al.* would need to occur in a functional device.[1, 2] This is important when considering potential functionality of rotaxanes at surfaces.

In Chapter 4 also, the example of the exopyridl rotaxane shows that the selection of appropriate molecule types will have a key role to play in the ordering of rotaxane films. Any rotaxane device will need to be well ordered and addressable. The reconstruction measured by high-resolution FM-AFM in Chapter 5 has therefore been a very useful experiment for showing clearly the high degrees of order in the film (not to mention having been a good demonstration of the power of FM-AFM in ambient conditions.) The fact that most images in Chapter 5 and all images in Chapter 4 and 6 were taken in ambient conditions, and that UHV conditions were not involved in any stage of the process demonstrated the robustness of both the film preparation technique and of the prepared films themselves.

In Chapter 6 I have shown that the robust film characteristics and order are not just properties of the films of simple rotaxanes, but can be carried over to the long-chain rotaxane molecular shuttles. The calculated reconstruction however suggests that this is likely to be at the expense of sub-molecular mobility since the structure shows an overlapping and interdigitation of neighbouring rotaxane threads. The technique described in Chapter 6 for measuring nanoscale rotaxane functionality will however still carry over to molecules that might be found to reconstruct with a higher likelihood of motion. The results show that distinct dissipation signatures as well as molecular-scale topography of multiple rotaxane types in neighbouring domains can be measured. The data in Chapter 6 thus represents a significant step towards the direct measurement of the nanoscale functionality of these molecules. This work does not prove either way that rotaxane switching at surfaces is possible, but it has taken some positive steps towards this goal.

7.3 Outlook

Using the techniques developed and knowledge generated in this thesis, the next step would be to explore further rotaxane types with a view towards finding a rotaxane with a surface reconstruction more favourable in terms of potential sub-molecular motion. Future work might incorporate molecular mechanics modelling of different rotaxane molecular permutations to calculate which monolayer films would have least crowded reconstruction. The required functionalities of the molecular shuttle thread stations will limit the number of possibilities, making the calculations easier. Because we know that this molecular family can form pure and well ordered films, the

deposition technique will likely be unchanged. Switching experiments could be carried out while measuring molecular-scale topography and dissipation signals of the shuttle under investigation, and a reference molecule with no activity.

The interdigitation noted in the molecular shuttle reconstruction seen in Chapter 6 (Figure *6.3*) points towards this particular molecular type not being sub-molecularly mobile at this surface. There are some alternative film types that could be proposed to make a functional rotaxane surface because of this result. For example it might be necessary to use rotaxanes with shorter chain lengths. In this way the reconstruction should change so that the stoppers cannot sterically overlap, which might allow more freedom for sub-molecular motion; the exact reconstruction however would need to be investigated.

When conducting experiments into the switching of rotaxane molecules I hasten to add the following two caveats. Care must be taken when interpreting the effect of external stimuli because the surface and any contaminants can also easily be affected. As well as this it is important not to perturb the rotaxane film with the AFM in a way that could be mistaken for switching. Two interesting examples from my studies follow.

Figure *7.1* shows interesting surface behaviour under exposure to UV radiation ($254\,nm$, $5mW/cm^2$) for 1 hour. Without any tip changes occurring in the series of images, and molecular-scale resolution evident in both topography and dissipation, interesting changes in the series of images can be seen. The tip was not disengaged from the sample during this entire time. The experiment was initially very misleading because it turned out that the molecular surface imaged here was in fact just contamination from the environment in the Lab (probably a dirty vacuum pump) and so this series of images represented some sort of cleaning of the graphite surface under the influence of the UV radiation. I confirmed this suspicion by a control experiment, generating the same structures on a bare HOPG substrate without adsorbed rotaxanes. This is a caution for future experiments because this type of surface behaviour could easily be mistaken for some kind of surface switching, yet the material is not rotaxane. This also reinforces the need for the multi-component films with an inactive control molecule as shown in chapter 6 when testing the rotaxane

functionality using AFM. A switching experiment where the material was definitely rotaxane is shown in Chapter 6 (Figure *6.10*) and I was unable to see any changes in films of this type.

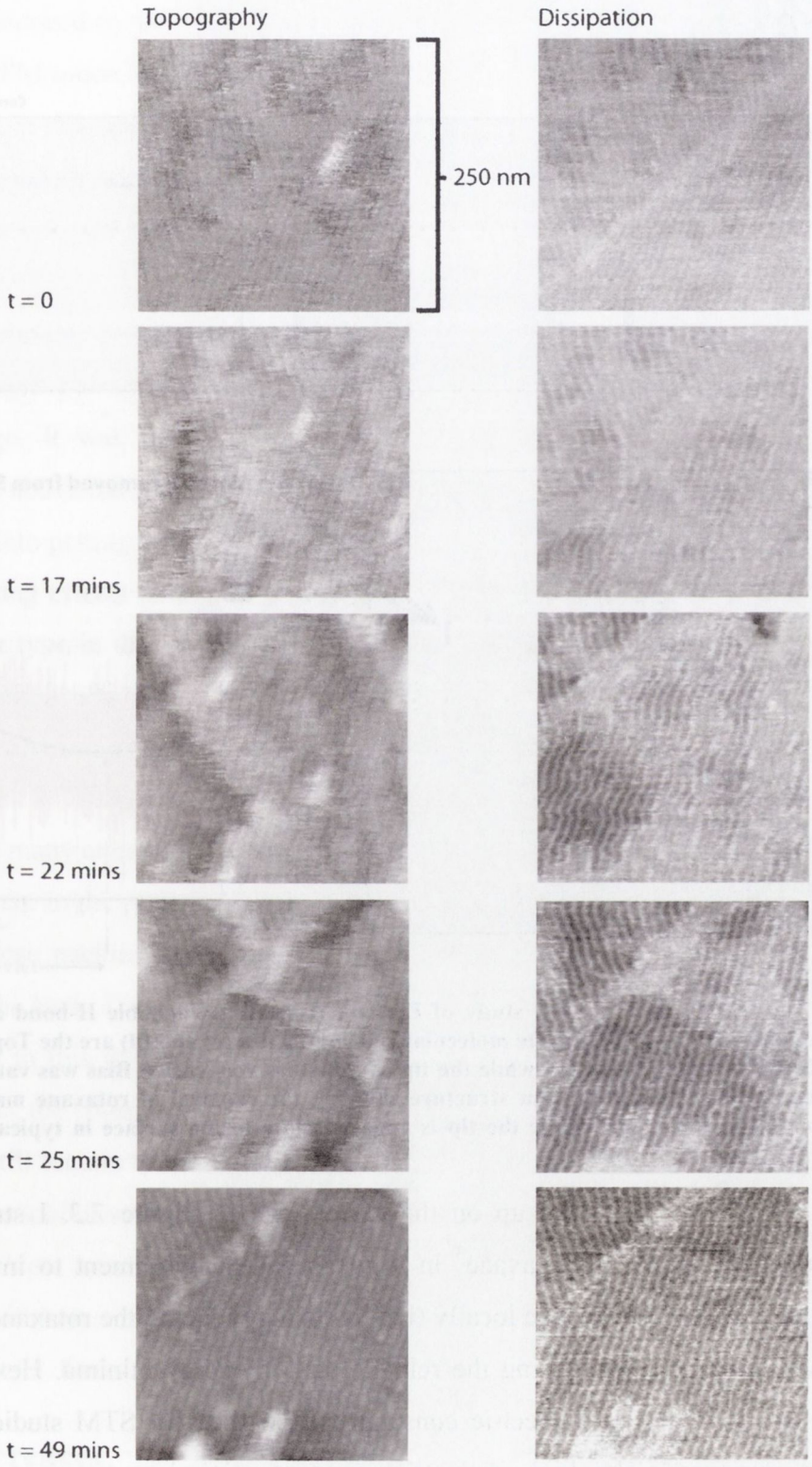


Figure 7.1: A series of FM-AFM topography and dissipation images of a contaminated HOPG surface in ambient conditions during exposure of the surface to UV radiation at ($254\,nm$, $5mW/cm^2$) for 1 hour.

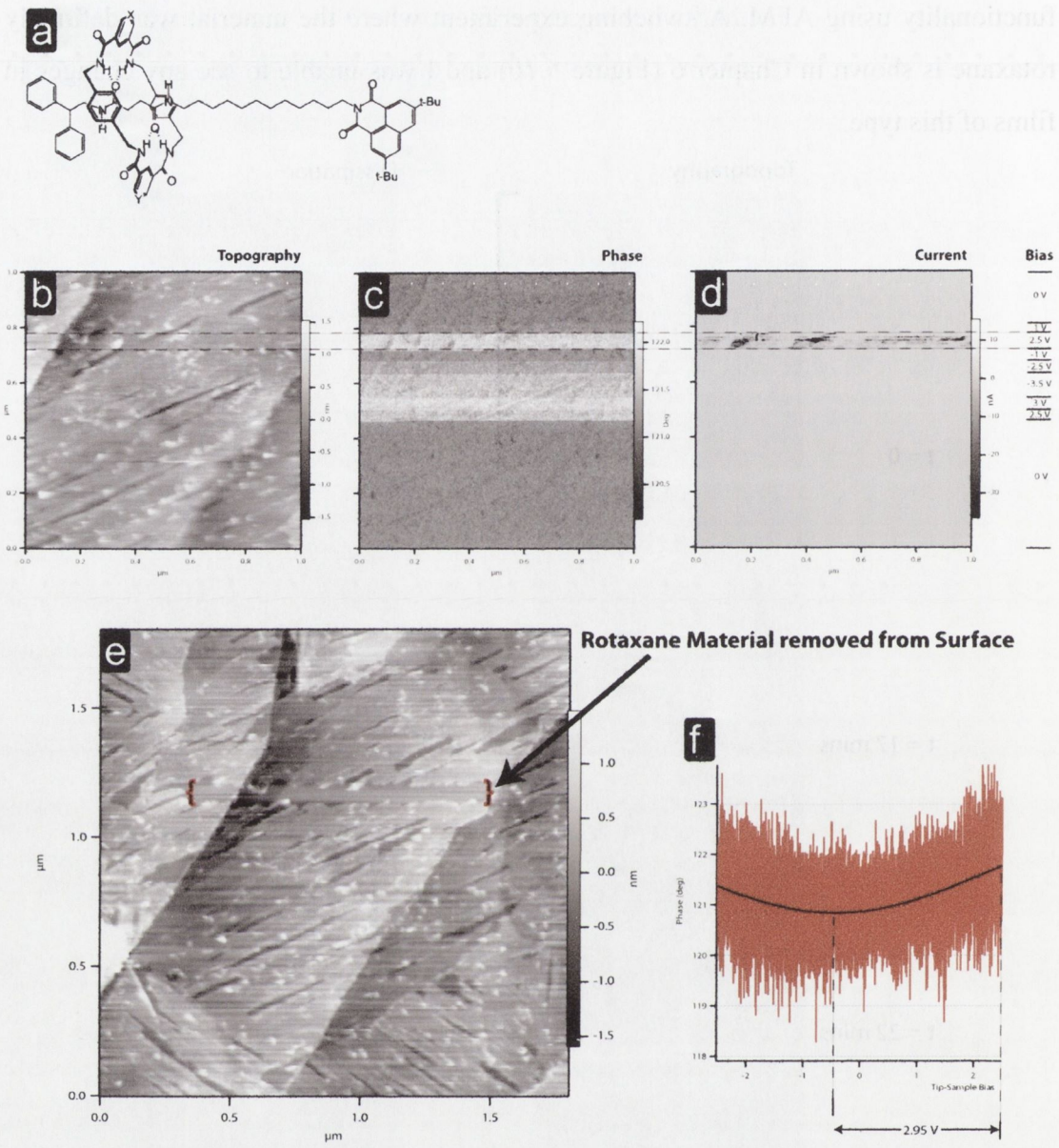


Figure 7.2: Illustration of AM-AFM study of Electrochemically switchable H-bond assembled rotaxane monolayer thin film. (a) is the molecular schematic. (b), (c) and (d) are the Topography, Phase and Current signals recorded while the tip-sample bias was varied Bias was varied (RHS of (d)). Image (e) is the resulting film structure showing the removal of rotaxane material. (f) shows the phase vs. Bias curve while the tip is engaged close to the surface in typical imaging conditions.

I spent a lot of time following up on the effect seen in Figure *7.2*. I studied an electrochemically switchable rotaxane[3] in a hexadecane environment to investigate the effects of charging the surface locally (i.e. oxidising/reducing the rotaxane) which should have the effect of reversing the relative station energy minima. Hexadecane and other liquids with high dielectric constant can be used for STM studies at the liquid/solid interface.[4] The high dielectric constant minimises transient currents between tip and sample, ensuring that the current flows only between the very end of the tip and the substrate. I used hexadecane for Conducting AFM experiments in this

capacity. Using this method under certain tip-sample bias conditions and with a conducting AFM tip, rotaxane material spontaneously desorbed from the surface. I spent some time investigating this effect, but could never demonstrate that the effect was not induced by the tip-sample force being changed. The experiments were done in AM-AFM mode, because I could not achieve the stable self-oscillation needed for FM-AFM in this dense liquid. Using this technique it is not easy to deconvolute forces (as discussed in section *3.3.1*). I believe material was essentially scraped from the surface because the force was changed with changing tip-sample bias.

The experiments described in this thesis initially gave very exciting and unique results, which might prompt one to jump ahead without having a complete foundation of knowledge. It was for this reason and because of warning signs such as those described above that I deliberately took a step back at this point in the work. I put a lot of effort into getting more fundamental data and establishing a method for observation of switching effects (Chapter 6), paying particular attention to the need for a control molecular type in the experimental protocol for testing rotaxane functionality. I was very thorough with establishing the effect of solvent (Chapter 4). This is despite the successes with topographic and dissipation resolutions (Chapter 5).

Although many attempts were made to induce the switching of rotaxanes at surfaces it may be that, in the particular film configurations investigated, motion was impossible due to close packing and strong inter-molecular and surface molecule interactions. Despite the lack of a successful observation of switching under the studied conditions presented in this thesis, a vast array of possible surface preparation parameters that may affect the rotaxane mobility in the final film, as well as a variety of molecular shuttles still remain to be investigated. I have, however, expanded upon the molecular mechanics toolkit available to researchers to include the powerful FM-AFM technique under ambient conditions and elucidated many properties of these rotaxanes that I believe will help in the design of useful functional surfaces or other rotaxane-based devices in the future.

7.4 References

1. Biscarini, F.; Cavallini, M.; Kshirsagar, R.; Bottari, G.; Leigh, D. A.; Leon, S.; Zerbetto, F., *Proc. Natl. Acad. Sci. U. S. A.* **2006** (103) 17650.

2. Cavallini, M.; Biscarini, F.; Leon, S.; Zerbetto, F.; Bottari, G.; Leigh, D. A., *Science* **2003** (299) 531.
3. Altieri, A.; Gatti, F. G.; Kay, E. R.; Leigh, D. A.; Martel, D.; Paolucci, F.; Slawin, A. M. Z.; Wong, J. K. Y., *J. Am. Chem. Soc.* **2003** (125) 8644.
4. De Feyter, S.; Uji-i, H.; Mamdouh, W.; Miura, A.; Zhang, J.; Jonkheijm, P.; Schenning, A.; Meijer, E. W.; Chen, Z.; Wurthner, F.; Schuurmans, N.; van Esch, J.; Feringa, B. L.; Dulcey, A. E.; Percec, V.; De Schryver, F. C., *International Journal of Nanotechnology* **2006** (3) 462.